


July 2016

## Alternative Methods for the Treatment of Chemo-Resistant Cancers

Kaitlyn Wong  
University of Massachusetts Amherst

Follow this and additional works at: [https://scholarworks.umass.edu/dissertations\\_2](https://scholarworks.umass.edu/dissertations_2)

 Part of the [Alternative and Complementary Medicine Commons](#), [Cancer Biology Commons](#), [Nanomedicine Commons](#), and the [Oncology Commons](#)

---

### Recommended Citation

Wong, Kaitlyn, "Alternative Methods for the Treatment of Chemo-Resistant Cancers" (2016). *Doctoral Dissertations*. 702.

<https://doi.org/10.7275/8294150.0> [https://scholarworks.umass.edu/dissertations\\_2/702](https://scholarworks.umass.edu/dissertations_2/702)

This Open Access Dissertation is brought to you for free and open access by the Dissertations and Theses at ScholarWorks@UMass Amherst. It has been accepted for inclusion in Doctoral Dissertations by an authorized administrator of ScholarWorks@UMass Amherst. For more information, please contact [scholarworks@library.umass.edu](mailto:scholarworks@library.umass.edu).

# **Alternative Methods for the Treatment of Chemo-Resistant Cancers**

**A Dissertation Presented  
by  
Kaitlyn E. Wong**

**Submitted to the Graduate School of the  
University of Massachusetts Amherst in partial fulfillment  
of the requirements for the degree of**

**DOCTOR OF PHILOSOPHY**

**May 2016**

**Molecular and Cellular Biology**



# **Alternative Methods for the Treatment of Chemo-Resistant Cancers**

**A Dissertation Presented**

**By**

**KAITLYN E. WONG**

**Approved as to Style and Content by:**

---

**Sallie S. Schneider, Chair**

---

**Todd S. Emrick, Committee Member**

---

**Richard B. Arenas, Committee Member**

---

**Kathleen F. Arcaro, Committee Member**

---

**Dominique Alfandari, Program Leader / GPD  
Molecular and Cellular Biology Program**

## **DEDICATION**

This work is dedicated to my amazing husband and soulmate, Sing Wai Wong, and our wonderful child, Liam Charles.

Additionally, this work is dedicated to the memory of my grandfather, Charles James Urban, and my dear friend, Lauren Marie Csorny. You were both taken far too early from this world and continue to influence and inspire me daily.

## ACKNOWLEDGEMENTS

I would like to thank Dr. Sallie S. Schneider for her overwhelming support, encouragement, and mentorship that she has provided me while under her tutelage. She has been supportive of my career goals whilst also allowing me to be creative and explore multiple avenues of research. Thank you for supporting me and my lofty dreams as well as encouraging me both in and outside of lab.

I would like to thank the fellow members of my lab and colleagues at Pioneer Valley Life Sciences Institute. It truly takes a village to train someone and everyone at PVLSI and the BACF were instrumental to my training and academic growth. I would like to personally thank Maxine Dudek and Dr. Lotfi Bassa, my partners in graduate education. I would like to acknowledge both Dr. Jean Henneberry and Dr. Giovanna Crisi for their assistance with histologic review of samples. I would like to also thank Nicholas Panzarino, Elizabeth Henchey, Matthew Skinner, Dr. Kelly Gauger, Dr. Carmen Mora, Dr. Erica Kane, Dr. Katharine Bittner, Dr. Negendra Yadava and Jennifer Ser-Delansky for their additional support of my research. Additionally I would like to acknowledge the members of Baystate Animal Care Facility for not only their support with animal care but for their patience in training and support of my various animal projects.

I wish to thank the Department of Surgery at Baystate Medical Center for their support of my extended time in lab to allow for me to obtain this degree during surgical residency training. I would like to overwhelmingly express my gratitude of the support and mentorship provided by Dr. Michael Tirabassi, whom I consider an honorary member of my defense committee. Additionally I would like to thank Dr. Kevin Moriarty, my

clinical advisor, who has provided mentorship and guidance and has been very supportive of my career choices. Additionally I would like to acknowledge the support of Dr. David Tashjian, Dr. Neal Seymour and Dr. Gladys Fernandez as well as all the faculty and residents of the Department of Surgery at Baystate Medical Center for their support, mentorship and guidance allowing me work toward obtaining a Ph.D.

I would like thank the University of Massachusetts Amherst and the Department of Molecular and Cellular Biology Program for allowing me to pursue a graduate degree in this program. I would particularly like to acknowledge Dr. Barbara Osbourne and Sarah Czerwonka for their assistance and support in my enrollment in the program. Additionally, I would like to thank Dr. Kathleen Arcaro, Dr. Todd Emrick and Dr. Richard Arenas for their support and guidance of my research as members of my thesis committee.

I would like to express overwhelming gratitude for the support, encouragement, love and guidance I have received from my all my close friends, family and mentors throughout my entire academic career. I would like to thank my in-laws, Lisa “Lai Shan” Ng and Paul “Kam Po” Wong for continuous support. I would like to thank my parents, Nancy and Henry Ellis, and my sisters, Dana and Amy Ellis, for their never-ending support and encouragement. Finally, the successes and achievements I have obtained would be impossible without the undying support, encouragement and assistance from my husband, Sing Wong and our son, Liam. I love you both, forever and always.

## ABSTRACT

# ALTERNATIVE METHODS OF THE TREATMENT OF CHEMO-RESISTANT CANCERS

MAY 2016

KAITLYN E. WONG B.S., STATE UNIVERSITY OF NEW YORK AT STONY  
BROOK

M.P.H., TUFTS UNIVERSITY

M.D., TUFTS UNIVERSITY

Ph.D., UNIVERSITY OF MASSACHUSETTS AMHERST

Directed by: Professor Sallie S. Schneider

Great strides have been made in cancer therapy in the past century, yet it remains one of the leading causes of death in the United States today. This work aimed to shed light on novel methods to treat a variety of aggressive and often chemo-resistant cancers both *in vitro* and *in vivo*.

The first aim of this work was to evaluate the therapeutic efficacy of poly(methacryloyloxyethyl phosphorylcholine) (polyMPC) prodrugs compared to standard chemotherapeutic agents. Conjugation of polyMPC to drugs such as doxorubicin (Dox) can result in its improved solubility, prolonged half-life and therapeutic efficacy. PolyMPC and polyMPC-Dox (at a dose less than 10mg/kg) was observed to be safe for systemic administration in a murine model. Additionally, treatment with polyMPC-Dox resulted in improved survival and reduced off target toxicities in mice with orthotopic human ovarian xenografts. Further, mesenchymal stem cells (MSCs) were observed to



successfully uptake polyMPC and home to breast cancer xenografts *in vivo* and thus can potential serve as a vehicle to improve drug delivery.

Additional aims of this work focused on evaluating the root extract of *Rhodiola crenulata* (RC) plants for the treatment of aggressive cancers derived from the neural crest, including neuroblastoma and melanoma. RC was observed to reduce growth and migration of melanoma *in vitro*. Further, RC resulted in reduction of aggressive tumor characteristics upon topical therapy as well as the reduced establishment of metastatic foci upon enteral administration in mice with melanoma. While no difference in outcomes was observed upon RC treatment in a disseminated neuroblastoma model *in vivo*, RC did result in striking cytotoxic effects upon treatment of neuroblastoma cells *in vitro*. These cytotoxic effects of RC likely resulted from derangements altering the cell's ability to undergo optimal cellular metabolism.

## TABLE OF CONTENTS

	Page
ACKNOWLEDGEMENTS.....	v
ABSTRACT.....	vii
LIST OF TABLES.....	xi
LIST OF FIGURES.....	xii
CHAPTER	
1. INTRODUCTION.....	1
1.1. Significance.....	1
1.2. Current Cancer Therapeutic Strategies.....	2
1.3 Polymer Based therapeutic Agents.....	3
1.4 Drug Delivery Vehicles.....	4
1.5 Phytochemicals and Cancer Therapy.....	5
1.6 References.....	7
2. EVALUATION OF POLYMPVC PRODRUGS IN A HUMAN OVARIAN TUMOR MODEL.....	11
2.1. Introduction.....	11
2.2. Materials and Methods.....	13
2.3. Results.....	16
2.4. Discussion.....	17
2.5. Conclusion.....	25
2.6. Figures.....	27
2.7. References.....	33
3. TARGETED CHEMOTHERAPY UTILIZING MESENCHYMAL STEM CELLS LOADED WITH POLYMPVC.....	35
3.1. Introduction.....	35
3.2. Materials and Methods.....	37
3.3. Results.....	40
3.4. Discussion.....	41
3.5. Conclusion.....	43
3.6. Figures.....	44
3.7. References.....	47

4. EVALUATION OF <i>RHODIOLA CREMULATA</i> ON THE TREATMENT OF MELANOMA.....	50
4.1. Introduction.....	50
4.2. Materials and Methods.....	51
4.3. Results.....	55
4.4. Discussion.....	58
4.5. Conclusion.....	61
4.6. Figures.....	62
4.7. References.....	67
5. EVALUATION OF <i>RHODIOLA CREMULATA</i> ON THE TREATMENT OF NEUROBLASTOMA.....	70
5.1. Introduction.....	70
5.2. Materials and Methods.....	71
5.3. Results.....	82
5.4. Discussion.....	89
5.5. Conclusion.....	93
5.6. Figures.....	94
5.7. Tables.....	106
5.8. References.....	107
6. CONCLUSION.....	109
6.1 General Discussion.....	109
6.2 Utilization of PolyMPC for Cancer Therapeutics.....	110
6.3 Utilization of <i>Rhodiola</i> Extract for the Treatment of Cancer.....	111
6.4. Conclusion.....	112
BIBLIOGRAPHY.....	113

## LIST OF TABLES

	Page
5.1 Primers Utilized in qRT-PCR.....	106

## LIST OF FIGURES

	Page
2.1 Maximal Tolerated Dose Evaluation of PolyMPC and PolyMPC-Dox.....	27
2.2 Biodistribution Analysis of PolyMPC-Dox.....	28
2.3 Evaluation of Efficacy of PolyMPC-Dox in Human Ovarian Tumor Model <i>In Vivo</i> .....	29
2.4 Evaluation of the <i>In Vivo</i> Cardiac Effects of PolyMPC-Dox Treatment.....	30
2.5 Evaluation of the <i>In Vivo</i> Pulmonary Effects of PolyMPC-Dox Treatment.....	31
2.6 Evaluation of the <i>In Vivo</i> Liver Effects of PolyMPC-Dox Treatment.....	32
3.1 MSC Drug Uptake and Viability.....	44
3.2 MSC Co-Culture Experiment.....	45
3.3 MSC Tumor Homing <i>In Vivo</i> .....	46
4.1 <i>In Vitro</i> Effects of RC treatment upon Melanoma.....	62
4.2 Outcomes of Topical RC Treatment of Melanoma <i>In Vivo</i> .....	63
4.3 Gross and Pathological Changes upon Topical RC Treatment of Melanoma.....	64
4.4 Outcomes of Enteral RC Treatment of Melanoma <i>In Vivo</i> .....	65
4.5 Effects of Enteral RC Treatment on the Establishment of Metastatic Melanoma.....	66
5.1 Morphological Effects of RC Treatment on Neuroblastoma Cells <i>In Vitro</i> .....	94
5.2 Cytotoxic Effects of RC on Neuroblastoma <i>In Vitro</i> .....	95
5.3 Evaluation of RC's Effect on Migration and Growth on Neuroblastoma <i>In Vitro</i> .....	96
5.4 Evaluation of RC vs Dox treatment on Neuroblastoma <i>In Vitro</i> .....	97
5.5 Effects on Gene Expression upon RC treatment in NB-1691 <i>In Vitro</i> .....	98
5.6 Evaluation of the Effects of Pyruvate Upon RC Treatment on Neuroblastoma.....	99
5.7 Evaluation of Nutrient Supplementation on RC Effects on Neuroblastoma Viability <i>In Vitro</i> .....	100
5.8 Evaluation of Citric Acid Cycle Intermediate Supplementation on RC Effects on Neuroblastoma Viability <i>In Vitro</i> .....	101
5.9 Effect of Metabolic Inhibitors on RC Treatment upon NB-1691 Cells <i>In Vitro</i> .....	102
5.10 RC Effects on Metabolic Enzyme Activity and Metabolic Intermediate Levels.....	103
5.11 Evaluation of the <i>In Vivo</i> Efficacy of RC Treatment of Disseminated Neuroblastoma.....	104
5.12 Outcomes of RC treatment in a disseminated <i>in vivo</i> neuroblastoma model.....	105

# CHAPTER 1

## INTRODUCTION

### 1.1 Significance

Cancer remains a critical public health concern as it continues to be one of the leading causes of death, not just in the United States, but throughout the world. The American Cancer Society projected that more than 1.6 million new cancer diagnoses, excluding basal and squamous skin cancers and non-invasive *in situ* cancers, were diagnosed in 2015 in the United States [1]. Further, more than half a million deaths in the United States were a result of cancer in 2015 [1]. Only heart disease and accidental trauma results in more deaths than cancer, in adults and children respectively, in the United States annually. There is a greater than 38% lifetime risk (38% female, 43% male) of developing cancer in the average American [1]. While significant improvements in detection and treatments for cancer over the last few decades have resulted in the downward trend of the incidence of cancer and death resulting from this disease [2], still it contributes a significant burden to the health care of our society.

Evaluation of novel methods to not only treat cancer but to improve currently available therapeutic options can enhance treatment efficacy and result in improved patient outcomes and survival. The research presented in this thesis seeks to evaluate polyMPC polymer prodrugs and *Rhodiola crenulata* (RC) plant extracts for the treatment of a variety of chemo-resistant cancers both *in vivo* and *in vitro*.

## **1.2. Current Cancer Therapeutic Strategies**

The treatment of cancer, depending on the stage of the disease at presentation, often requires a multidisciplinary approach to therapy combining medicine, surgery and/or radiation. While surgery and radiation are more loco-regional based efforts of treatment, chemotherapeutic drugs, typically provided systemically, are utilized in more invasive and disseminated stages of disease [3]. A variety of classes of chemotherapeutic agents are available, many of which non-specifically target rapidly growing and dividing cells, including cancer cells. These drugs are also associated with severe side effects related to dosing, biodistribution and the pharmacokinetics of these agents. While side effects can be as generalized as fatigue and gastrointestinal complaints, specific drugs can result in significant toxicities, resulting in devastating morbidities such as cardiac, renal or neurotoxicities [3]. The severity of these side effects can limit optimal dosing or even the utilization of these agents entirely despite their potential therapeutic benefit.

Investigation into novel agents and means to improve current therapy is ongoing. Novel treatment classes, such as immunologic agents, have been developed. These agents enhance immune function, promoting both innate and adaptive immunologic anti-tumor defenses [4]. Additionally, genetic and proteomic profiling have also been evaluated to optimize therapy for each patient based on their specific tumor characteristics. Investigation also continues to identify naturally available treatment agents, such as bioactive fractions of plant based phytochemicals that may provide us with novel treatment or preventative agents. Finally, additional strategies to improve traditional chemotherapeutic agents have also been employed. A variety of methods have been

utilized to improve tumor targeting and drug delivery through both active and passive mechanisms, thus improving the efficacy and tolerance of these agents.

### **1.3 Polymer Based Therapeutic Agents**

The creation of prodrugs is one method to improve the effectiveness of available chemotherapeutic agents. Prodrugs are created through the modification of drugs by means of binding biologically inactive moieties to these agents to alter their biologic properties upon administration *in vivo* [5]. When administered systemically, the drug is often inert given its attachment to the bound chemical molecules. The prodrug can be modified by a variety of means, including enzymatic and chemical modifications, in order to release the drug in its active form and at the optimal site of action, such as within a tumor. The goals of utilizing prodrugs are to increase drug uptake by tumors and reduce unintended uptake of these drugs by other organs [4-6]. Utilization of prodrugs can allow for improved drug tolerance through allowance of higher drug administration or through reduction of harmful side effects that could limit drug tolerance.

The chemical moieties employed to create prodrugs can also allow for improved pharmacokinetic and biodistributive profile as the utilized scaffolds can improve drug solubility and half life of the index agent. Further, improved tumor uptake of the drug in prodrug form can result secondary to the enhanced permeability and retention (EPR) effect. This effect states that larger and bulkier molecules bound to drugs are more likely to be taken up by the leaky, disorganized vasculature of the tumor micro-environment



[6-9]. Uptake is further enhanced secondary to its prolonged circulation and decreased rate clearance provided by the conjugation of these drugs to polymers.

A variety of polymer nanocarriers, such as poly(ethylene glycol) (PEG) have been utilized for prodrug creation [4-6]. Several strategies are utilized to create prodrugs using polymers in which the drug can be conjugated to a preformed polymer, the drug can be bound to a monomer prior to polymerization or polymerization can be initiated following binding to the agent of interest [5]. Utilization of polymers as a means to create prodrugs provide several benefits as the synthesis of these facile molecules can be tailored in a variety of ways including shape, size and drug binding capacity allowing for alterations of drug availability and release. Investigation into alternative polymers, such as poly (2-methacryloyloxyethyl phosphorylcholine) (polyMPC), can result in more efficacious and potentially better tolerated prodrugs [7-8].

#### **1.4 Drug Delivery Vehicles**

In order to further enhance drug delivery, additional means to deliver treatment agents are necessary. A variety of “carriers” have been evaluated as vehicles for drug delivery to improve targeting of drugs, such as liposomes or polymer micelle formulations [5,6,9]. These vehicles serve to not only shield drugs while in systemic circulation, thus preventing unintended exposure of these agents to certain tissues, but can also result in improved drug targeting specifically within the tumor bed. Several clinically relevant drug formulations employ these techniques. For example, doxil is a liposomal formulation of the anthracycline agent, doxorubicin (Dox) [10,11]. Through

utilization of a liposomal carrier, Dox uptake within the tumor is enhanced and its uptake in cardiac tissues is reduced, resulting in improved therapeutic efficacy and less cardiotoxicity [11].

Active targeting methods often employ ligand mediated targeting whereby ligands, such as antibodies, which are specific for cell surface molecules or receptors on tumors are bound to drugs resulting in very specific interactions required for drug delivery [6]. Alternative methods can also be utilized to further deliver drug directly to a tumor. Cellular vehicles hold promise as an alternative and potentially active means to promote drug delivery. A variety of cells including T-cells, macrophages and stem cells are known to have inherent migratory and tumorotropic abilities. The micro-environment of tumor stroma is similar to that of a healing wound and thus releases chemoattractant molecules which stimulate the migration of these cells to tumors. Mesenchymal stem cells (MSCs) are pluripotent progenitor cells with tumorotropic characteristics that are found throughout the body [12-16]. The therapeutic advantages of these cells have already been harnessed clinically, given their attraction to sites of injury, in order to treat tissue damaged from myocardial infarctions and strokes [17,18]. The tumorotropic properties displayed by MSCs can be taken advantage of therapeutically, as MSCs can be physically or genetically modified to deliver drugs or anti-cancer agents directly to tumors.

## **1.5 Phytochemicals and Cancer Therapy**

Natural products are agents derived from plants, animals and microbes that are potentially biologically and pharmaceutically active [19-21]. Almost a quarter of novel drugs developed for cancer treatment between 1981-2002 were composed of, derived from or were discovered in natural agents [20]. Many continue to remain under investigation, and are even undergoing evaluation in active clinical trials. Phytochemicals, or natural agents derived from plants, comprise a significant proportion of the products. Many phytochemicals are used for both the prevention or treatment of cancer [19-22]. There are four classes of plant based compounds that are currently utilized clinically for the treatment of cancer including vinca alkaloids, epipodophyllotoxins, taxanes, and camptothecins [21]. While phytochemicals are one of the key sources of agents utilized to treat cancer, still many of these plant based agents have yet to be evaluated critically for their ability to treat cancer or provide insight into potential novel targets for cancer therapy.

Bioactive fractions from a variety of dietary plants or plant extracts have been utilized in traditional medicines for centuries and are known to treat or prevent the development of cancer. These agents can be derived from a vast array of plants, including licorice, ginger, green tea, as well as many others [21]. These plant based products result in the prevention or treatment of cancer through a variety of mechanisms. Several of the means to which these phytochemicals result in anti-tumorigenic effects on a wide array of cancers (either *in vitro* or *in vivo*) include anti-inflammatory and pro-apoptotic properties, prevention of cellular epithelial to mesenchymal transitions, as well as prevention of metastatic spread and establishment [20,22].

*Rhodiola* plants have been utilized medicinally for centuries in Eurasian cultures. The genus *Rhodiola* is composed of nearly 90 different species of plants which grow throughout Eastern Europe and Asia [19,23]. *Rhodiola* plants grow throughout regions of high altitude, cold climates and barren soil. Given this, these plants have evolved to produce a numerous adaptogenic compounds which allow the plant to thrive in such harsh environments. Many of the fractions of *Rhodiola* plants that display medicinal properties, such as salidroside, tyrosol, caffeic acid, rosin and rosavin, are classified as adaptogens as they are utilized to prevent the effects of cellular stressors [19,23-29]. Today *Rhodiola* extracts are available as a natural supplement used for the treatment of fatigue, depression, anemia, impotence, gastrointestinal ailments, infections, and nervous system disorders. These extracts are believed to convey improved physical endurance and boost the immune system [19,24-29]. Extracts from *Rhodiola crenulata* (RC) are known to be bioactive and bioavailable and are under investigation as a therapy in several types of cancers, including breast and bladder cancer [24-29]. RC extracts, and the compounds contained within it, have the potential to serve as a novel adjunct for the treatment of a variety of cancers.

## 1.6 References

1. American Cancer Society. Cancer Facts and Figures. 2015. Accessed 2/10/15. Available from <http://www.cancer.org/acs/groups/content/@editorial/documents/document/acspc-044552.pdf>.
2. Weir, H.K., Thompson, T.D., Soman, A, et al. The Past, Present, and Future of Cancer Incidence in the United States: 1975-2020. *Cancer*. 2015. DOI: 10.1002/cncr.2925
3. Siegal, R., DeSantis, C., Virgo, K., et al. Cancer Treatment and Survivorship Statistics, 2012. *CA A Cancer Journal for Clinicians*. 2012. DOI: 10.3322/caac.21149
4. Pardoll, D., Allison, J. Cancer Immunotherapy: Breaking the Barriers to Harvest the Crop. *Nature Medicine*. 2004. 10: 887-892.
5. Delplace, V., Couvreur, P., Nicolas, J. Recent Trends in the Design of Anticancer Polymer Prodrug Nanocarriers. *Polym. Chem*. 2014. 5:1529-1544.
6. Bertrand, N., Wu, J., Xu, X., et al. Cancer Nanotechnology: The Impact of Passive and Active Targeting in the Era of Modern Cancer Biology. *Advanced Drug Delivery Reviews*. 2014. 66:2-25.
7. Greish, K. Enhanced Permeability and Retention Effect for Selective Targeting of Anticancer Nanomedicine: Are we There Yet? *Drug Discovery Today: Technologies*. 2012. 9(2):e161-166.
5. Maeda, H. Enhanced Permeability and Retention Effect in Relation to Tumor Targeting. *Drug Delivery in Oncology: From Basic Research to Cancer Therapy*. Chapter 3: 65-84
6. Maeda, H., Wu, J., Sawa, T., et al. Tumor Vascular Permeability and the EPR Effect in Macromolecular Therapeutics: A Review. *Journal of Controlled Release* 2000 65; 271-284.
7. Chen, X., Parelkar, S.S., Henchey, E., et al. PolyMPC-Doxorubicin Prodrugs. *Bioconjugate Chemistry*. 2012 23: 1753-1763.
8. McRae Page, S., Henchey, E., Chen, X., et al. Efficacy of PolyMPC-DOX Prodrugs in 4T1 Tumor-Bearing Mice. *Molecular Pharmaceutics* 2014 11:1715-1720.
9. Saenz del Burgo, L., Pedraz, J.L., Orive, G., et al. Advanced Nanovehicles for Cancer Management. 2014. 19 (10): 1659-1670.

10. Tacar, O., Sriamornsak, P. and Dass, C.R. Doxorubicin: an Update on Anticancer Molecular Action, Toxicity and Novel Drug Delivery Systems. *Journal of Pharmacy and Pharmacology*. 2013. 65(2): 157-170.
11. Pastorino, F., Di Paolo, D., Piccardi, F., et al. Enhanced Antitumor Efficacy of Clinical-Grade Vasculature-Targeted Liposomal Doxorubicin. *Clinical Cancer Research* 2008 14; 7320-7329.
12. Deans, R.J. and Moseley, A.B. Mesenchymal Stem Cells: Biology and Potential Clinical Uses. *Experimental Hematology* 2000 28; 875-884.
13. Hall, B., Dembinski, J., Sasser, A.K., et al. Mesenchymal Stem Cells in Cancer: Tumor-Associated Fibroblast and Cell-Based Delivery Vehicles. *International Journal of Hematology* 2007 86; 8-16.
14. Huang, X., Zhang, F., Wang, H., et al. Mesenchymal Stem Cell-based Cell Engineering with Multifunctional Mesoporous Silica Nanoparticles for Tumor Delivery. *Biomaterials* 2013 24; 1772-1780.
15. Roger, M., Clavreul, A., Venier-Julienne, M., et al. Mesenchymal Stem Cells as Cellular Vehicles for Delivery of Nanoparticles to Brain Tumors. *Biomaterials* 2010 31; 8393-8401.
16. Studeny, M., Marini, F.C., Champlin, R.E., et al. Bone Marrow-derived Mesenchymal Cells as Vehicles for Interferon-beta Delivery into Tumors. *Journal of Cancer Research* 2002 62; 3603-3608.
17. Bang, O.Y., Lee, J.S., Lee, P.H., et al. Autologous Mesenchymal Stem Cell Transplantation in Stroke Patients. *Annals of Neurology* 2005 57; 874-882
18. Chen, S., Fang, W., Ye, F., et al. Effect on Left Ventricular Function of Intracoronary Transplantation of Autologous Bone Marrow Mesenchymal Stem cells in Patients with Myocardial Infarction. *The American Journal of Cardiology*. 2004 94; 92-95.
19. Brown, R.P., Gerbarg, P.L., Ramazanov, Z. *Rhodiola Rosea A Phytomedicinal Overview*. HerbalGram. 2002. 56:40-52.
20. Agbarya, A., Ruimi, Nili, Epelbaum, R., et al. Natural Products as Potential Cancer Therapy Enhancers: A Preclinical Update. Sage. 2014. doi: **10.1177/2050312114546924**
21. Khazir, J., Ahmad Mir, B., Pilcher, L., et al. Role of Plants in Anticancer Drug Discovery. *Phytochemistry Letters*. 2014. 7: 173-81.

22. Mehta, R.G., Murillo, G., Naithani, R., et al. Cancer Chemoprevention by Natural Products: How Far Have we Come? *Pharm Res.* 2010. 27:950-61.
23. Gauger, K.J. *Rhodiola Rosea*: A Possible Plant Adaptogen. *Alternative Medicine Review.* 2001. 6:293-30
24. Bocharova, O. A., B. P. Matveev, et al. The effect of a *Rhodiola rosea* extract on the incidence of recurrences of a superficial bladder cancer (experimental clinical research). *Urol Nefrol (Mosk).* 1995. 2: 46-47.
25. Gauger, K.J., Rodríguez-Cortés A, Hartwich, M., et al. *Rhodiola crenulata* inhibits the tumorigenic properties of invasive mammary epithelium cells with stem cell characteristics. *Journal of Medicinal Plants Research.* 2010. 4(6): 446-454.
26. Mora, M.C., Bassa, L.M., Wong, K.E., et al. *Rhodiola Crenulata* Inhibits Wnt/ $\beta$ -catenin Signaling in Glioblastoma. *Journal of Surgical Research.* Accepted for publication February, 2015
27. Dudek, MC, Wong, KE, Bassa, LM, et al. Antineoplastic Effects of *Rhodiola Crenulata* Treatment on B16-F10 Melanoma. *Tumor Biology.* 2015. DOI 10.1007/s13277-015-3742-2
28. Pannossian, A., Wikman, G., Sarris, J. *Rosenroot (Rhodiola Rosea)*: Traditional use, chemical composition, pharmacology and clinical efficacy. *Phytomedicine.* 2010. 17:481-493
29. Tu, Y., L. Roberts, et al. *Rhodiola crenulata* induces death and inhibits growth of breast cancer cell lines. *J Med Food.* 2008. 11(3): 413-423.

## **CHAPTER 2**

### **EVALUATION OF POLYMPC PRODRUGS IN A HUMAN OVARIAN TUMOR**

#### **MODEL**

*This research was performed in close collaboration with Matthew Skinner and Dr.*

*Carmen Mora.*

#### **2.1 Introduction**

Ovarian cancer is the most lethal gynecological malignancy among women in the United States, and remains a leading cause of death with approximately 22,000 diagnoses and 14,000 deaths annually [1]. Early tumor detection is challenging, and patients often present with advanced, metastatic or disseminated disease at diagnosis. Conventional treatment involves surgical de-bulking of solid tumor accompanied by chemotherapy. Doxorubicin (Dox), an anthracycline chemotherapeutic, is a prominent treatment option for various hematologic cancers and solid tumors, including malignant ovarian neoplasms [2,3]. While Dox is a powerful anti-tumor agent, its efficacy is limited by rapid clearance kinetics and non-specific accumulation in healthy tissue. This poor specificity leads to off-target toxicity that causes myelosuppression, gastrointestinal irritation, and cardiotoxicity, thus limiting Dox dosing even when its use is effective for tumor reduction [2,4].

To improve the therapeutic efficacy of Dox, specifically its pharmacokinetics, conjugation to polymers offers a convenient and attractive strategy. Polymer-drug



conjugation produces prodrugs of larger hydrodynamic size than the drug alone. This lengthens renal clearance half-life and prolongs *in vivo* circulation [5]. Coupling this improved pharmacokinetic profile with the enhanced permeability and retention (EPR) effect, whereby polymer-drug conjugates penetrate into the leaky vasculature of tumors and become entrapped due to poor tumoral lymphatic drainage, drug uptake in solid tumors is enhanced and off-target organ accumulation is reduced [6-8]. For ease of delivery, hydrophilic polymers solvate otherwise water insoluble drugs at high loadings [9-11], and are potential replacements for other excipients, such as ethanol, which are problematic in some patient populations as they can cause severe or even fatal anaphylactic reactions [12-13].

Poly(2-methacryloyloxyethyl phosphorylcholine) (polyMPC) [14-15], is a hydrophilic polymer noted for its exceptional water solubility and biocompatibility [16-18]. Dox conjugation to polyMPC was achieved by formation of hydrazone bonds, which are acid-sensitive and thus cleavable *in vivo*. Previous evaluation of polyMPC-Dox prodrugs exhibited an *in vivo* circulation half-life of greater than two hours. Upon evaluation of polyMPC-Dox treatment on an aggressive mouse breast tumor model (4T1 cell line), its administration reduced the mean tumor size and resulted in a two-fold increase in survival time over free Dox treated mice. Dox in the prodrug animal group accumulated in tumors at twice the level of that observed in mice treated with free Dox. A corresponding reduction in off-target organ uptake was also observed.

To gauge the therapeutic breadth and clinical relevance of polyMPC-Dox, its efficacy was evaluated in human cancer through utilization of the SKOV-3 ovarian tumor

model *in vivo*. Experiments were performed with polyMPC and polyMPC-Dox to evaluate its *in vivo* biocompatibility and establish a maximum tolerated dose (MTD) of the prodrug. Mice with subcutaneously established SKOV-3 xenografts were treated with Dox, polyMPC-Dox or Doxil, an alternate liposomal Dox formulation [2], using a recurring dosing schedule resembling that employed for human patients [19]. Animals were monitored for symptoms of treatment associated toxicity, change in tumor size, and survival. The overall accumulation of Dox and polyMPC-Dox in solid ovarian tumors was compared, as was the specificity for uptake in tumor tissue versus off-target organs.

## **2.2 Materials and Methods**

### **2.2.1 Cell Culture.**

Human ovarian adenocarcinoma SKOV-3 cells were maintained in Roswell Park Memorial Institute (RPMI)-1640 medium supplemented with 10% fetal bovine serum, 100U/mL penicillin, and 100µg/mL streptomycin at 37°C under 5% CO<sub>2</sub> (Thermo fisher, Grand Island, NY).

### **2.2.2 Maximum Tolerated Dose of polyMPC and polyMPC-Dox.**

The MTD of the polyMPC scaffold carrier and polyMPC-Dox prodrug were evaluated in seven week old non-obese diabetic severe combined immunodeficient (NOD SCID) mice, as they are commonly utilized for human tumor xenograft models [20, 21]. In order to evaluate the MTD of polyMPC, three mice per treatment group were administered two doses of polyMPC dissolved in Hank's balanced salt solution (HBSS,

Thermo fisher, Grand Island, NY) at doses of 50, 100, 200, 400 or 800 mg/kg via lateral tail vein injections administered on day 0 and day 17. The MTD of polyMPC-Dox was evaluated both via intraperitoneal and intravenous administration. Three mice per treatment group were administered a single dose of polyMPC-Dox in solutions of Dox equivalent doses of 10, 20, 30, 40 or 50 mg/kg administered via a single lateral tail vein injection or intraperitoneal injection.

Weight, appearance and behavior of the mice were monitored daily for a total of 35 days. Symptoms of toxicity were defined as weight loss greater than 15% or evidence of distress in appearance or behavior. Animals exhibiting these criteria were euthanized prior to the end of the study. At the completion of the study, all remaining mice were euthanized and necropsy was performed to collect tissues for histologic evaluation

### 2.2.3 Biodistribution.

The uptake and accumulation of Dox within tumor tissue and off-target organs was evaluated in four week old NOD SCID mice following treatment with either free Dox or polyMPC-Dox. SKOV-3 ovarian human adenocarcinoma subcutaneous xenografts were established following injection of  $1 \times 10^7$  cells in the right flanks of nine mice. Following tumor establishment and growth to a volume of 100-500mm<sup>3</sup> (calculated by length X width<sup>2</sup>/2), three mice per treatment group were administered HBSS, polyMPC-Dox (6 mg/kg Dox equivalent) or free Dox (6 mg/kg) via lateral tail vein injection. Three days following the injections, mice were euthanized and organs (liver, kidneys, spleen, heart, lungs) and tumor were resected, weighed, and then flash frozen in

liquid nitrogen. All tissues were stored at  $-80^{\circ}\text{C}$  prior to analysis. Dox accumulation in the resected tissues was assessed by HPLC and normalized to HBSS values in order to determine Dox concentration.

#### 2.2.4 Tumor Efficacy.

The therapeutic efficacy of polyMPC-Dox was evaluated using a human ovarian tumor model in NOD SCID mice. Human ovarian tumors were established by injecting  $1 \times 10^7$  SKOV-3 cells subcutaneously in the right flanks of 24 four week old NOD SCID mice. Mice identified to have intramuscular tumors were excluded from analysis. Once tumors reached a volume of 250-500  $\text{mm}^3$ , mice were randomly divided into four treatment groups of 7-8 mice. Treatment groups included: HBSS (control), 2mg/kg free Dox (half of the reported Dox MTD in NOD SCID mice) [23], polyMPC-Dox at 5mg/kg Dox equivalent dosing (half of the polyMPC-Dox MTD dose), and 5mg/kg Doxil (Dox dose equivalent to polyMPC-Dox). Mice were administered treatment via lateral tail vein injections every 7-8 days. Treatment was withheld if the animals exhibited significant weight loss approaching 20% or excessive injection site wounds or scarring prohibiting further injections. Animals were evaluated every 24-48 hours for overall health, tumor volume and weight. Mice were removed from the study and euthanized if they experienced weight loss greater than 20%, exhibited signs of distress or if tumor volume exceeded  $1500\text{mm}^3$ . At time of euthanasia, necropsy was performed and tumors and organs (liver, kidneys, spleen, heart and lungs) were collected for histologic evaluation.

### 2.2.5 Statistical analysis

All graphs were created and statistical analysis was performed using GraphPad Prism Software (Prism, GraphPad Software, Inc., San Diego, CA).

## 2.3 Results

### 2.3.1 Maximum tolerated dose (MTD) of polyMPC.

For the entirety of the study, the polymer was well tolerated at all doses with no physical or behavioral concerns for toxicity. All mice treated with polymer exhibited weight gain similar to those of control mice (Fig 2.1A). Histological evaluation of the heart, kidney, spleen and lungs resected from mice treated with polyMPC exhibited no differences from the organs of the control animals. Livers of mice administered polyMPC did exhibit an increase in lymphocyte concentration at higher polymer doses, however, these changes were minor and were observed with no corresponding effect on the health of the hepatocytes (Fig 2.1D).

### 2.3.2 MTD of polyMPC-Dox Establishment.

Mice were unable to tolerate polyMPC-Dox at all doses following intraperitoneal administration secondary to weight loss and ill health necessitating euthanasia (Fig 2.1B). Mice administered PolyMPC-Dox intravenously at doses of 20-50 mg/kg experienced weight loss and required removal from the study by euthanasia. However, mice treated with 10mg/kg polyMPC-Dox survived throughout the course of the study period with no overt signs of systemic toxicity observed (Fig 2.1C). Histologic analysis of liver sections

of mice administered intravenous polyMPC-Dox demonstrated evidence of lymphocytic infiltration and hepatocyte enlargement otherwise no significant histologic changes were observed upon polyMPC-Dox treatment (Fig 2.1D).

### 2.3.3 Biodistribution of PolyMPC-Dox in a human ovarian tumor model.

Three days after intravenous treatment of either polyMPC-Dox (Dox equivalent dose of 6mg/kg) or free Dox (6mg/kg), the mean tumor uptake of polyMPC-Dox and free Dox was 1120 ng/g and 567 ng/g of tissue, respectively. The accumulation of polyMPC-Dox in solid tumors was nearly two-fold that of free Dox after a single injection, resulting in a significant difference of  $\alpha=0.10$  ( $p=0.064$ ). However, no significant differences were observed for polyMPC-Dox and free Dox accumulation in off-target organs.

### 2.3.4 Tumor efficacy.

The efficacy of polyMPC-Dox was evaluated using NOD SCID mice with subcutaneously established SKOV-3 tumors. Following tumor establishment, one mouse from the polyMPC-Dox group was excluded due to formation of an intramuscular tumor which precluded accurate measurement of tumor volume. Mice administered HBSS alone and polyMPC-Dox received a total of eight doses. Mice treated with free Dox received 6-7 doses of drug secondary to the development of ulcers in the tail at sites of drug infusion which prevented administration of drug. Mice treated with doxil were only able to tolerate 5-6 doses of drug given significant weight loss necessitating withholding drug administration or euthanasia (Fig2.3B). The mean weight of mice treated with polyMPC-

Dox and free Dox increased similarly to the control group. In contrast, mice treated with doxil exhibited significant weight loss following drug administration (Fig 2.3C). By Day 50, seven of eight control animals were euthanized due to excessive tumor growth and as a result, final treatments for all groups were administered at Day 53.

Mice treated with polyMPC-Dox exhibited mean survival time of 79 days, almost twice that of the control mice of 47 days, 15 days longer than the mean survival of mice treated with free Dox (~64 days) and 40 days longer than mean survival of mice treated with doxil (~38.5 days) (Fig 2.3A). Moreover, by Day 60, all control mice had been euthanized, 86% of the animals treated with polyMPC-Dox were still alive, 50% of the mice from the free Dox group had survived and only 38% of doxil treated mice remained alive. Overall survival of mice treated with polyMPC-Dox was 121 days, 35 days longer than the free Dox group and 56 days longer than doxil treated mice. Treatment with polyMPC-Dox reduced tumor growth compared to the free Dox and control groups. By day 49 the increase in mean tumor volume for HBSS and free Dox groups was 1991% and 1113% of the original tumor volume, respectively (Fig 2.3D) while the mean tumor growth in the polyMPC-Dox group was 440% at Day 49. In contrast, the tumor volumes of mice treated with doxil exhibited minimal growth by day 49 (~84% of initial tumor volume).

Upon necropsy, the organs and tumors were weighed and evaluated for any gross changes and H+E's of the organs were further evaluated to assess for off target toxicities. Upon evaluation of the heart, mice treated with doxil were observed to have a significantly larger heart size in proportion to overall weight. Histologic evaluation of

heart sections for mice treated with free Dox, polyMPC-Dox as well as doxil showed evidence of minor myocyte eosinophilic bands. The lungs of mice treated with doxil were also noted to be significantly larger in proportion to the total animal weight. Upon evaluation of the lung tissue in mice treated with doxil, foamy cells present within the lungs were observed which were not identified in other treatment groups. Differences were also noted between the proportional weights of the liver and kidneys of control mice in mice treated with polyMPC-Dox. Histological review of liver sections from mice treated with free Dox and polyMPC-Dox revealed evidence of enlarged hepatocytes, increased mitotic activity and lymphocytic infiltration.

## **2.4 Discussion**

This work is the first reported evaluation of a polyMPC cancer prodrug in a human tumor model. We have shown that the polyMPC construct is a safe scaffold for administration *in vivo* and therefore can be utilized for the creation of prodrugs, such as polyMPC-Dox. The performance of polyMPC-Dox was then compared to that of free Dox and doxil in a human ovarian tumor model to assess its toxicity, tumor accumulation properties, and therapeutic efficacy. PolyMPC-Dox treatment resulted in increased tumor uptake and improved survival compared to free Dox. Additionally, polyMPC-Dox was observed to be better tolerated than doxil, resulting in less systemic toxicity.

The maximum tolerated dose is the greatest amount of drug that can be tolerated without evidence of toxicity. All mice tolerated administration of polyMPC throughout



the course of the study without any outward signs of weight loss or distress. Even mice treated with a cumulative 1600mg/kg (800mg/kg per dose) of polyMPC exhibited weight gain similar to that of HBSS control. Treatment utilizing higher doses of polymer were unable to be performed given the high viscosity of the solution at polymer doses required above 800mg/kg dosing. Upon gross inspection of internal organs following euthanasia, there were no obvious abnormalities observed. Only the spleen and lung of mice treated with 800mg/kg polyMPC exhibited a significant increase of the total percent body weight of these organs. The livers of mice administered polyMPC exhibited an increase in lymphocyte concentration at higher polymer doses, however, these changes were minor and were observed with no corresponding effect on the health of the hepatocytes. This study revealed that polyMPC is non-toxic even at very high doses. Further, this work established the suitability of polyMPC as an injectable carrier for delivery of many types of drugs.

Previously it was observed that polyMPC-Dox was well tolerated in athymic nude mice at Dox equivalent doses greater than three-fold the reported MTD of 8 mg/kg for free Dox [14,22]. NOD SCID mice, however, are known to be uniquely sensitive to Dox [23], with systemic toxicity to Dox observed at doses as low as 4 mg/kg. Given this, an MTD analysis of polyMPC-Dox was necessary to re-establish the prodrug MTD specifically in NOD SCID mice. At a dose of 10mg/kg DOX equivalent polyMPC-DOX, mice were able to tolerate intravenous administration of the prodrug, although higher doses of polyMPC-Dox were not tolerated. PolyMPC-DOX was not tolerated upon intraperitoneal administration, potentially secondary to a more acidic environment found

within the peritoneal fluid. This would result in disruption of the hydrazine linkage binding Dox to polyMPC, resulting in a bolused release of free drug greater than its MTD. Histologic analysis of liver sections of mice administered polyMPC-Dox intravenously did demonstrate evidence of lymphocytic infiltration and hepatocyte enlargement. However, as Dox treatment is commonly accompanied by hepatotoxicity, these changes are most likely attributed to Dox itself [24,25]. Therefore the estimated MTD of polyMPC Dox was an intravenous dose of 10mg/kg or lower in NOD SCID mice.

The *in vivo* biodistribution of both polyMPC-Dox and free Dox was assessed in mice bearing human ovarian tumors, comparing drug accumulation in tumor tissue and off-target organs. Subcutaneous SKOV-3 tumors were established in the right flanks of NOD SCID mice, and single doses of free Dox, at 6 mg/kg, or polyMPC-Dox at a Dox equivalent dose of 6 mg/kg, were administered by tail vein injection. These selected doses were consistent with previous biodistribution analysis of polyMPC-Dox in a breast tumor model [15]. Three days after drug administration, mean tumor uptake of Dox was observed to be increased in mice treated with polyMPC-Dox compared to that of free Dox treated mice. No significant differences were observed for prodrug and Dox accumulation in off-target organs. Improved drug uptake by mice treated with polyMPC-Dox can likely be attributed to the EPR effect or increased half life associated with polyMPC conjugation to Dox.

The efficacy of polyMPC-Dox for treating a human cancer was evaluated using a SKOV-3 ovarian tumor model. SKOV-3 tumors are Dox-resistant at dosing levels

tolerated by animals [3], and thus this model allows for evaluation of polyMPC-Dox in a challenging human tumor model. Approximately half the MTD was utilized for dosing of free Dox (2mg/kg) and polyMPC-Dox (5mg/kg Dox equivalent). This was performed in an attempt to minimize dose-limiting toxicity during the weekly dosing schedule designed to mimic current clinical dosing practice [19]. Doxil, an alternative formulation of Dox utilized clinically to treat a variety of cancers including ovarian cancer, is a liposomal formulation of Dox. In order to compare the efficacy of polyMPC-Dox to an alternate Dox formulation (Doxil), both drugs were administered at a Dox equivalent doses (5mg/kg).

We observed that mice treated with polyMPC-Dox were able to tolerate more frequent administration of drug compared to free Dox or doxil treated mice. Mice treated with free Dox received between 12-14 mg/kg, mice treated with doxil received between 25-30mg/kg and mice treated with polyMPC-Dox received a total of 40 mg/kg cumulative Dox over the course of this study. Further, multiple free Dox treated mice developed local wounds overlying the site of tail vein administration which prevented repeated drug administration. Only one mouse treated with polyMPC-Dox developed a ulcer at the site of tail vein injection. In contrast, mice treated with doxil displayed significant weight loss following drug administration approaching the 20% weight loss cutoff necessitating euthanasia. Given the significant weight loss, additional drug administration were withheld in these mice. In comparison, no significant weight loss was observed in mice treated with HBSS, free Dox or polyMPC-Dox.

Mice treated with polyMPC-Dox displayed improved survival compared to other treatment groups. PolyMPC-Dox treated mice survived almost twice that of control and doxil treated mice and approximately two weeks longer than that of free Dox treated mice. In addition to improved survival, treatment with polyMPC-Dox displayed a reduced rate of tumor growth compared to free Dox and control groups. Tumors in mice administered HBSS or free Dox grew slowly for 40 days, after which the tumor growth rate in both groups rapidly increased most likely secondary to cessation of drug administration. The rate of tumor growth in mice treated with polyMPC-Dox remained nearly stagnant for approximately 80 days well beyond the final drug administration. In contrast, mice treated with doxil did not exhibit any enlargement of tumor growth. Despite minimal tumor growth, mice displayed significant weight loss and health issues, including hair loss and abnormal gait, necessitating euthanasia much earlier than other treatment groups.

To assess systemic toxicity, the organs of animals were evaluated histologically to assess for tissue damage. Upon evaluation of cardiac and lung tissues, we observed that doxil treated mice had a significantly larger proportional weight of these organs. Histologic evaluation of heart sections for mice treated with free Dox, doxil and polyMPC-Dox only showed evidence of myocyte eosinophilic bands indicative of ischemic changes in the cardiac tissue. Upon evaluation of the lung tissue, doxil treated mice were observed to have foamy cells present within the lungs, secondary to the presence of macrophages. These changes most likely are attributable to the development of cardiac injury resulting in pulmonary edema and inflammation.

Differences were noted between the proportional weights of the livers upon treatment with free Dox and polyMPC-Dox were observed in which there was evidence of enlarged hepatocytes, increased mitotic activity and lymphocytic infiltration indicative of hepatotoxic injury. These findings were even more striking within the liver sections of mice administered free Dox, which is consistent with the known hepatotoxic nature of Dox [24, 25]. The changes observed in liver tissue, therefore, are likely attributable to Dox itself, and not the prodrug or polymer carrier. Moreover, given the serial administration of drug used in the efficacy study, accumulation of Dox in organs involved in drug clearance would be expected resulting in observed histologic changes. Further research is warranted to examine polyMPC-Dox clearance, especially under such treatment conditions that resemble current clinical regimens.

Upon comparison of outcomes of the different treatment groups evaluated in the efficacy study, polyMPC-Dox was the best tolerated Dox formulation allowing for the most consistent administration of drug with minimal side effects. While comparable Dox doses were provided upon each dose of polyMPC-Dox or doxil provided, significant toxicities were observed both grossly and histologically in mice treated with doxil that far outweigh the benefits of the the minimal tumor growth that it afforded. As NOD SCID mice are exquisitely sensitive to Dox administration, it is possible that the liposomal based Dox resulted in a bolused release of Dox systemically that exceeded the maximally tolerated dose of Dox in animals. In contrast, polyMPC conjugation may have allowed for a more gradual release and uptake within not just the tumor but off target organs, thus resulting in improved drug tolerance and less side effects.

## 2.5 Conclusion

Through this work, we not only established the safety of the polyMPC scaffold for use in prodrug development but determined the efficacy of polyMPC-Dox prodrugs through evaluation of its effect upon treatment in a human tumor xenograft *in vivo*. PolyMPC itself was well-tolerated in NOD SCID mice, even at very high doses, demonstrating its utility as an injectable polymer. Upon biodistribution analysis, Dox accumulation from polyMPC-Dox treatment in the tumor tissue was nearly two-fold higher than that of free Dox, without observation of enhanced uptake in off-target organs. Toxicity and efficacy studies demonstrated that polyMPC-Dox could be administered to mice at greater than twice the dose of free Dox without causing systemic toxicity. Ovarian tumor-bearing mice receiving weekly prodrug dosing exhibited improved survival time and reduced tumor growth relative to free Dox treatment. Additionally, polyMPC-Dox treatments provided at the same Dox dose as doxil, was much better tolerated and resulted in less systemic toxicity despite reduced tumor growth observed in doxil treated mice. These results demonstrate the advantages of treating human ovarian tumors using the polyMPC-Dox prodrug, including enhanced tumor uptake with reduced off-target toxicity, higher dosing capabilities, and improved therapeutic efficacy. *In vivo* evaluation in human ovarian tumors suggests that the polyMPC-Dox prodrug is safer and more effective in the treatment of solid tumors compared to Dox or alternative Dox formulations such as doxil. Thus, this study demonstrates the viability of polyMPC-Dox

cancer therapy, and that a simple water-soluble polymer-drug conjugate is useful for improving drug delivery to tumors.

## 2.6 Figures

Figure 2.1: Maximal Tolerated Dose Analysis

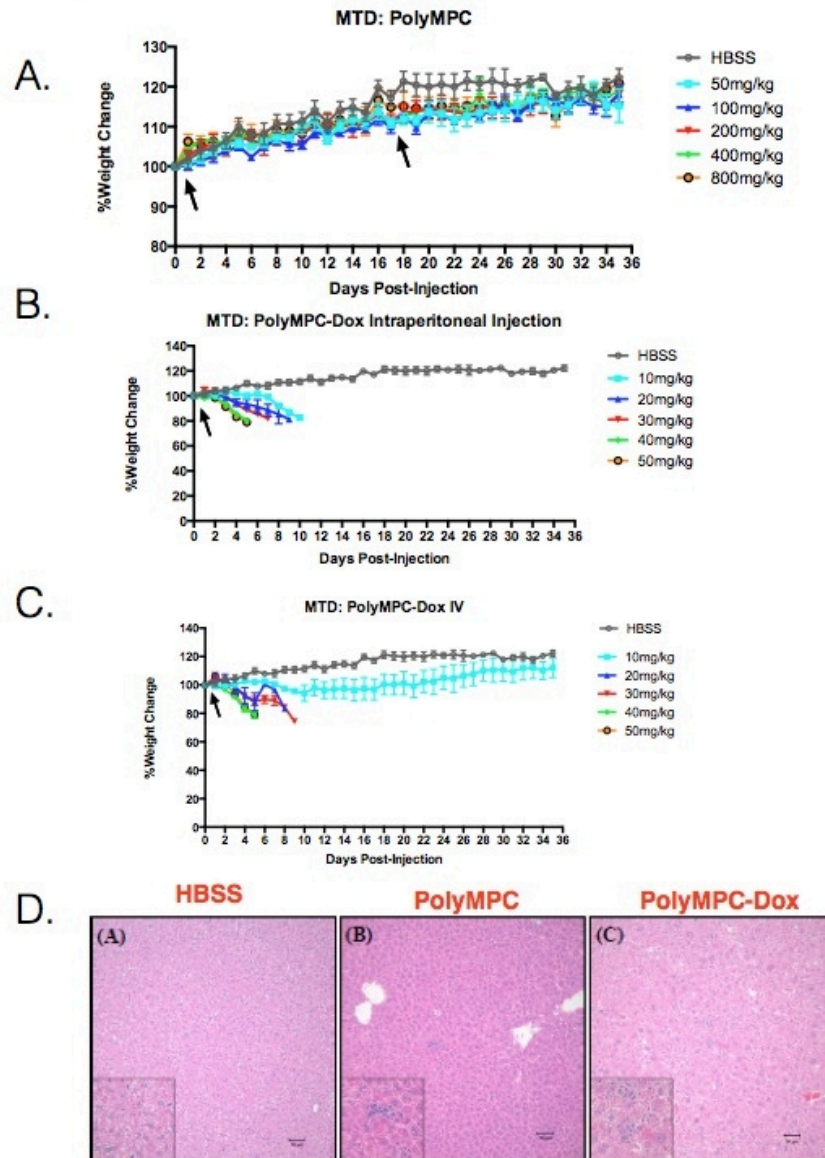
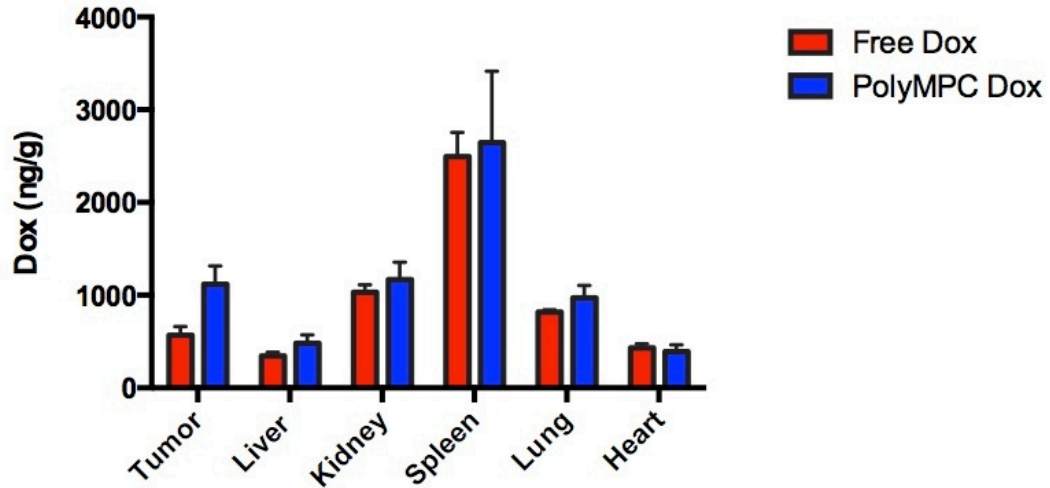


**Figure 2.1. Maximal Tolerated Dose Evaluation of PolyMPC and PolyMPC-Dox** A) PolyMPC MTD-Weight change over time of NOD-SCID mice treated with intravenous administration of polyMPC scaffold, doses ranging from 50-800mg/kg polyMPC. B) Intraperitoneal PolyMPC-Dox MTD-Weight change of NOD-SCID mice treated with intraperitoneal administration of polyMPC-Dox, ranging from 10-50mg/kg polyMPC-Dox, over time. C) Intravenous PolyMPC-Dox MTD-Weight change of NOD-SCID mice treated with intravenous administration of polyMPC-Dox, ranging from 10-50mg/kg polyMPC-Dox, over time. D) Representative H&E staining of liver sections of mice administered (A) HBSS, (B) 800 mg/kg polyMPC, and (C) polyMPC-Dox at a 10 mg/kg Dox equivalent dose. All error Bars indicate  $\pm$  SEM, arrows represent days of polymer or polyMPC-Dox administration. Images were taken at 20X magnification with 40X magnification inlay images. All scale bars represent 50  $\mu$ m.



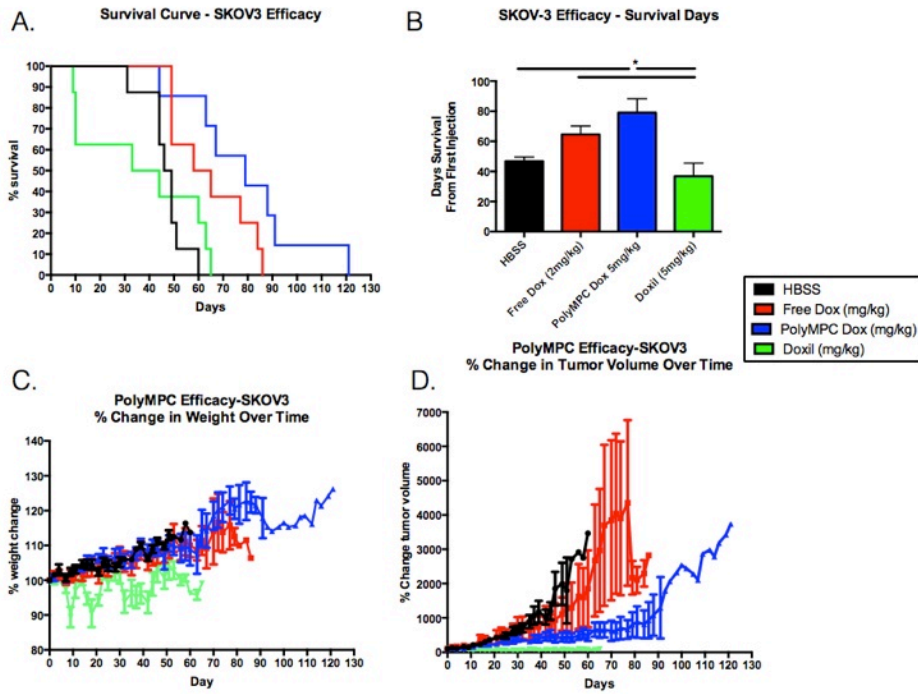
Figure 2.2: Biodistribution Evaluation

**Biodistribution HPLC:  
Free Dox vs PolyMPC Dox**



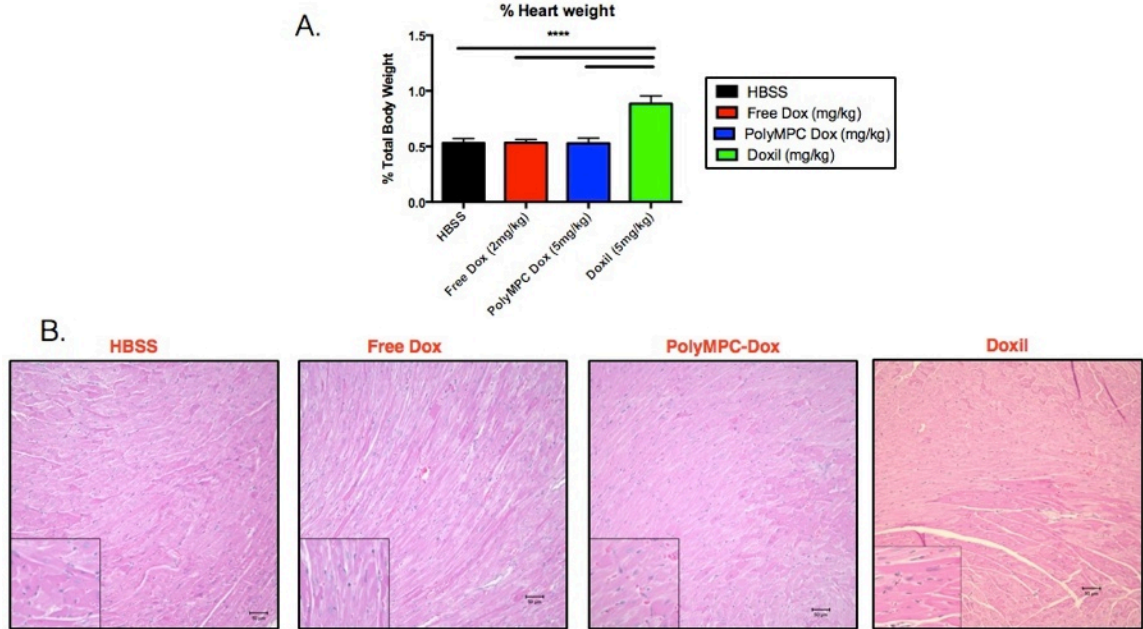
**Figure 2.2 Biodistribution Analysis of PolyMPC-Dox.** Biodistribution results following a single injection of free Dox (6 mg/kg) or polyMPC-DOX (6 mg/kg Dox equivalent) in SKOV-3 tumor-bearing mice. Accumulation, expressed as ng Dox/g of tissue, was measured in tumors and major organs using HPLC. Error bars represent  $\pm$  the SEM.

Figure 2.3: PolyMPC-Dox Efficacy Results



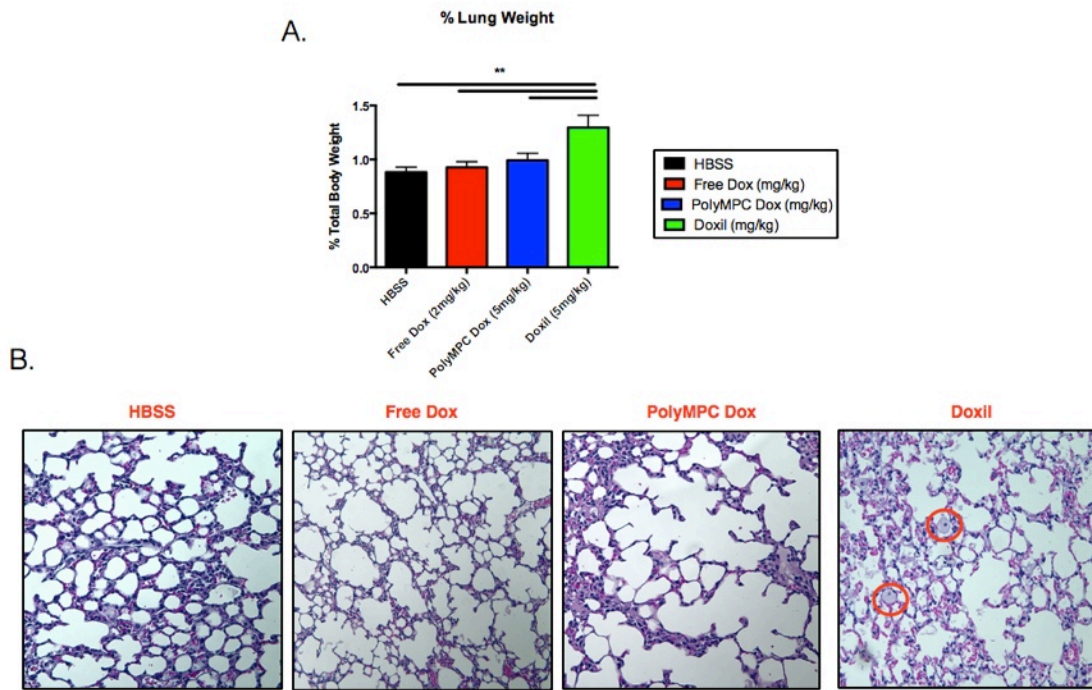
**Figure 2.3 Evaluation of Efficacy of PolyMPC-Dox in Human Ovarian Tumor Model *In Vivo*.** Efficacy results for SKOV-3 tumor-bearing mice treated with HBSS (control), free Dox (2 mg/kg), polyMPC-Dox (5 mg/kg Dox equivalent dose) or doxil (5mg/kg) A) Survival curve B) Average survival days C) Percent change in mean mouse weights D) percent change in mean tumor volumes. Black=HBSS, Red=Free Dox, Blue=PolyMPC-Dox, Green=Doxil. Error bars represent  $\pm$  SEM,  $*=p<0.05$ .

Figure 2.4: PolyMPC-Dox Efficacy Heart Outcomes



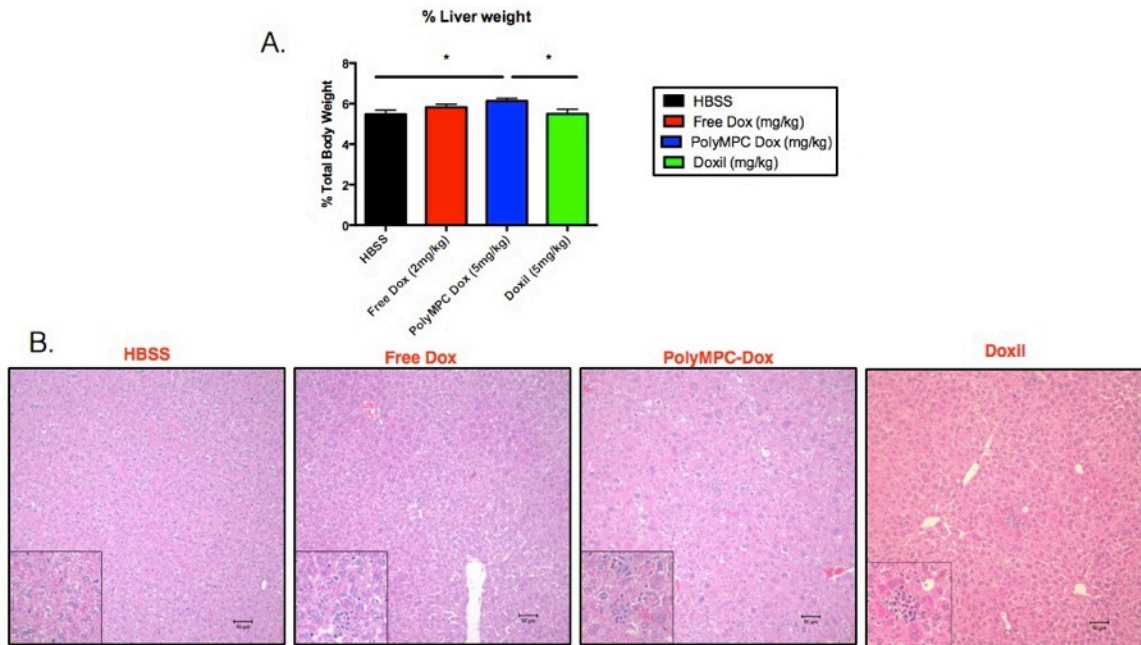
**Figure 2.4** Evaluation of the *In Vivo* Cardiac Effects of PolyMPC-Dox Treatment A) Proportional heart weights at time of euthenasia for NOD SCID mice, bearing subcutaneous SKOV-3 human ovarian tumors, treated with multiple administrations of HBSS, Dox (2 mg/kg), or polyMPC-Dox (5 mg/kg Dox equivalent dose) and doxil (5mg/kg). B) Representative H&E staining of cardiac sections of mice administered HBSS, Dox (2 mg/kg), polyMPC-Dox (5 mg/kg Dox equivalent dose) or doxil (5mg/kg) in a SKOV-3 human ovarian tumor efficacy study. Error bars represent  $\pm$  SEM. \*\*\*\*= $p < 0.0001$ . Images were taken at 20X magnification with 40X magnification inlay images. Scale bars represent 50  $\mu$ m.

Figure 2.5: PolyMPC-Dox Efficacy Lung Outcomes



**Figure 2.5 Evaluation of the *In Vivo* Pulmonary Effects of PolyMPC-Dox Treatment A)** Proportional lung weights at time of euthanasia for NOD SCID mice, bearing subcutaneous SKOV-3 human ovarian tumors, treated with multiple administrations of HBSS, Dox (2 mg/kg), or polyMPC-Dox (5 mg/kg Dox equivalent dose) and doxil (5mg/kg). B) Representative H&E staining of lung sections of mice administered HBSS, Dox (2 mg/kg), polyMPC-Dox (5 mg/kg Dox equivalent dose) or doxil (5mg/kg) in a SKOV-3 human ovarian tumor efficacy study. Red circles represent foamy cells likely indicative of lymphocytes within the lung. Error bars represent  $\pm$  SEM. \*\*\*\*= $p < 0.0001$ . Images were taken at 20X magnification with 40X magnification inlay images. Scale bars represent 50  $\mu$ m.

Figure 2.6: PolyMPC-Dox Efficacy Liver Outcomes



**Figure 2.6 Evaluation of the *In Vivo* Liver Effects of PolyMPC-Dox Treatment** A) Proportional liver weights at time of euthanasia for NOD SCID mice, bearing subcutaneous SKOV-3 human ovarian tumors, treated with multiple administrations of HBSS, Dox (2 mg/kg), or polyMPC-Dox (5 mg/kg Dox equivalent dose) and doxil (5mg/kg). B) Representative H&E staining of liver sections of mice administered HBSS, Dox (2 mg/kg), polyMPC-Dox (5 mg/kg Dox equivalent dose) or doxil (5mg/kg) in a SKOV-3 human ovarian tumor efficacy study. Error bars represent  $\pm$  SEM.  $*=p<0.05$ . Images were taken at 20X magnification with 40X magnification inlay images. Scale bars represent 50  $\mu$ m.

## 2.7 References

1. National Cancer Institute. A Snapshot of Ovarian Cancer. <http://www.cancer.gov/research/progress/snapshots/ovarian> (accessed Sep 28, 2015).
2. Rahman, A. M.; Yusuf, S. W.; Ewer, M. S. Anthracycline-induced Cardiotoxicity and the Cardiac Sparing Effect of Liposomal Formulation. *Int. J. Nanomedicine*. 2007, 2, 567-583.
3. Shim, G-s.; Manandhar, S.; Shin, D.; Kim, T-H.; Kwak, M-K. Acquisition of Doxorubicin Resistance in Ovarian Carcinoma Cells Accompanies Activation of the NRF2 Pathway. *Free Radic. Biol. Med.* 2009, 47, 1619-1631.
4. Singal, P.K.; Iliskovic, N. Doxorubicin-Induced Cardiomyopathy. *N. Engl. J. Med.* 1998, 339, 900-905.
5. Fox, M. E.; Szoka, F. C.; Fréchet, J. M. J. Soluble Polymer Carriers for the Treatment of Cancer: The Importance of Molecular Architecture. *Acc. Chem. Res.* 2009, 42, 1141- 1151
6. Matsumura, Y.; Maeda, H. A New Concept for Macromolecular Therapeutics in Cancer Chemotherapy: Mechanism of Tumor Tropic Accumulation of Proteins and Antitumor Agents SMANCS. *Cancer Res.* 1986, 46, 6387-6392.
7. Maeda, H.; Wu, J.; Sawa, T.; Matsumura, Y.; Hori, K. Tumor Vascular Permeability and the EPR Effect in Macromolecular Therapeutics: a Review. *J. Control. Release.* 2000, 65, 271-284.
8. Maeda, H.; Nakamura, H.; Fang, J. The EPR Effect for Macromolecular Drug Delivery to Solid Tumors: Improvement of Tumor Uptake, Lowering of Systemic Toxicity, and Distinct Tumor Imaging In Vivo. *Adv. Drug Deliv. Rev.* 2013, 65, 71-79.
9. Khandare, J.; Minko, T. Polymer-Drug Conjugates: Progress in Polymeric Prodrugs. *Prog. Polym. Sci.* 2006, 31, 359-397.
10. Larson, N.; Ghandehari, H. Polymeric Conjugates for Drug Delivery. *Chem. Mater.* 2012, 24, 840-853
11. Luxenhofer, R.; Schulz, A.; Li, S.; Bronich, T. K.; Batrakova, E. V.; Jordan, R.; Kabanov A. V. Doubly Amphiphilic Polymers as High-Capacity Delivery Systems for Hydrophobic Drugs. *Biomaterials*. 2010, 31, 4972-4979.
12. Gelderblom, H.; Verweij, J.; Nooter, K.; Sparreboom, A. Cremophor EL: the Drawbacks of Vehicle Selection for Drug Formulation. *Eur. J. Cancer*. 2001, 37, 1590-1598.



13. Ten Tjie, A. J.; Verweij, J.; Loos, W. J.; Sparreboom A. Pharmacological Effects of Formulation Vehicles: Implications for Cancer Chemotherapy. *Clin. Pharmacokinet.* 2003, 42, 665-685.
14. Chen X, Parelkar S, Henchey E, Schneider S, Emrick T. PolyMPC-Doxorubicin Prodrugs. *Bioconjugate Chem.* 2012, 23, 1753-1763.
15. Page, S. M.; Henchey, E.; Chen, X.; Schneider, S.; Emrick, T. Efficacy of polyMPCDOX Prodrugs in 4T1 Tumor-Bearing Mice. *Mol. Pharmaceutics.* 2014, 11, 1715-1720
16. Ishihara, K. New Polymeric Biomaterials—Phospholipid Polymers with a Biocompatible Surface. *Front Med. Biol. Eng.* 2000, 10, 83-95.
17. Iwasaki, Y.; Ishihara, K. Phosphorylcholine-Containing Polymers for Biomedical Applications. *Anal. Bioanal. Chem.* 2005, 381, 534-546.
18. Ishihara, K. Highly Lubricated Polymer Interfaces for Advanced Artificial Hip Joints through Biomimetic Design. *Polym. J.* 2015, 47, 585-597.
19. Rose, P. G. Pegylated Liposomal Doxorubicin: Optimizing the Dosing Schedule in Ovarian Cancer. *Oncologist.* 2005, 10, 205-214.
20. Hasan, N.; Ohman, A. W.; Dinulescu, D. M. The Promise and Challenge of Ovarian Cancer Models. *Transl. Cancer. Res.* 2015, 4.
21. Richmond, A.; Su, Y. Mouse Xenograft Models vs GEM Models for Human Cancer Therapeutics. *Dis. Model Mech.* 2008, 1, 78-72.
22. Houba, P. H. J.; Boven, E.; van der Meulen-Muileman, I. H.; Leenders, R. G. G.; Scheeren, J. W.; Pinedo, H. M.; Haisma, H. J. Pronounced Antitumor Efficacy of Doxorubicin When Given as the Prodrug DOX-GA3 in Combination with a Monoclonal Antibody  $\beta$ -Glucuronidase Conjugate. *Int. J. Oncol.* 2001, 91, 550-554.
23. Kratz, F.; Mansour, A.; Soltau, J.; Warnecke, A.; Fichtner, I.; Unger, C.; Drevs, J. Development of Albumin-Binding Doxorubicin Prodrugs that are Cleaved by Prostate-Specific Antigen. *Arch. Pharm.* 2005, 338, 462-472.
24. Injac, R.; Strukelj, B. Recent Advances in Protection Against Doxorubicin-Induced Toxicity. *Technol. Cancer Res. Treat.* 2008, 6, 497-516.
25. Joshi, M.; Sodhi, K. S.; Pandey, R.; Singh, J.; Goyal, S.; Prasad, S.; Kaur, H.; Bhaskar, N.; Mahajan. Cancer Chemotherapy and Hepatotoxicity: An Update. *IAJPS.* 2014, 6, 2976-2984.

**CHAPTER 3**

**TARGETED CHEMOTHERAPY UTILIZING MESENCHYMAL STEM CELLS**

**LOADED WITH POLYMPC**

*This research was performed in close collaboration with Nicholas Panzarino.*

### **3.1 Introduction**

Limitations associated with conventional systemic administration of chemotherapeutics include off target drug effects that damage healthy tissue, thus constraining therapeutic agents to a narrow window and diminishing their efficacy. The therapeutic effect of cancer drugs is, in many cases, improved by their conversion to prodrugs [1]. In principle, prodrugs transport the therapeutic agent in a nontoxic form through the bloodstream, thereby shielding the body from off target toxic effects and improving the therapeutic profile of the drug [2,3]. In addition, polymer prodrugs also improve drug delivery by passive tumor targeting via the enhanced permeability and retention (EPR) effect, in which the fenestrated tumor vasculature preferentially traps and retains the polymer prodrugs within the tumor [4-6]. After reaching the tumor, the drug is released from the polymer by a variety of tunable mechanisms, such as hydrolysis and enzyme driven chemistry [7].

Numerous examples of polymer pro-drugs exhibit improved pharmacokinetic and biodistribution profiles [1]. Nevertheless, challenges remain for passively targeted agents to overcome the physical defenses of solid tumors, including elevated interstitial and



hydrostatic tumor pressure [8-11]. These elevated pressures arise from irregular tumor vasculature [12], a disabled tumor lymphatic system [13], and the density of tightly packed cancer cells [14], collectively impairing drug penetration. Furthermore, the elevated pressures also impair uniform drug diffusion throughout the tumor, consequently exposing tumor regions to ineffective drug concentrations and limiting their therapeutic effect [15]. This represents a principle barrier to the efficacy of passively administered agents, and may also facilitate the development of drug resistance in solid tumors [13].

MSCs are a pluripotent progenitor cell type which are most abundant in bone marrow and adipose tissue. MSCs differentiate into adipocytes, chondrocytes, and osteoblasts, and have been observed to migrate to sites of injury and to promote wound healing. MSC specific migration holds potential for the treatment of damaged tissues resulting from myocardial infarction and stroke, as well as for delivering secreted therapeutic proteins to wounds [16].

MSCs have been reported to actively migrate to solid tumors and therefore hold potential to actively transport therapeutic agents directly to tumors in order to overcome their physical tumor defenses [17]. Use of MSCs in cancer therapeutics may ultimately improve drug targeting, increase drug penetration, and reduce off target toxicities. Such an approach has been evaluated previously as MSCs transduced to produce interferon  $\beta$  reduced tumor growth in melanoma bearing mice [15]. Subsequent studies have delivered a wider range of biologics or nanoparticles as a strategy to transport chemotherapeutics agents to tumors utilizing MSCs [18-25]. For example, Zhang et al., loaded MSCs with doxorubicin (Dox) polymer conjugates which were intracranially

injected into mice with glioma xenografts. Mice treated with MSCs carrying Dox polymer conjugates experienced prolonged survival compared to control animals [25]. However, the therapeutic potential of drug loaded MSCs administered systemically has yet to be evaluated.

## **3.2 Materials and Methods**

### **3.2.1 Cell culture.**

Human bone marrow mesenchymal stem cells (Cell Engineering Technologies, (CET), Coralville, IA) were cultured in CET Mesenchymal Stem Cell Expansion Medium (CET, Coralville, IA) without phenol red. MDA MB-231 breast cancer cells and DO11.10 T-cells were grown in Dulbecco's Modified Eagle Medium (DMEM, Thermo Fisher, Grand Island, NY). All media was supplemented with 10% fetal bovine serum, 100U/mL penicillin and 100µg/mL streptomycin (Thermo Fisher, Grand Island, NY) and cells were grown at 37°C and 5% CO<sub>2</sub>.

### **3.2.2 Polymer loading into MSCs.**

Polymer loading was carried out with  $1 \times 10^6$  cells per mL in Live Cell Imaging Solution Physiological Buffered Saline (LCIS, Thermo fisher, Grand Island, NY) suspension containing 10µM polymer solution of polyMPC-Rhodamine B (RhdB), 10µM doxorubicin (Dox) equivalent polyMPC-Dox or 10µM free Dox at 37°C for 15 minutes. Cells were centrifuged at 200 x g for five minutes at 37°C and the pellet was washed with

LCIS to remove unbound polymer. Polymer uptake was confirmed with confocal microscopy.

### 3.2.3 Cell viability.

Cell viability was evaluated using trypan blue exclusion performed on a Beckman Coulter Vi-Cell Cell Viability Counter (Beckman Coulter, Brea, Ca). Viability was determined after polymer loading on MSCs with either polyMPC-RhdB or polyMPC-Dox daily for up to 72 hours following polymer loading. Qualitative cell viability was evaluated for up to 96 hours following polymer loading by transmitted light differential interference contrast images utilizing live cell confocal microscopy.

### 3.2.4 Co-culture Experiment.

Drug release from MSCs was evaluated utilizing T-cell viability as a marker for Dox release as T-cell viability is exquisitely sensitive to the presence of Dox. T-cells were cultured with MSCs loaded with Dox or polyMPC-Dox. The viability of T-cells was evaluated over 72 hours utilizing trypan blue exclusion with a Beckman Coulter Vi-cell Viability Counter.

### 3.2.5 Evaluation of PolyMPC loaded MSC *in vivo* migration.

Non-obese diabetic severe combined immunodeficient (NOD SCID) mice were implanted with  $1 \times 10^7$  MDA MB-231 breast cancer cells in the right lateral flank. When tumor volumes (calculated by tumor length X tumor width<sup>2</sup>/2) grew to a minimum of

500 mm<sup>3</sup>, mice were administered HBSS or 100,000-500,000 MSCs loaded with polyMPC-RhdB provided via lateral tail vein injection. Five days following injection, the mice were euthanized. Tumors were divided and sections were either flash frozen in liquid nitrogen or formalin fixed and subsequently paraffin embedded.

### 3.2.6 Evaluation of polymer loaded MSC migration to tumor.

Frozen tumor sections embedded in optimal cutting temperature (OTC) compound were cut at 4 µm thickness. Tumor sections were first imaged for RhdB fluorescence to detect for the presence of polyMPC-RhdB loaded MSCs. Images for polyMPC-RhdB were captured with a Nikon Eclipse Ti microscope equipped with an Xcite Mercury Arc lamp and a Texas Red HyQ filter set (Nikon).

Immunohistochemistry (IHC) was performed on a Dako Cytomation autostainer using the Envision HRP Detection system (Dako, Carpinteria, CA) following paraffin embedding of formalin fixed tumor samples to evaluate for human CD105 (Ab169545, Abcam, Cambridge, MA), specific to human bone marrow MSCs. Each mammary tissue block was sectioned at 4µm on a graded slide, deparaffinized in xylene, rehydrated in graded ethanols, and rinsed in Tris-phosphate-buffered saline (TBS). Heat induced antigen retrieval was performed in a microwave at 98°C in 0.01M citrate buffer. After cooling for 20 minutes, sections were rinsed in TBS and subjected to an antibody specific for human CD105 at 1:400 dilution for 45 minutes. Immunoreactivity was visualized by incubation with chromogen diaminobenzidine (DAB) for 5 minutes. Tissue sections were counterstained with hematoxylin, dehydrated through graded ethanols and xylene, and

cover-slipped. Images were captured with an Olympus BX41 light microscope using SPOT™ Imaging Solutions (Detroit, MI).

### 3.2.7 Statistical Analysis

All graphs were created and statistical analysis was performed utilizing GraphPad Prism Software (Prism, GraphPad Software, Inc., San Diego, CA).

## 3.3 Results

### 3.3.1 PolyMPC-RhdB and PolyMPC-Dox Polymers are Stably Loaded onto MSCs.

Following incubation of MSCs with polyMPC-RhdB, no reduction in viability was observed up to 72 hours following treatment (Fig 3.1C). Further, no reduction in viability was observed upon loading of MSCs with polyMPC-Dox as well (Fig 3.1D). Confocal microscopy revealed a distinctive filamentous pattern of cytoplasmic fluorescence with sparing in the nucleus observed in both polyMPC-RhdB and polyMPC-Dox (Fig 3.1B) loaded MSCs. This pattern of fluorescence was observed to be stable for up to 96 hours. In contrast, MSCs loaded with Dox exhibited a diffuse pattern of fluorescence (Fig. 3.1A)

### 3.3.2 MSC Co-Culture Experiment

Drug release from MSCs was evaluated utilizing T-cell viability as a marker for Dox release, given exquisite T-cell sensitivity to Dox. Co-culture of T-cells with MSCs loaded with Dox led to a reduction in T-cell viability over 72 hours (Fig 3.2A). In

contrast, MSCs loaded with polyMPC-Dox did not lead to appreciable T-cell death (Fig 3.2B).

### 3.3.3 PolyMPC-RhdB Loaded MSCs Home to Tumors *In Vivo*.

Mice with established subcutaneous human mammary tumor (MBA MB-231) xenografts were treated with polyMPC-RhdB loaded MSCs. Five days after the MSCs were administered, mice were euthanized, necropsy was performed and tumors were evaluated in order to determine if MSCs had transported their polymer cargo to the solid tumors. Frozen tumor sections imaged for RhdB fluorescence to detect for the presence of MSCs containing polyMPC-RhdB revealed distinct fluorescent foci present throughout the tumor sections. In contrast, tumors from mice treated with saline were not fluorescent (Fig 3.3). Immunohistochemistry (IHC) was performed on paraffin-embedded tumor sections using a human CD105 antibody specific for human MSCs. We observed anti-CD105 antibody to stain tumor sections from mice treated with polyMPC-RhdB loaded MSCs while negligible staining was observed in the saline control tumors (Fig. 3.3).

## 3.4 Discussion

While a wide variety of treatment options are available for the treatment of cancer, therapy is often limited by the toxicities associated with these chemotherapeutic agents. Means to improve drug targeting directly to tumors can result in increased uptake of the drugs into the tumor as well as reduced uptake in other off target organs. Conjugation of these drugs to polymers, such as polyMPC, can allow for passive

targeting of the tumor through the enhanced permeability and retention (EPR) effect [26, 27]. Delivery of these prodrugs can be further improved through utilization of a more active and targeted method. Here, we evaluated a cellular tumorotropic vehicle for polymer drug delivery through utilization of MSCs.

MSCs were able to stably uptake both polyMPC-RhdB and polyMPC-Dox. For this work, Rhodamine B (RhdB) bound to polyMPC was utilized in addition to polyMPC-Dox because RhdB's brighter fluorescence allowed for a facile analysis of cellular uptake. Following incubation of MSCs with polyMPC-RhdB, no reduction in viability was observed for up to 72 hours following treatment. Repeat analysis utilizing polyMPC-Dox also revealed stable uptake. Confocal microscopy confirmed uptake of both polymers without altering viability for upto 96 hours. Compared to free Dox, both polyMPC-RhdB and polyMPC-Dox exhibited a filamentous pattern of fluorescence throughout the cytoplasm consistent with intracellular localization within the mitochondria. In contrast, free Dox uptake within MSCs was noted to be diffuse throughout both the cytoplasm and nucleus.

Drug release from MSCs was evaluated utilizing T-cell viability as a marker for Dox release, given exquisite T-cell sensitivity to Dox. Co-culture of T-cells, a suspensatory cell line, with MSCs, an adherent cell line, which were loaded with Dox led to a reduction in T-cell viability over 72 hours. This provided evidence that MSCs can not only be loaded with Dox, but can also release the drug. In contrast, MSCs loaded with polyMPC-DOX did not lead to appreciable T-cell death. It remains unclear this difference in outcome is secondary to reduced drug uptake or reduced drug release by the MSCs.

Following the observation that MSCs can be stably loaded with polyMPC- Dox and have the potential for drug release *in vitro*, the *in vivo* migratory capabilities of polymer loaded MSCs was evaluated. We observed that MSCs containing their polymer cargo maintained their tumorigenic abilities. MSC migration was evaluated both with fluorescent microscopy to evaluate for the presence of polyMPC-RhdB as well as through IHC to assess for human cd105, which is specific for MSCs. Together, fluorescent imaging and IHC confirmed that systemically administered MSCs actively transport to a solid tumor while loaded with polymer cargo. This suggests that MSCs can serve as vehicles for actively targeted delivery of drugs, including polyMPC prodrugs.

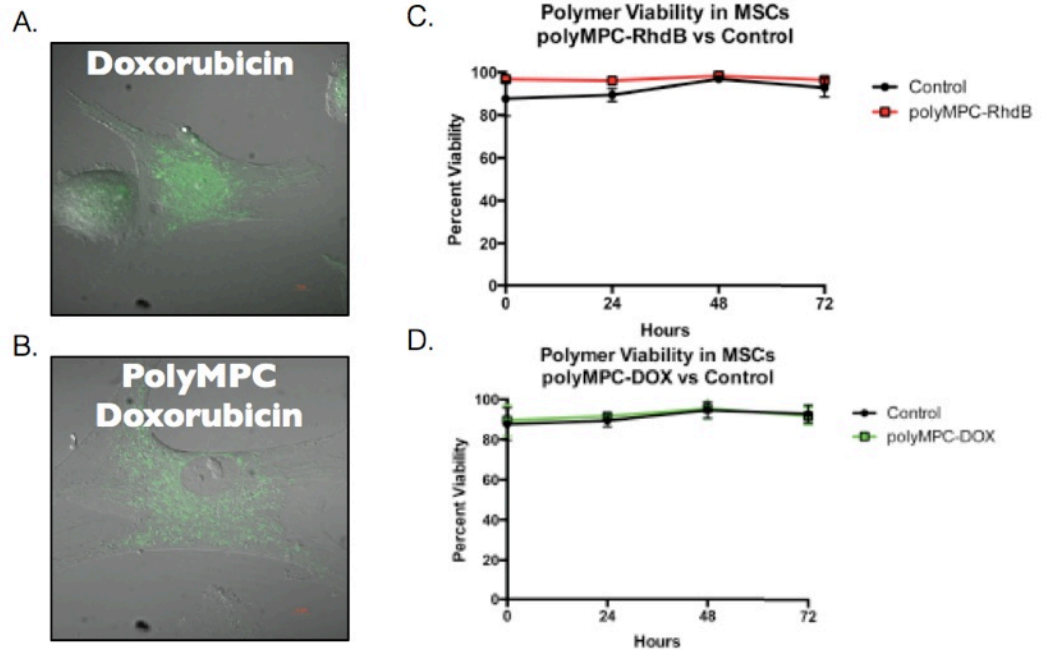
### **3.5 Conclusion**

In summary, cellular vehicles with inherent tumorigenic properties, such as MSCs, provide the unique ability to actively target and deliver chemotherapeutic drugs to tumors. This potentially allows for improved efficacy and reduced off target toxicity. We found that polyMPC can be stably loaded into MSCs and that the cells maintain their tumorigenic capabilities and can migrate to established tumor xenograft upon systemic administration *in vivo*. This work provides evidence that MSCs hold potential to improve active tumoral drug delivery of polymer prodrugs and future work will focus on drug release and therapeutic efficacy of drug loaded MSCs.



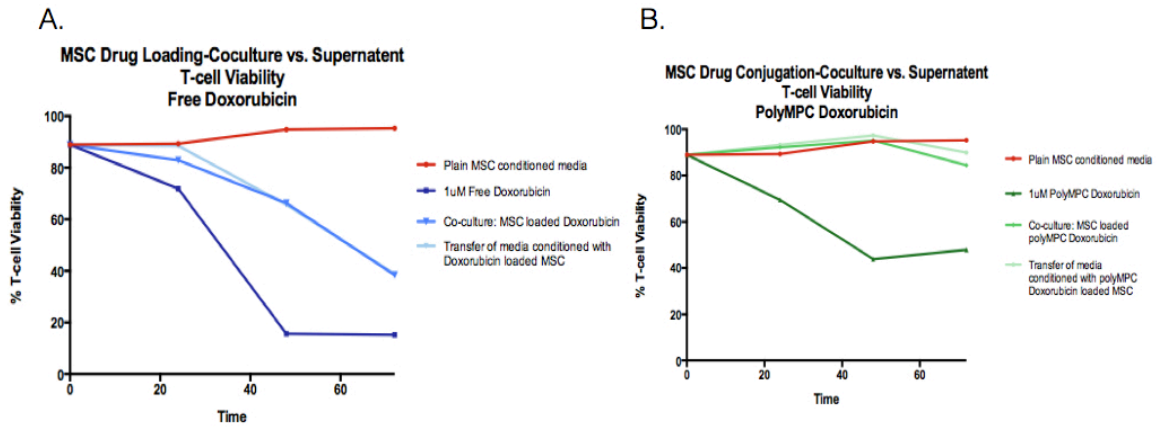
### 3.6 Figures

Figure 3.1: MSC Drug Uptake and Viability



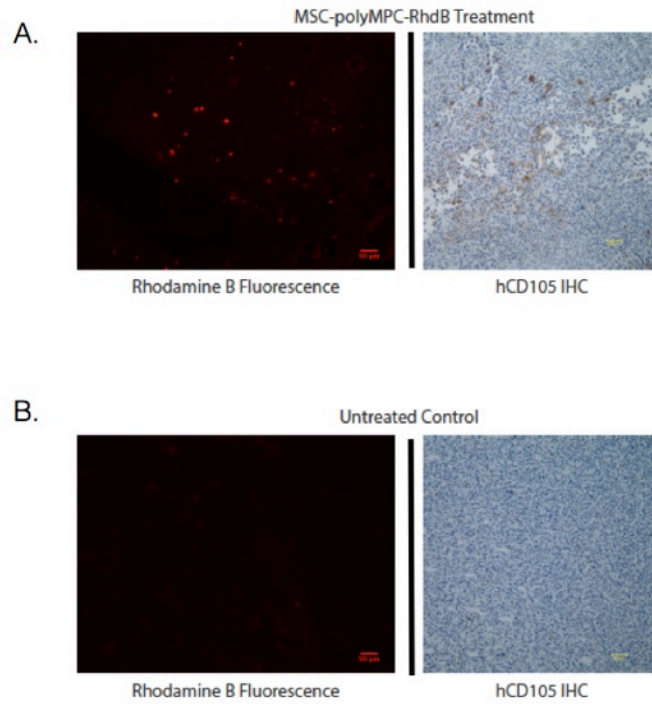
**Figure 3.1 MSC Drug Uptake and Viability.** A) Live cell confocal microscopic image (63X) of MSCs loaded with Dox B) Live cell confocal microscopic image (63X) of MSCs loaded with PolyMPC-Dox. C) Viability of polyMPC-RhdB loaded MSCs evaluated by trypan blue exclusion. Red=polyMPC-RhdB MSCs, Black=untreated MSCs. D) Viability of polyMPC-Dox loaded MSCs evaluated by trypan blue exclusion. Green=polyMPC-Dox MSCs, Black=untreated MSCs. Error bars represent standard deviation.

Figure 3.2: MSC Co-Culture Experiment



**Figure 3.2 MSC Co-culture Experiment.** A) 72 hour viability analysis, evaluated by trypan blue exclusion, of T-cells (DO11.10) grown in either MSC conditioned media (red), 1uM FD (dark blue), co-culture with MSC loaded DOX (blue) or with DOX loaded MSC conditioned media (light blue). B) 72 hour viability analysis, evaluated by trypan blue exclusion, of T-cells grown in either MSC conditioned media (red), 1uM DOX equivalent polyMPC DOX (dark green), co-culture with MSC loaded with polyMPC-DOX (green) or with polyMPC-loaded MSC conditioned media (light green).

Figure 3.3: MSC Tumor Homing *In Vivo*



**Figure 3.3 Polymer Loaded MSC Tumor Homing *In Vivo*** A) Left: Fluorescent microscopic images (10X) of RhdB fluorescence from a frozen tumor section from a mouse treated with polyMPC-RhdB loaded MSCs. Right: Microscopic images (20X) of a paraffin embedded tumor section from a mouse treated with polyMPC-RhdB loaded MSCs immunohistochemically stained with human CD105. B) Fluorescent microscopic images (10X) of RhdB fluorescence from a frozen tumor section from a mouse treated with saline. Right: Microscopic images (20X) of a paraffin embedded tumor section from a mouse treated with saline immunohistochemically stained for human CD105. Scale bars for all images represent 50uM

### 3.7 References

1. Duncan R. Polymer conjugates as anticancer nanomedicines. *Nat Rev Cancer*. 2006;6(9):688-701.
2. Haag R, Kratz F. Polymer therapeutics: concepts and applications. *Angew Chem Int Ed Engl*. 2006;45(8):1198-215.
3. Pasut G, Veronese FM. PEG conjugates in clinical development or use as anticancer agents: an overview. *Adv Drug Deliv Rev*. 2009;61(13):1177-88.
4. Matsumura Y, Maeda H. A new concept for macromolecular therapeutics in cancer chemotherapy: mechanism of tumorotropic accumulation of proteins and the antitumor agent smancs. *Cancer Res*. 1986;46(12 Pt 1):6387-92.
5. Maeda H, Matsumura Y. Tumorotropic and lymphotropic principles of macromolecular drugs. *Crit Rev Ther Drug Carrier Syst*. 1989;6(3):193-210.
6. Maeda H, Sawa T, Konno T. Mechanism of tumor-targeted delivery of macromolecular drugs, including the EPR effect in solid tumor and clinical overview of the prototype polymeric drug SMANCS. *J Control Release*. 2001;74(1-3):47-61.
7. Chen X, Parelkar SS, Henchey E, Schneider S, Emrick T. PolyMPC-doxorubicin prodrugs. *Bioconj Chem*. 2012;23(9):1753-63.
8. Minchinton AI, Tannock IF. Drug penetration in solid tumours. *Nat Rev Cancer*. 2006;6(8):583-92.
9. Milosevic MF, Fyles AW, Wong R, Pintilie M, Kavanagh MC, Levin W, et al. Interstitial fluid pressure in cervical carcinoma: within tumor heterogeneity, and relation to oxygen tension. *Cancer*. 1998;82(12):2418-26.
10. Heldin CH, Rubin K, Pietras K, Ostman A. High interstitial fluid pressure - an obstacle in cancer therapy. *Nat Rev Cancer*. 2004;4(10):806-13.
11. Jain RK. Delivery of molecular and cellular medicine to solid tumors. *Adv Drug Deliv Rev*. 2001;46(1-3):149-68.
12. Less JR, Skalak TC, Sevick EM, Jain RK. Microvascular architecture in a mammary carcinoma: branching patterns and vessel dimensions. *Cancer Res*. 1991;51(1):265-73.

13. Leu AJ, Berk DA, Lymboussaki A, Alitalo K, Jain RK. Absence of functional lymphatics within a murine sarcoma: a molecular and functional evaluation. *Cancer Res.* 2000;60(16):4324-7.
14. Grantab R, Sivananthan S, Tannock IF. The penetration of anticancer drugs through tumor tissue as a function of cellular adhesion and packing density of tumor cells. *Cancer Res.* 2006;66(2):1033-9.
15. Primeau AJ, Rendon A, Hedley D, Lilge L, Tannock IF. The distribution of the anticancer drug Doxorubicin in relation to blood vessels in solid tumors. *Clin Cancer Res.* 2005;11(24 Pt 1):8782-8.
16. Wei X, Yang X, Han ZP, Qu FF, Shao L, Shi YF. Mesenchymal stem cells: a new trend for cell therapy. *Acta Pharmacol Sin.* 2013;34(6):747-54.
17. Studeny M, Marini FC, Champlin RE, Zompetta C, Fidler IJ, Andreeff M. Bone marrow-derived mesenchymal stem cells as vehicles for interferon-beta delivery into tumors. *Cancer Res.* 2002;62(13):3603-8.
18. Ren C, Kumar S, Chanda D, Chen J, Mountz JD, Ponnazhagan S. Therapeutic potential of mesenchymal stem cells producing interferon-alpha in a mouse melanoma lung metastasis model. *Stem Cells.* 2008;26(9):2332-8.
19. Ren C, Kumar S, Chanda D, Kallman L, Chen J, Mountz JD, et al. Cancer gene therapy using mesenchymal stem cells expressing interferon-beta in a mouse prostate cancer lung metastasis model. *Gene Ther.* 2008;15(21):1446-53.
20. Seo SH, Kim KS, Park SH, Suh YS, Kim SJ, Jeun SS, et al. The effects of mesenchymal stem cells injected via different routes on modified IL-12-mediated antitumor activity. *Gene Ther.* 2011;18(5):488-95.
21. Loebinger MR, Eddaoudi A, Davies D, Janes SM. Mesenchymal stem cell delivery of TRAIL can eliminate metastatic cancer. *Cancer Res.* 2009;69(10):4134-42.
22. Cheng H, Kastrup CJ, Ramanathan R, Siegwart DJ, Ma M, Bogatyrev SR, et al. Nanoparticulate cellular patches for cell-mediated tumoritropic delivery. *ACS Nano.* 2010;4(2):625-31.
23. Roger M, Clavreul A, Venier-Julienne MC, Passirani C, Sindji L, Schiller P, et al. Mesenchymal stem cells as cellular vehicles for delivery of nanoparticles to brain tumors. *Biomaterials.* 2010;31(32):8393-401.

24. Li L, Guan Y, Liu H, Hao N, Liu T, Meng X, et al. Silica nanorattle-doxorubicin-anchored mesenchymal stem cells for tumor-tropic therapy. *ACS Nano*. 2011;5(9):7462-70.
25. Zhang X, Yao S, Liu C, Jiang Y. Tumor tropic delivery of doxorubicin-polymer conjugates using mesenchymal stem cells for glioma therapy. *Biomaterials*. 2015;39:269-81.
26. McRae Page S, Martorella M, Parelkar S, Kosif I, Emrick T. Disulfide cross-linked phosphorylcholine micelles for triggered release of camptothecin. *Mol Pharm*. 2013;10(7):2684-92.
27. McRae Page S, Henchey E, Chen X, Schneider S, Emrick T. Efficacy of polyMPC-DOX prodrugs in 4T1 tumor-bearing mice. *Mol Pharm*. 2014;11(5):1715-20.

## **CHAPTER 4**

# **EVALUATION OF *RHODIOLA CRENULATA* ON THE TREATMENT OF MELANOMA**

*This research was performed in close collaboration with Maxine Dudek and Dr. Carmen Mora.*

### **4.1 Introduction**

Each year, more than 76,000 people in the United States are diagnosed with melanoma, the most aggressive form of skin cancer [1]. Melanoma arises from the malignant transformation of melanocytes. Melanocytes specialize in melanogenesis or the production of melanin, a pigment that protects the skin by absorbing and scattering harmful solar radiation [2]. During the development of melanoma, mutated melanocytes display rapid proliferation and growth. Melanomas that grow laterally or display a radial growth phase (RGP) pattern are typically less aggressive than those displaying a vertical growth phase (VGP) pattern [3]. At present, primary cutaneous melanomas are staged according to their thickness or vertical growth. With increasing T stage category, cancerous cells are more likely to invade into through the basement membrane resulting in an increased risk of metastatic spread [4-6]. Given its aggressive behavior the five year survival rate for patients diagnosed with metastatic melanoma is less than 16% [1].

At present, early detection of melanoma is the most important means to improve disease survival. Primary treatment involves surgical resection, brachytherapy, targeted

molecular therapy, and/or immunotherapy. Despite these aggressive interventions, treatment options for patients with metastatic disease remain limited and typically is associated with a poor prognosis. Consequently, investigations into novel treatment options are necessary for patients with this aggressive disease. One promising treatment option is the extract derived from *Rhodiola crenulata* (RC) plant roots. RC is a small perennial plant cultivated in barren soils and high altitudes in the tundra regions of Siberia and the highlands of Tibet. Traditionally, the phenolic phytochemicals extracted from the root of RC have been used to treat disorders such as depression, anxiety, and fatigue [7-10]. Recent studies have demonstrated the therapeutic potential of RC in a variety of malignancies including bladder cancer, breast cancer, and glioblastoma [11-14]. Given the anti-tumorigenic properties observed with the use of *Rhodiola* plant extracts both *in vitro* and *in vivo*, this current study was designed to evaluate the therapeutic potential of RC root extract on a melanoma cell line.

## **4.2. Materials and Methods**

### **4.2.1 *R. crenulata* Preparation.**

RC root extract was obtained in powdered form from Barrington Chemical Corporation (Harrison, NY). For cell culture and oral administration experiments, RC powder was dissolved in a 10% ethanol solution in distilled water and was filter sterilized. Cream-based RC for topical experiments was prepared by the addition of 5% or 10 % RC by weight to a 10% DMSO-Eucerin™-based cream.



#### 4.2.2 Cell Culture.

B16-F10 (CRL-6475™) murine melanoma cell culture line was obtained from ATCC® (Manassas, VA). Cells were cultured in Dulbecco's Modified Eagle's Medium (DMEM) supplemented with 10% fetal bovine serum, 100 U/mL penicillin, and 100 µg/mL streptomycin (Thermo Fisher, Grand Island, NY) at 37°C under 5% CO<sub>2</sub>.

#### 4.2.3 Evaluation of viability and proliferation.

A CellTiter96® Aqueous One Solution MTS Assay (Promega, Madison, WI) assay was performed according to the manufacturer's directions in order to test for cell growth and proliferation. A total of 5X10<sup>3</sup> B16-F10 cells were seeded on a 96-well microtiter plate and treated with 200 µg/mL RC or ethanol vehicle control and assay was performed in quintuplicate. After incubation for 24, 48, and 72 hours following treatment, the plate was spun at 2000 X g for one minute, treated media was decanted and replaced with 100µL of 1X PBS with 20 µL of MTS reagent per well. The plate was then incubated at 37°C in a humidified, 5% CO<sub>2</sub> atmosphere for three hours. The absorbance of each well was recorded at 490 nm using an Enspire® multimode automated plate reader (PerkinElmer, Waltham, MA).

#### 4.2.4 Clonogenicity assay.

A total of 200 B16-F10 cells were seeded onto 60-mm tissue culture plates. After allowing the cells to adhere for 24 hours, plates were treated with 100 µg/mL RC or vehicle control for 1 hour +/- exposure to 5 Gy radiation or sham treatment. The media

was replaced with appropriate treatment every four days. On day 11, colonies were fixed in methanol and stained with 2% crystal violet in a 50% methanol solution. Colonies were defined as a cluster of five or more cells. The number of colonies were quantified visually and compared between treatment groups. The experiment was performed in triplicate.

#### 4.2.5 Migration assay

Migration and cell growth were evaluated using a scratch wound assay. B16-F10 cells were plated on 30-mm dishes and allowed to reach 100% confluency and then a scratch was made down the center of each culture with a pipette tip. Plates were then treated with 100 µg/mL RC or ethanol vehicle control, and cell growth was monitored over 48 hours. Images of the plates were captured daily with Nikon Eclipse TE2000-U using Metaview™ software (Universal Imaging Corporation).

#### 4.2.6 Evaluation of Topical RC Therapy on a Subcutaneous Melanoma *In Vivo*.

Thirty 8-week-old virgin C57BL/6 female mice were housed in plastic cages and were permitted free access to food and water. A total of  $1 \times 10^6$  B16-F10 cells were implanted subcutaneously above the scapular fat pad. Daily topical RC treatment was initiated 24 hours following tumor implantation. Treatment groups (10 animals/group) included the following: 5% RC cream, 10% RC cream, and DMSO control cream. Mice were evaluated daily, and tumor volume measurements were obtained once tumors became palpable. Tumor volume was calculated by  $(\text{tumor length} \times \text{tumor width}^2)/2$ , in

which the tumor width was the smaller of the two measured values. Mice were euthanized if they appeared to be in any distress, exhibited greater than 15% weight loss, or when tumor volume exceeded 1500 mm<sup>3</sup>. Upon euthanasia, necropsy was performed, and tissues were preserved in 10% formalin. Excised tumors were paraffin embedded and stained with hematoxylin and eosin (H&E, Poly Scientific, Bay Shore, NY). The total number of mitotic cells was quantified in three representative images at 40X power per tumor sample obtained from each mouse in the DMSO and 10% RC treated groups. Images were captured with an Olympus BX41 light microscope using SPOTS SOFTWARE (Diagnostic Instruments, Inc.).

#### 4.2.7 Evaluation of Enteral RC Therapy on a Subcutaneous Melanoma *In Vivo*.

Subcutaneous B16-F10 tumors were established overlying the scapula of 20 C57BL/6 mice. Beginning 24 hours prior to tumor implantation, drinking water of ten mice per treatment group was supplemented with either 50mg/kg RC or ethanol vehicle control. Mice were evaluated daily, and tumor volume measurements were obtained once tumors became palpable. Tumor volume was calculated by  $(\text{tumor length} \times \text{tumor width}^2)/2$ , in which the tumor width was the smaller of the two measured values. Mice were euthanized if greater than 15% weight loss was observed, tumor volume exceeded 1500mm<sup>3</sup> or mice exhibited any signs of distress. Necropsy was performed at time of euthanasia. Outcomes, including length of survival and tumor growth were compared between treatment groups.

#### 4.2.8 Evaluation of RC to Prevent the Establishment of Metastatic Melanoma *In Vivo*

Sixteen 8-week-old C57BL/6 female mice were pretreated for three days with 100mg/kg RC or vehicle supplemented water (8 mice/group). A total of  $1 \times 10^5$  B16-F10 cells were injected via lateral tail vein to model a disseminated disease state. Mice were evaluated daily, and water was replaced with appropriate treatment every 48 hours. Mice were euthanized if they appeared to be in any distress or exhibited more than 15% weight loss. All surviving mice were euthanized 30 days following tumor injection. At the time of euthanasia, the lungs were preserved in Fekete's solution [15], while remaining organs were preserved in 10% formalin. The lungs were evaluated for gross establishment of metastatic foci, and photos were obtained of gross lung specimens. Formalin-fixed paraffin-embedded lungs were further analyzed histologically by H&E staining. Representative images of H&E-stained lung sections were taken using an Olympus BX41 light microscope using SPOTSOFTWARE (Diagnostic Instruments, Inc.).

#### 4.2.9 Statistical analysis

All results were analyzed using either a two-tailed student's t-test with one-way analysis of variance (ANOVA) or a two-ANOVA with a Bonferroni's correction. Statistical outliers were identified utilizing a rout test [16]. All graphs were created and statistical analysis was performed using GraphPad Prism Software (Prism, GraphPad Software, Inc., San Diego, CA).

### 4.3. Results

#### 4.3.1 RC induces morphological changes in B16-F10 cells.

B16-F10 cells are typically adherent, flat, and have multiple dendritic projections. Upon treatment of these cells with increasing doses of RC, we observed phenotypic changes at doses greater than 200  $\mu\text{g}/\text{mL}$  RC. Cells treated with RC exhibited reduced dendritic projections, became rounder, and were less adherent (Fig 4.1A).

#### 4.3.2 RC decreases B16-F10 proliferation

To assess RC's effect on growth and proliferation, we performed an MTS assay on B16-F10 cells treated with either RC (200  $\mu\text{g}/\text{mL}$ ) or vehicle control. Following 24 hours of treatment an initial trend toward decreased proliferation was observed in RC treated cells. By 48 and 72 hours, a significant reduction in proliferation was observed upon RC treatment ( $p < .01$  and  $p < .0001$ , respectively, Fig. 4.1B).

#### 4.3.3 RC Decreases Colony Formation of B16-F10 Cells

To evaluate RC treatment efficacy, a clonogenicity assay was performed. RC treatment significantly reduced the number of colonies established ( $p < .001$ ) compared to vehicle control (Fig. 4.1C). However, radiation sensitivity did not appear to be enhanced by treatment with RC.

#### 4.3.4 RC Decreases Cellular Migration of B16-F10 Cells

To determine if RC affects migration of B16-F10 cells, a scratch wound assay was performed. Cultures treated with vehicle control exhibited complete wound closure by 48

hours, while cells treated with RC maintained distinct wound boundaries with minimal growth at 48 hours (Fig 4.1D).

#### 4.3.4 Evaluation of the Topical RC treatment on subcutaneous B16-F10 Tumors *In Vivo*

A trend toward increased survival was observed in mice treated with RC. Mice treated with 5% RC and 10% RC met requirements for euthanasia by days 15 and 20, respectively, while mice treated with vehicle met requirements for euthanasia by 14 days (Fig 4.2A). Further, one mouse treated topically with 5% RC exhibited complete regression of the subcutaneous tumor and survived for over 30 days. There was no difference in the final weights of mice at the time of euthanasia (Fig 4.2C). While no significant difference was observed in the overall size of the measured tumor volume (Fig 4.2B, D), tumors in mice treated with vehicle control tended to be raised, while animals treated with RC displayed a more horizontal growth pattern (Fig 4.3A). Additionally, tumors treated with RC exhibited a significantly lower number of active mitotic figures per high power field compared to the vehicle-treated mice (Fig 4.3C, D,  $p=.0374$ ).

#### 4.3.5 Evaluation of the Enteral RC treatment on subcutaneous B16-F10 Tumors *In Vivo*

Similar to the topical RC experiments, there was no significant difference observed in the survival and tumor growth in mice treated with RC enterally compared to vehicle control (Fig 4.4A). At the time of euthanasia, there was no difference in the weight of the mice, tumor volume or tumor weight (Fig 4.4 B, C, D respectively).

Additionally, there were no gross difference in tumor growth patterns observed amongst treatment groups.

#### 4.3.6 Evaluation of Enteral RC to Prevent Establishment of Metastatic Melanoma

Upon necropsy performed 30 days following tumor injection, a striking difference in the tumor establishment within the lungs was observed. Mice treated with RC exhibited a reduction in tumor burden established in the lungs compared to mice treated with ethanol vehicle control (Fig 4.5A). No other organs bore a similar difference in tumor establishment. Total lung weights confirmed our gross findings, in which there was a significant decrease in the weight of lungs treated with RC compared to vehicle control (Fig 4.5B,  $p < 0.05$ ). Additionally, histologic examination of the lungs confirmed reduced establishment of tumor foci in animals treated with RC.

### 4.4 Discussion

Melanoma is the most aggressive and deadliest form of skin cancer. The SEER database estimated that melanoma was responsible for the death of more than 9,000 Americans in 2015 [1]. Currently, prevention and early detection are the best methods to reduce the mortality rate associated with melanoma. Unfortunately, effective treatment options for cases of advanced and disseminated disease remain limited. Consequently, there may be significant value in identifying natural products that possess potent anticancer properties. *Rhodiola* plant extracts have exhibited a number of anti-tumorigenic properties in a variety of cancers and have been shown to promote cell death

and inhibit both proliferation and angiogenesis within a variety of cancers [11,12,14,17]. Based on the data presented above, RC extract, and the compounds contained within it, may represent a potentially novel and effective melanoma therapy.

In this study, we evaluated the effect of RC on an aggressive melanoma cell line, B16-F10. Upon treatment with RC *in vitro*, B16-F10 cells exhibited morphological changes, reduced proliferation, increased cell death, and reduced colony formation compared to vehicle controls. Given the promising effects observed with RC treatment upon melanoma cells *in vitro*, investigation of the therapeutic effects of this extract were then evaluated *in vivo*.

While no overt difference in the survival and tumor growth in mice with subcutaneous tumors treated with RC were observed, differences in growth patterns and mitotic activity was observed in tumors treated with topical RC. Upon topical RC treatment, tumors displayed more horizontal growth patterns while the tumors of vehicle control treated mice tended to grow more vertically. Of note, the endpoint for the investigation of RC treatment of subcutaneous tumors was based on the length and width of the pigmented area, but not on the vertical axis in tumor volume measurements. If the vertical axis had been a consideration, then the overall survival time of RC-treated animals compared to vehicle control-treated animals may have resulted in a significant improvement in survival. The differences in growth patterns observed is critical as melanoma displaying radial growth patterns are associated with considerably lower rates of metastatic disease compared to the more aggressive and vertically growing phenotypes.



Upon further histologic analysis of tumor sections, topical RC treated tumors displayed reduced mitotic activity. High mitotic rates in cutaneous melanomas are known to be associated with more aggressive disease phenotypes and significantly lower survival rates [19-23]. Therapeutic agents that reduce the mitotic rates of melanomas have the potential to reduce tumor growth and improve overall survival. This further suggests that RC can reduce the aggressive potential of melanoma tumors *in vivo*.

Topical application of RC creams resulted in phenotypic changes in the tumor that are associated with less aggressive behavior. While RC has previously been used topically to reduce the size of pigmented lesions [24], this work is the first to suggest that the RC is bioactive when applied topically in the setting of a cutaneous neoplasm. In contrast, enterally administered RC did not result in any changes in tumor growth or histologic characteristics. While RC has previously been shown to be bioavailable upon enteral administration in the setting of other cancers, there are several reasons as to why RC administered topically was more effective than enterally administered RC in this study. First, RC doses provided enterally may have led to poor tumor uptake while topically administered RC may have led to more concentrated uptake within the tumor bed directly. Additionally, B16-F10 melanoma is a syngeneic line with C57BL/6 mice, resulting in very aggressive growth and dissemination following tumor implantation. As such, tumor growth may have exceeded the ability to observe any efficacious changes following RC treatment administered enterally.

Upon *in vivo* evaluation of RC treatment in a disseminated model of melanoma, a dramatic reduction in the establishment of metastatic foci in the lungs was observed.

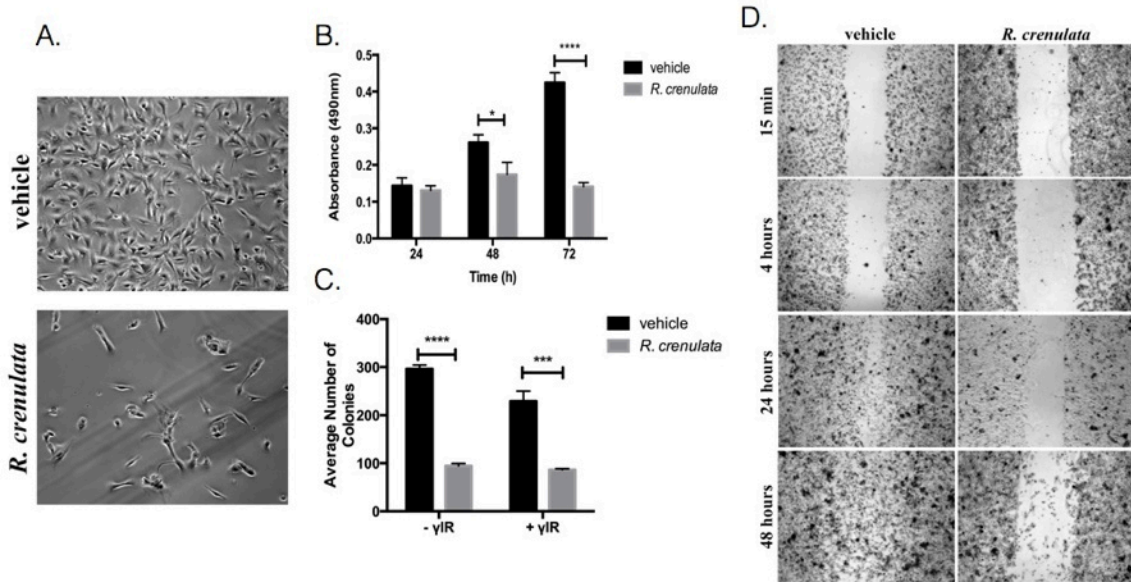
Given this, RC's ability to prevent establishment of metastatic disease is very promising as a novel therapy for melanoma. The molecular detection of circulating tumor cells in patients with melanoma has been established as a negative prognostic indicator, emphasizing the impact of hematogenous spread on overall survival [25, 26]. Current treatments for locally or regionally advanced disease, such as interferon, provide only minimal improvements in patient survival. Treatments that may further prevent the development of metastatic lesions, such as RC, can potentially be utilized as an adjunct to other chemotherapeutic agents to prevent further dissemination of the disease.

#### **4.5 Conclusion**

In summary, treatment of B16-F10 melanoma with RC resulted in promising anti-neoplastic properties noted both *in vitro* and *in vivo*. We observed that RC was cytotoxic to melanoma cells and reduced cell proliferation and migration *in vitro*. We also observed that topical RC could impede more aggressive vertical growth characteristics of tumors critical for the establishment of metastatic disease. Furthermore, our findings demonstrate the potential anti-metastatic activity of this extract when utilized in a disseminated model of melanoma. The identification of novel agents with chemotherapeutic potential, such as RC, is important for the improvement of overall patient survival. Thus, *Rhodiola* plant extracts may have a place in the future as an adjuvant therapeutic agent for the treatment of melanoma.

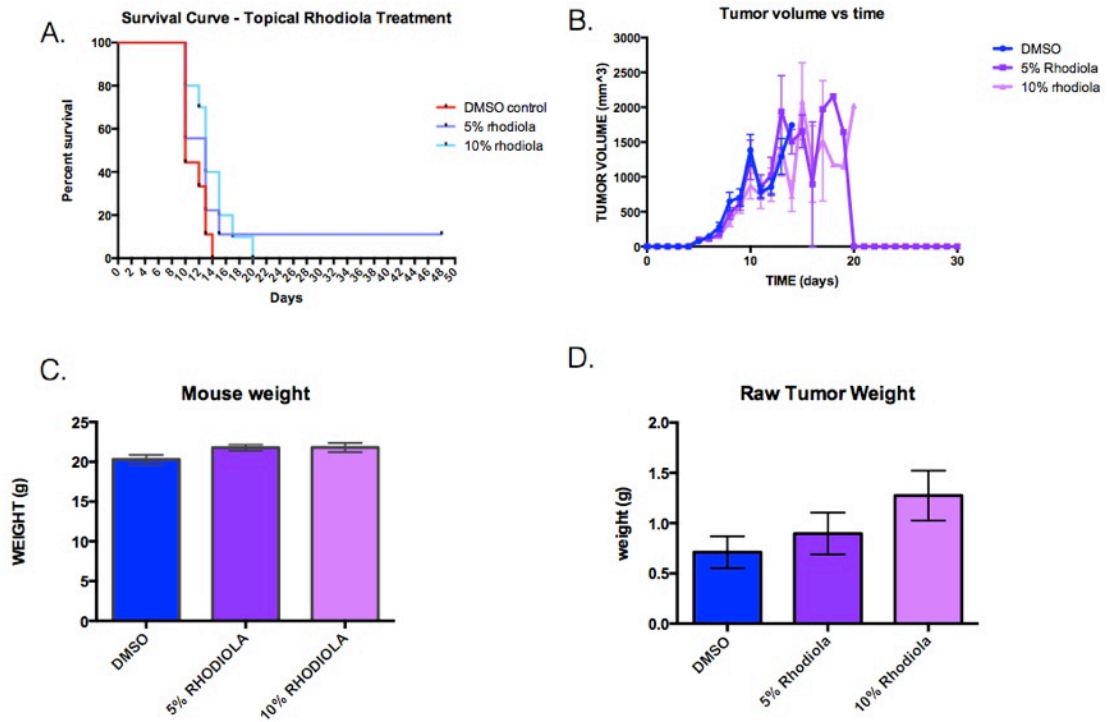
## 4.6 Figures

Figure 4.1: *In Vitro* Effects of Rhodiola on Melanoma



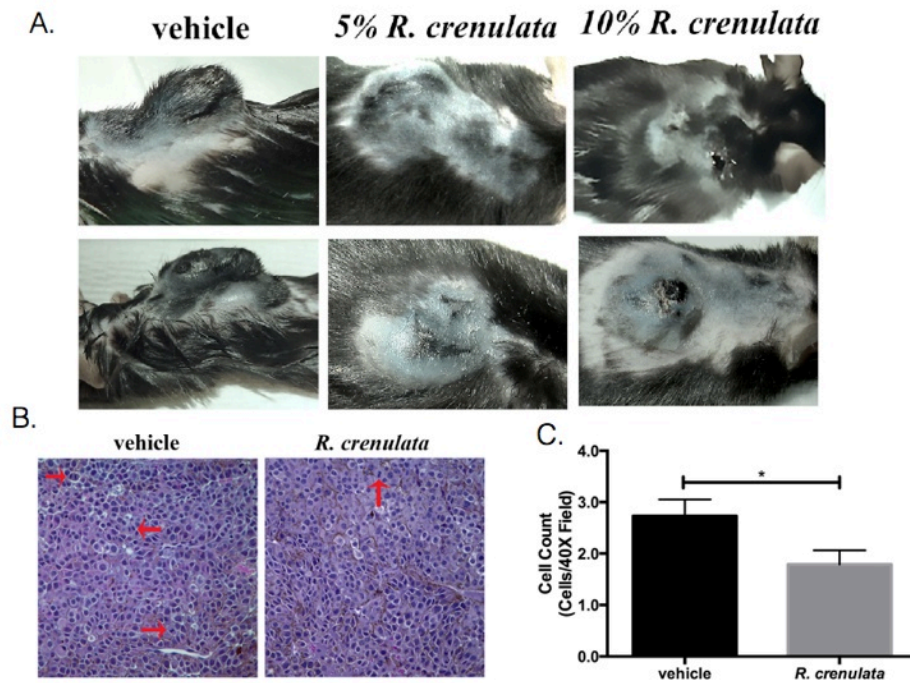
**Figure 4.1** *In Vitro* Effects of RC treatment upon Melanoma A) Phase contrast image representation of B16-F10 cells treated for 72 hours with 100  $\mu$ g/mL *R. crenulata* or ethanol vehicle. B) MTS assay performed on cells treated with Rhodiola or vehicle control evaluated at 24, 48 and 72 hours. C) Clonogenicity assay performed on cells treated with either Rhodiola on vehicle control with or without exposure to 5 Gy radiation. All colonies containing more than five cells that grew following 8 days of therapy were quantified. D) Scratch wound healing assay performed on a confluent monolayer of cells treated with either Rhodiola or vehicle control. Scratch wound healing was observed at 15 minute, 4, 24 and 48 hour time intervals. All images were obtained at 20X magnification. Error bars represent  $\pm$  standard error of the mean. \*= $p < 0.05$ , \*\*\*= $p < 0.001$ , \*\*\*\*= $p < 0.0001$ .

Figure 4.2: Topical Rhodiola Treatment of Melanoma Outcomes



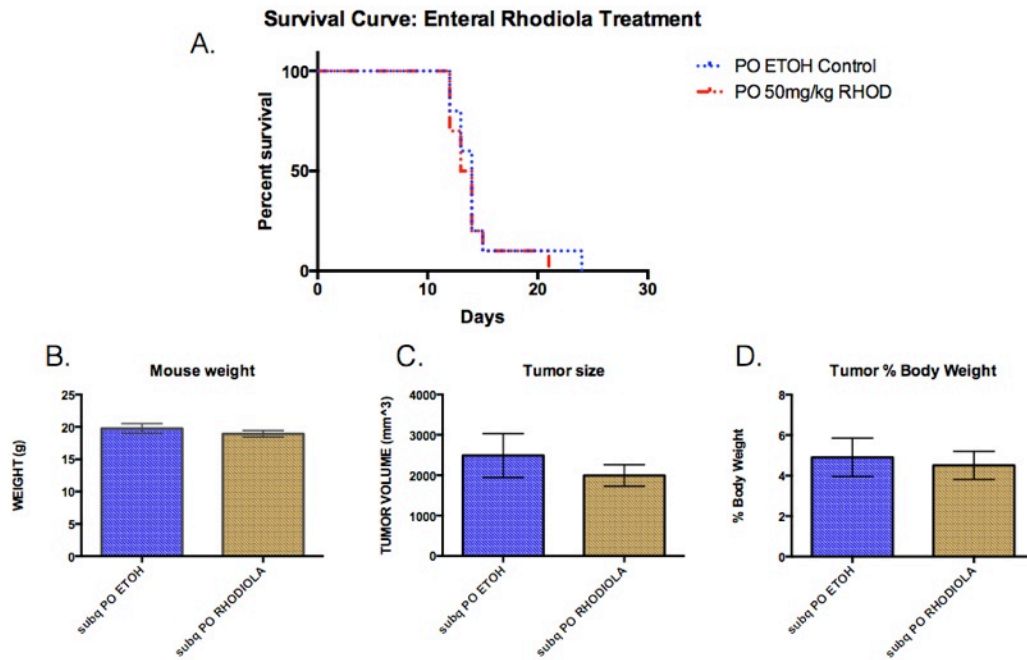
**Figure 4.2 Outcomes of Topical RC Treatment of Melanoma *In Vivo*.** A) Survival Curve of C57BL/6 mice with B16-F10 subcutaneous tumors treated with topical DMSO cream (red), 5% RC (dark blue) and 10% RC (light blue). NS=non-significant. B) Change in tumor growth over time among treatment groups including DMSO cream (Dark blue), 5% RC cream (dark purple) and 10% RC (light purple). C) Average mice weight at time of euthanasia. D) Tumor weight (g) at time of euthanasia. Error bars indicate  $\pm$  standard error of the mean.

Figure 4.3: Topical Rhodiola Treatment of Melanoma Gross and Pathological Changes



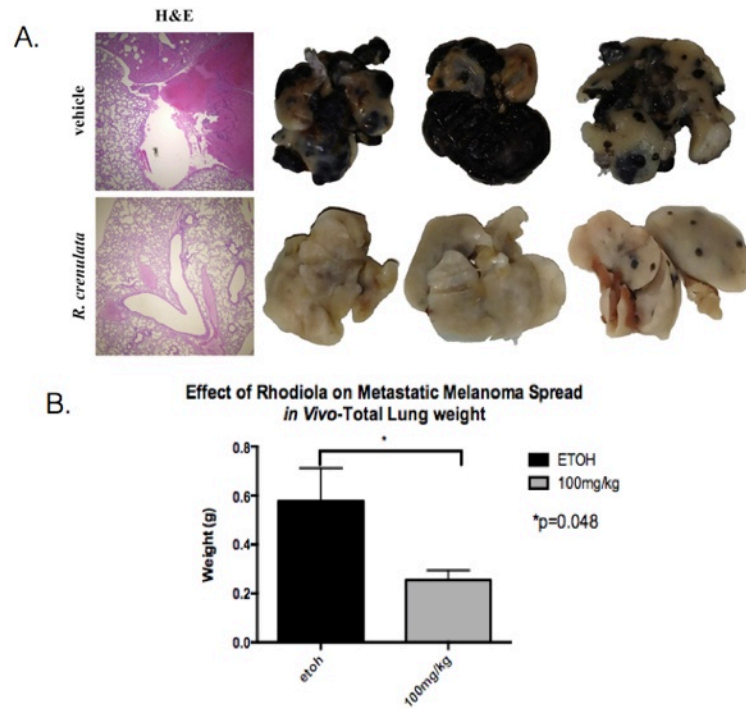
**Figure 4.3** Gross and Pathological Changes upon Topical RC Treatment of Melanoma. A) Photographic representation of tumors treated topically with 5% or 10% *R.crenulata* cream or vehicle cream. B) Image representation of histological tumor specimens stained with hematoxylin and eosin. Red arrows indicate mitotic cells. Images were captured at 40X magnification. C) Average number of mitotic cells present within each representative 40X field and compared between mice treated with vehicle cream and 10% Rhodiola cream. Error bars represent  $\pm$  standard error of the mean, \* $p < 0.05$ .

Figure 4.4: Enteral *Rhodiola* Treatment of Subcutaneous Melanoma



**Figure 4.4 Outcomes of Enteral RC Treatment of Melanoma *In Vivo*.** A) Survival Curve of C57BL/6 mice with B16-F10 subcutaneous tumors treated with enteral 50mg/kg RC or ethanol vehicle control. B) Mouse weight (g) at time of euthanasia comparing ethanol treated (blue) to RC treated (yellow). C) Tumor volume at time of euthanasia. D) % Total body weight of tumor compared to total mouse weight at time of euthanasia. Error bars indicate  $\pm$  standard error of the mean.

Figure 4.5: Enteral Rhodiola Effects on Metastatic Establishment of Melanoma



**Figure 4.5 Effects of Enteral RC Treatment on the Establishment of Metastatic Melanoma**  
A) Photographic representation of lungs of C57BL/6 mice at 30 days following disseminated B16-F10 tumor administration via lateral tail vein injection in mice treated with ethanol supplemented water or 100mg/kg RC supplemented water B) Lung weight (g) at time of euthanasia of mice treated with ethanol or 100mg/kg RC, ROUT Test was performed to identify statistical outliers. Error bars indicate  $\pm$  standard error of the mean,  $*=p<0.05$ .



#### 4.7 References

1. Melanoma of the Skin. In: turning cancer data into discovery. surveillance, epidemiology, and end results (SEER) program. 2004–2010. <http://seer.cancer.gov/statfacts/html/melan.html>. Accessed 12 March 2015.
2. Tadokoro Tet al. UV-induced DNA damage and melanin content in human skin differing in racial/ethnic origin. *FASEB J*. 2003. doi:10.1096/fj.02-0865fje.
3. Breslow A. Thickness, cross-sectional areas and depth of invasion in the prognosis of cutaneous melanoma. *Ann Surg*. 1970;5:902–8.
4. Balch CM, Gershenwald JE, Soong S, et al. Staging and primary tumor mitotic rate. *J Surg Oncol*. 2011;104:379–85.
5. Chin L. The genetics of malignant melanoma: lessons from mouse and man. *Nat Rev Cancer*. 2003;3:559–70.
6. Bedrosian I, FariesMB, Guerry D, et al. Incidence of sentinel node metastasis in patients with thin primary melanoma (#1 mm) with vertical growth phase. *Ann Surg Oncol*. 2000;7:262–7.
7. Brown RP, Gerbarg PL. *The rhodiola revolution*. 1st ed. Holtzbrinck Publishers; 2004.
8. Darbinyan V, Aslanyan G, Amrovan E, et al. Clinical trial of *Rhodiola rosea* L. extract SHR-5 in the treatment of mild to moderate depression. *Nord J Psychiatry*. 2007;61:343–8.
9. Dwyer AV, Whitten DL, Hawrelak JA. Herbal medicines, other than St. John's Wort, in the treatment of depression: a systematic review. *J Clin Ther*. 2001;16:40–9.
10. Pannossian A, Wilkman G, Sarris J. Rosenroot (*Rhodiola rosea*): traditional use, chemical composition, pharmacology and clinical efficacy. *Phytomedicine*. 2010;17:481–93.
11. Gauger KJ, Rodríguez-Cortés A, Hartwich M, et al. *Rhodiola crenulata* inhibits the tumorigenic properties of invasive mammary epithelial cells with stem cell characteristics. *J Med Plants Res*. 2010;4:446–54.
12. Tu Y, Roberts L, Schneider SS. *Rhodiola crenulata* induces death and inhibits growth of breast cancer cell lines. *J Med Food*. 2008;11:413–23.



13. Liu Z, Li X, Simoneau AR, Jafari M, et al. Rhodiola rosea extracts and salidroside decrease the growth of bladder cancer cell lines via inhibition of the mTOR pathway and induction of autophagy. *Mol Carcinog*. 2012;51:257–67.
14. Mora MC, Bassa LM, Wong KE, et al. Rhodiola Crenulata inhibits Wnt/ $\beta$ -catenin signaling in glioblastoma. *J Surg Res*. 2015;197(2): 247–55.
15. Overwijk WW, Restifo NP. B16 as a mouse model for human melanoma. *Curr Protoc Immunol*. 2001. doi:10.1002/0471142735.im2001s39.
16. Motulsky HJ, Brown RE. Detecting outliers when fitting data with nonlinear regression – a new method based on robust nonlinear regression and the false discovery rate. *BMC Bioinf*. 2006. doi: 10.1186/1471-2105-7-123.
17. Skopińska-Różewska E, Hartwich M, Siwicki AK, et al. The influence of Rhodiola rosea extracts and rosavin on cutaneous angiogenesis induced in mice after grafting of syngeneic tumor cells. *Cent Eur J Immunol*. 2008;33:102–7.
18. Elder DE. Pathology of melanoma. *Clin Cancer Res*. 2006;12: 2309–11.
19. Meier F, Satyamoorthy K, Nesbit M, et al. Molecular events in melanoma development and progression. *Front Biosci*. 1998;3: 1005–10.
20. Thompson JF, Soong S, Balch S, et al. Prognostic significance of mitotic rate in localized primary cutaneous melanoma: an analysis of patients in the Multi-Institutional American Joint Committee on cancer melanoma staging database. *J Clin Oncol*. 2011;29:2199–205.
21. Azzola MF, Shaw HM, Thompson JF, et al. Tumor mitotic rate is a more powerful prognostic indicator than ulceration in patients with primary cutaneous melanoma. *Cancer*. 2003;97:1488–98.
22. Balch CM, Gershenwald JE, Soong S, et al. Final version of 2009 AJCC melanoma staging and classification. *J Clin Oncol*. 2009;27: 6199–206.
23. Francken AB, Shaw HM, Thompson JF, et al. The prognostic importance of tumor mitotic rate confirmed in 1317 patients with primary cutaneous melanoma and long follow-up. *Ann Surg Oncol*. 2004;11:426–33.
24. Chiang H, Chien Y, Wu C, et al. Hydroalcoholic extract of Rhodiola rosea L. (Crassulaceae) and its hydrolysate inhibit melanogenesis in B16F0 cells by regulating the CREB/MITF/tyrosinase pathway. *Food Chem Toxicol*. 2014;65:129–39.

25. Mellado B, Gutierrez L, Castel T, et al. Prognostic significance of the detection of circulating malignant cells by reverse transcriptase polymerase chain reaction in long-term clinically disease-free melanoma patients. *Clin Cancer Res.* 1999;5:1843–8.
26. Hoon DS, Bostick P, Kuo C, et al. Molecular markers in blood as surrogate prognostic indicators of melanoma recurrence. *Cancer Res.* 2000;60:2253–7.

**CHAPTER 5**  
**EVALUATION OF *RHODIOLA CRENULATA* ON THE TREATMENT OF**  
**NEUROBLASTOMA**

**5.1 Introduction**

Neuroblastoma is the most common extra-cranial solid malignancy in infants and children. Occurring in approximately 1 in 100,000 children, neuroblastoma is responsible for 15% of all pediatric cancer deaths [1-4]. While these tumors of neurocrest origin may arise anywhere along the sympathetic ganglion chain, they most commonly arise from the adrenal medulla[1]. The clinical course of this highly malignant neoplasm is quite variable depending on the location of the primary tumor, age of the patient, and stage of disease at presentation. The DNA content of cells, amplification status of the proto-oncogene MYCN, the stage of disease, and age of the patient at presentation are important variables for determining the treatment and outcomes of this aggressive disease [1]. Despite intensive research therapeutic options for these patients, outcomes of children with aggressive variants of neuroblastoma continues to remains poor.

The treatment of neuroblastoma typically involves surgical resection and multi-agent chemotherapy. The toxicity of chemotherapy required often limits therapy in this young and fragile population. Children who receive chemotherapy at such of a young age are susceptible to the life long effects of the morbidities associated with these drugs including hepatotoxicity, nephrotoxicity or cardiotoxicity [5]. Further, children are at increased risk for developing long term side effects of these agents, such as the

development of myelodysplastic syndromes [5]. Any novel agent that can effectively treat this disease or serve as an adjunct to reduce the toxicities associated with current therapeutic options, offers the potential to limit or eliminate these devastating systemic toxicities and improve therapeutic outcomes in children with neuroblastoma.

Given the anti-cancer properties that RC has displayed in a variety of cancers [6-10], such as breast cancer [7-8], glioblastoma [9] and melanoma [10], this work sought to evaluate the effects that RC extract has both *in vitro* and *in vivo* as a novel method for the treatment of neuroblastoma.

## **5.2 Materials and Methods**

### **5.2.1 RC Preparation**

RC root extract was obtained in powdered form from Barrington Chemical Corporation (Harrison, NY). For cell culture and oral administration experiments, RC powder was dissolved in a 10% ethanol solution in distilled water and was filter sterilized.

### **5.2.2 Cell Culture**

Two human neuroblastoma cell lines were evaluated for this work which were graciously provided by Dr. Andrew Davidoff's labs of St. Jude's Hospital for Children. The first cell line, NB-1691, is a MYCN amplified neuroblastoma line derived from a recurrent retroperitoneal tumor in a 1.9 year old male [11]. The second line evaluated is SK-N-AS, which are non-MYCN amplified cells obtained from the bone marrow of an

eight year old female with recurrent neuroblastoma [11]. Cells were cultured in either Roswell Park Memorial Institute (RPMI)-1640 medium containing 2mM of glutamine (Thermo Fisher, Grand Island, NY) or Dulbecco's Modified Eagle's Medium (DMEM, Thermo Fisher, Grand Island, NY). All media was supplemented with 10% fetal bovine serum (FBS), 100 U/mL penicillin, and 100 µg/mL streptomycin (Gibco®, Grand Island, NY) and all cells were cultured at 37°C under 5% CO<sub>2</sub>.

### **5.2.3 Evaluation of Viability with Trypan Blue Exclusion.**

Cell viability was determined by trypan blue exclusion performed on a Beckman Coulter Vi-Cell Cell Viability Counter (Beckman Coulter, Brea, Ca).

### **5.2.4 MTS Proliferation Assay**

A CellTiter96® Aqueous One Solution MTS (Promega, Madison, WI) assay was performed according to the manufacturer's directions in order to test for cell growth and proliferation. A total of  $1 \times 10^4$  cells were seeded on a 96-well microtiter plate and treated with 0-200 µg/mL RC or ethanol vehicle control. After incubation for up to 96 hours, media was removed and replaced with 100µL of 1X PBS mixed with 20 µL of MTS reagent per well. The plate was then incubated at 37°C until color development occurred (between 1-4 hours). The absorbance of each well was evaluated at a wavelength of 490 nm using an Enspire® multimode automated plate reader (Perkin Elmer, Waltham, MA).

### **5.2.5 Clonogenicity assay.**

A total of 300 NB-1691 cells were seeded onto 60-mm tissue culture dishes in which three plates were evaluated per treatment group. After allowing the cells to adhere for 24 hours, plates were then treated with 50 µg/mL RC or vehicle control. Plates were also additionally treated with +/- exposure to 5 Gy radiation one hour following RC treatment. The media was replaced with the appropriate treatment every 3-4 days. Once colonies were grown and established (approximately two weeks), cells were then fixed in methanol and stained with 2% crystal violet in a 50% methanol solution. Colonies were defined as a cluster of five or more cells. The number of colonies were quantified visually and compared between treatment groups. The experiment was performed in triplicate.

#### **5.2.6 Scratch Wound Migration Assay**

NB-1691 and SK-N-AS cells were plated on 30-mm dishes and allowed to reach 100% confluency. Following this, a scratch was made down the center of each culture dish using a pipette tip. Plates were then treated with 100 µg/mL RC or ethanol vehicle control. Cell growth was monitored over 72 hours. Images of the plates were captured daily with Nikon Eclipse TE2000-U using Metaview™ software (Universal Imaging Corporation).

#### **5.2.7 Transwell Migration Assay**

NB-1691 cells were pretreated with 100 µg/mL RC or vehicle control (three wells per treatment group). After 24 hours,  $1 \times 10^5$  cells were seeded onto a BD BioCoat™ migration chamber (8 µm pore) plate (Corning, Tewksbury, MA) and treated with serum-

free RPMI. Migration chambers were placed in a 24-well plate so that they hovered above RPMI containing 10% FBS in order to create a gradient for cell migration. After 24 hours of incubation, migration chamber membranes were fixed for 10 minutes with 10% formalin, stained with 2% crystal violet for 20 minutes, and rinsed 3 times with distilled H<sub>2</sub>O. Non-migrating cells were removed from the upper surface of the membrane with a cotton-tipped swab moistened with 1X PBS. The membrane was then mounted on a microscope slide with Cytoseal™ XYL mounting medium (Richard-Allan Scientific™) in order to evaluate the under surface of the membrane for migrated cells. Images were captured with an Olympus BX41 light microscope using SPOTS SOFTWARE (Diagnostic Instruments, Inc., Sterling Heights, MI). The total number of migrating cells was quantified in representative images per each membrane sample obtained 10X magnification.

### **5.2.9 RNA isolation and quantitative RT-PCR**

NB-1691 cells were treated with 10% ethanol vehicle control or 100µg/ml RC for 24 hours. RNA was extracted from cells using Trizol (Invitrogen, Carlsbad, CA) per protocol utilizing acid-phenol extraction method. Following RNA extraction, up to 10µg of RNA samples were then treated with DNase (Thermo Fisher, Grand Island, NY) in order improve purity of samples. RNA levels were quantified utilizing Nanodrop (Thermo Scientific, Wilmington, DE).

Relative levels of mRNA were determined by quantitative real-time polymerase chain reaction (qRT-PCR) using the Stratagene Mx3005P real time PCR system (Agilent

Technologies, La Jolla, CA). All values were normalized to the amplification of GAPDH. The PCR primer sequences evaluated are listed in Table 5.1. The assays were performed using the one-step 2X Brilliant SYBR Green qRT-PCR Master Mix Kit (Agilent Technologies, Santa Clara, CA) containing both 200nM of forward primer and reverse primer as well as 50ng total mRNA. The conditions for target mRNA amplification were performed as follows: one cycle of 50°C for 30 minute; one cycle of 95°C for 10 minutes; 35 cycles each 95°C for 30 seconds, 55°C for one minute, and 72°C for 30 seconds.

#### **5.2.10 Hypoxia Inducible Factor Transfection and Luciferase Assay**

NB-1691 cells were plated in a 24 well plate at  $8 \times 10^4$  cells/well and were transfected the following day with a reporter construct containing an inducible hypoxia inducible factor (HIF) promoter (Qiagen, Valencia, CA) as well as non-inducible reporter construct (negative control) and a constitutively active reporter construct (positive control). Vectors were transfected using Lipofectamine® 2000 (Invitrogen, Carlsbad, CA) as per manufacturer instructions. After 24 hours of transfection, the cells were then treated with either ethanol vehicle control or 100µg/ml RC for 24 hours. Cells were then washed with 1X PBS and lysed using 1X passive lysis buffer (Promega). Luciferase activity was measured using the Dual-Luciferase® reporter assay system (Promega) according to the manufacture's instructions. Light output was measured with a TD-20/20 Luminometer (Turner Designs, Sunnyvale, CA), and relative luciferase activity was



calculated by firefly luciferase activity/renilla luciferase activity. Luciferase activity of vehicle control treated cells were compared to RC treated cells.

#### **5.2.11 Evaluation of Pyruvate Supplementation on the Effects of RC on NB-1691 Viability**

In order to evaluate if media supplementation with pyruvate alters the outcomes of RC treatment on NB-1691 cells, viability and growth were evaluated with trypan blue exclusion, an MTS assay and a clonogenicity assay. Prior to performance of these assays, NB-1691 cells were grown in media conditioned with 1mM of pyruvate. For MTS and viability assays, cells were treated in suspension with 200µg/mL RC or ethanol +/- 1mM pyruvate. Cells were then incubated for 24 hours and assays were performed. For clonogenicity assays, 300 NB-1691 cells were allowed to adhere to the plate. Cells were then treated to 200µg/mL RC +/- 1mM pyruvate throughout experiment. Cells were allowed to grow for approximately three weeks in which colonies were established. Colonies were then fixed, stained and quantified.

#### **5.2.12 Evaluation of Nutrient Supplementation on the Effects of RC on NB-1691 Viability**

All experiments were performed on  $1 \times 10^4$  NB-1691 added to DMEM media lacking pyruvate, glucose and glutamine. Cells were then treated with 200µg/mL RC or ethanol vehicle control. Media was then additionally supplemented with either 25mM glucose, 2mM glutamax or 0.4mM non-essential amino acids (NeAA). Treatment was

added to cells in suspension and cells were then plated on a 96 well microtiter plate and incubated for 24 hours. MTS assay was then performed to assess for viability.

#### **5.2.13 Evaluation of Citric Acid Cycle Intermediates on the Effects of RC on NB-1691 Viability.**

All experiments were performed on  $2 \times 10^5$  NB-1691 cells which were treated with  $200 \mu\text{g/mL}$  RC or vehicle control +/- one of four citric acid cycle intermediates. Those evaluated included:  $5 \text{mM}$   $\alpha$ -ketoglutarate ( $\alpha\text{kg}$ ),  $5 \text{mM}$  malate,  $5 \text{mM}$  succinate, or  $5 \text{mM}$  isocitrate. Treatment was added to cells in suspension and cells were then incubated for 24 hours. Cells were washed with PBS, treated with trypsin, and viability was then evaluated using trypan blue exclusion using a Vi-cell counter.

#### **5.2.14 Evaluation of Metabolic Inhibitors on the effects of RC on NB-1691 Viability**

NB-1691 cells were treated with one of three metabolic inhibitors including: 2-deoxy-D-glucose (2DG) which is a glucose analog that inhibits glycolysis [12], dichloroacetate (DCA) which inhibits pyruvate dehydrogenase kinase (PDK) which drives cells to utilize mitochondrial respiration [13], or rotenone which inhibits oxidative phosphorylation through inhibition of complex I in the mitochondrial electron transport chain [14]. In order to evaluate the effects of glycolytic inhibition on RC,  $1 \times 10^4$  NB-1691 were treated with  $200 \mu\text{g/mL}$  RC or ethanol +/-  $11.1 \text{mM}$  2DG (equimolar to glucose concentration in the media). Cells were treated in suspension and plated on a 96 well microtiter plate for 24 hours, following which an MTS assay was performed to

assess for viability. In order to evaluate mitochondrial metabolism on the effects of RC,  $2 \times 10^5$  cells were treated with  $200 \mu\text{g}/\text{mL}$  RC or ethanol +/-  $20 \text{ nM}$  DCA, treated in suspension. Trypan blue exclusion performed utilizing a Vicell counter was performed 24 hours after treatment to assess for viability. Finally, in order to evaluate oxidative phosphorylation inhibition on the effects of RC,  $2 \times 10^5$  cells treated with  $200 \mu\text{g}/\text{mL}$  RC or ethanol +/-  $50 \text{ nM}$  rotenone, treated in suspension for 24 hours. Trypan blue exclusion performed utilizing a Vicell counter to assess for viability.

#### **5.2.15 Lactate Dehydrogenase Activity Assay**

NB-1691 cells were treated in microcentrifuge tubes in which  $1 \times 10^6$  cells were treated in suspension with  $200 \mu\text{g}/\text{mL}$  RC or ETOH for a total of two hours. Samples were evaluated in triplicate. After two hours, samples were prepared per Lactate Dehydrogenase (LDH) Activity Assay (Sigma Aldrich, St. Louis, MO) protocol. Cells were homogenized in LDH Activity buffer and centrifuged at  $10000 \times g$  for 15 minutes at  $4^\circ\text{C}$ . Samples were ran on a 96 well plate along with a positive control and NADH standards (standard concentrations evaluated included: 0 (blank), 2.5, 5, 7.5, 10, and  $12.5 \text{ nmole}/\text{well}$ ). Following homogenization,  $5 \mu\text{L}$  of each soluble fraction of unknown samples were added to  $45 \mu\text{L}$  of LDH assay buffer. To each sample and standard,  $50 \mu\text{L}$  of master mix containing LDH assay buffer and LDH substrate mix was added. Samples were allowed to develop in the dark at  $37^\circ\text{C}$  for 2-3 minutes and then samples were evaluated on an Enspire® multimode automated plate reader (Perkin Elmer, Waltham, MA) to determine the initial  $[(A_{450})_{\text{initial}}]$  absorbance at a wavelength of  $450 \text{ nm}$ . The plate

was then incubated at 37°C in the dark and repeat measurements were obtained every 5-10 minutes. The samples were allowed to continue to develop until the absorbance value of most active samples exceeded that of the highest NADH standard (12.5nmole/well). The measurement prior to this was determined the “penultimate” or final [(A<sub>450</sub>)<sub>final</sub>] measurement. LDH Activity was determined by subtracting the blank value from each standard and unknown value. The [(A<sub>450</sub>)<sub>final</sub>] was then subtracted from the [(A<sub>450</sub>)<sub>initial</sub>] and this value was compared to the standard curve to calculate the amount of NADH generated by LDH over the evaluated time period. Results of samples treated with ethanol were compared to those treated with RC.

#### **5.2.16 Pyruvate Kinase Activity Assay**

NB-1691 cells were treated in microcentrifuge tubes in which 5X10<sup>5</sup> cells were treated in suspension with 200µg/mL RC or ETOH for a total of two hours. Samples were evaluated in triplicate. After two hours, samples were prepared per Pyruvate Kinase (PK) Activity Assay (Sigma Aldrich, St. Louis, MO) protocol. Cells were homogenized in PK assay buffer and centrifuged at 15,000 X g for 10 minutes. Samples were ran on a 96 well plate along with pyruvate standards (standard concentrations evaluated included: 0 (blank), 2, 4, 6, 8, and 10nmole/µL). Following homogenization, 5µL of each soluble fraction of unknown samples were added to 40µL of PK assay buffer. To each sample and standard, 50µl of master mix containing PK assay buffer, PK substrate mix, PK enzyme mix and fluorescent peroxidase substrate mix was added. Samples were allowed to develop for 2-3 minutes and then samples were evaluated on an Enspire® multimode

automated plate reader (Perkin Elmer, Waltham, MA) to determine the initial  $[(A_{570})_{\text{initial}}]$  absorbance at a wavelength of 570nm. The plate was then incubated at room temperature in the dark and repeat measurements were obtained every 5-10 minutes. The samples were allowed to continue to develop until the absorbance value of most active samples exceeded that of the highest pyruvate standard (10nmole/ $\mu\text{L}$ ). The measurement prior to this was determined the “penultimate” or final  $[(A_{570})_{\text{final}}]$  measurement. PK Activity was determined by subtracting the blank value from each standard and unknown value. The  $[(A_{570})_{\text{final}}]$  was then subtracted from the  $[(A_{570})_{\text{initial}}]$  and this value was compared to the standard curve to calculate the amount of pyruvate generated by PK over the evaluated time period. Results of samples treated with ethanol were compared to those treated with RC.

#### **5.2.17 Nicotinamine Adenine Dinucleotide Quantification Assay**

NB-1691 cells were treated in microcentrifuge tubes in which  $8 \times 10^5$  cells were treated in suspension with 200 $\mu\text{g}/\text{mL}$  RC or ETOH +/-1mM pyruvate for a total of two hours. Samples were evaluated in triplicate. After two hours, samples were prepared per Nicotinamine adenine dinucleotide ( $\text{NAD}^+$ ) Quantification protocol (Sigma Aldrich, St. Louis, MO). Cells were pelleted and then homogenized in 400 $\mu\text{L}$  of NADH/NAD extraction buffer. Samples were vortexed and then centrifuged at 13000 X g for 10 minutes. Samples were run on a 96 well plate along with NADH standards (standard concentrations evaluated included: 0 (blank), 2, 4, 6, 8, and 10pmole/well). Following homogenization, samples were then filtered through a 10kDa microcentrifuge cut-off spin

filter (Thermo Scientific, Grand Island, NY). Then 50 $\mu$ L of each sample was plated on 96 well plate and then 100 $\mu$ L of master mix containing NAD<sup>+</sup> cycling buffer and NAD<sup>+</sup> cycling enzyme mix was added. Samples were allowed to develop for 5 minutes and then 10 $\mu$ L of NADH developer was added to each well to convert NAD to NADH. Samples were allowed to develop at room temperature from 1-4 hours in which measurements were obtained on an Enspire® multimode automated plate reader (Perkin Elmer, Waltham, MA) to determine the absorbance at a wavelength of 450nm ( $A_{450}$ ) to assess for a total level of NADH and NAD<sup>+</sup> together. The blank value was subtracted from each standard and unknown value and this value was compared to the standard curve to calculate the amount of NAD (NAD<sup>+</sup> plus NADH) generated. This was then compared between samples treated with ethanol and RC.

#### **5.2.18** Evaluation of RC treatment of Disseminated Neuroblastoma *In Vivo*

Twenty 6-week-old non-obese diabetic severe combined immunodeficient (NOD SCID) mice were pretreated for three days with RC (100 mg/kg) or ethanol vehicle supplemented into drinking water. A total of  $1 \times 10^6$  NB-1691 cells were injected via lateral tail vein to model a disseminated disease state. Mice were evaluated daily, and water was replaced with appropriate treatment every 48 hours. All mice were euthanized 38 days following tumor injection as mice began to exhibit decreasing weight. At the time of euthanasia, the lungs were injected with india ink and then preserved in Fekete's solution. All remaining organs were preserved in 10% formalin or flash frozen in liquid nitrogen. Formalin-fixed paraffin-embedded livers and kidneys were further analyzed

histologically by H&E staining. Representative images of H&E-stained liver and kidney sections were taken using an Olympus BX41 light microscope using SPOTSOFTWARE and metastatic foci from 10X images were quantified. (Diagnostic Instruments, Inc.).

### **5.2.19 Statistical analysis**

All results were analyzed using either a two-tailed student's t-test with one-way analysis of variance (ANOVA) or a two-ANOVA. Statistical outliers were identified utilizing a Grubb's test. All graphs were made and statistical analysis was performed using GraphPad Prism Software (Prism, GraphPad Software, Inc., San Diego, CA).

## **5.3 Results**

### **5.3.1 *In Vitro* effects of RC on Neuroblastoma**

Both cell lines were treated with 200 $\mu$ g/mL RC or ethanol vehicle control for 24 hours. Upon microscopic analysis, RC treated cells in both lines were noted to have a significant proportion of dead or abnormal appearing cells. Morphological changes of RC treatment consisted of more rounded appearing cells, which were less adherent (Fig 5.1). Further, cells treated with RC were associated with the development of cytoplasmic vacuoles within several hours of treatment.

### **5.3.2 Cytotoxic Effects on RC on Neuroblastoma *In Vitro***

In order to quantify the cytotoxic effects of RC, both cell lines were treated with graduated doses of RC ranging from 50 $\mu$ g/ml to 200 $\mu$ g/mL over 72 hours. Strikingly, the

viability of NB-1691 was reduced by more than 50% upon RC treatment. SK-N-AS cells, in contrast, exhibited an approximate 40% decrease in viability upon RC treatment (Fig 5.2A, B). The cytotoxic effects were noted to be greater upon application of RC treatment while cells were in suspension compared to RC treatment following adherence to the culture plate, especially in the NB-1691 cells. An MTS calorimetric proliferation assay performed on both cell lines following treatment with graduated doses of RC revealed an approximate 20-25% reduction in proliferation compared to vehicle control upon RC treatment (Fig 5.2C, D).

### **5.3.3 RC effects on Neuroblastoma Migration and Proliferation**

The growth and proliferation of neuroblastoma cells was also markedly affected by RC therapy. A scratch wound assay performed in both cell lines revealed a reduction in cell migration and wound healing upon RC treatment compared to ethanol vehicle control (Fig 5.3A). Additionally, a clonogenic assay of NB-1691 cells exposed to continuous 50µg/mL RC +/- 5gy radiation treatment resulted in a significant reduction in the number of established colonies ( $p < 0.0001$ ). Strikingly, upon RC treatment, no colonies were observed, regardless of radiation exposure (Fig 5.3B). However, no difference in cellular migration, assessed utilizing Transwell migration inserts, was observed upon RC treatment on NB-1691 cells *in vitro* compared to vehicle control.

### **5.3.4 Evaluation of the Cytotoxic Effects of RC Compared to Dox**



The cytotoxic effects of RC were compared to that of Dox, a common drug utilized in multi-agent treatment for high risk neuroblastoma. The cytotoxic effects of RC treatment was observed to be much greater than that observed with Dox treatment in NB-1691 cells, especially upon RC treatment with cells in suspension. In contrast, SK-N-AS cells were more susceptible to Dox treatment compared to RC treatment (Fig 5.4A, B).

### **5.3.5 RC Effects on Gene Expression Regulating Cellular Differentiation**

Inhibitor of DNA (Id) genes are known to play a role in cellular differentiation [7,9]. Reduction in the expression of ID 1, 2 and 3 was observed upon RC treatment. ID1 and ID3 expression was significantly reduced ( $p < 0.05$ ) upon treatment with RC compared to ethanol vehicle control (Fig 5.5A).

### **5.3.6 RC Effects on HIF and HIF Related Gene Expression**

In order to evaluate potential genes related to the Warburg Effect including those involved with nutrient uptake and cellular metabolism, qRT-PCR was performed evaluating the mRNA expression of HIF-1 $\alpha$  subunit and several HIF-1 downstream targets including genes involved in glycolysis (HK2, PKM2), cellular transport (MCT1, SLC7A11, GLUT1) and angiogenesis (VEGF $\alpha$ , VEGF $\alpha$ 165). This revealed a significant up-regulation of HIF-1 $\alpha$  expression upon RC treatment ( $p < 0.05$ ). Additional up-regulation of PKM2, VEGF and MCT1 was also observed (Fig 5.5B). Given the increased expression of HIF-1 $\alpha$ , further confirmation of alterations in HIF-1 activity was

performed. NB-1691 cells transfected with a HIF-luciferase reporter element exhibited a significant up-regulation in HIF promoter activity upon RC treatment ( $p=0.0094$ ) compared to vehicle control, which corroborated with qRT-PCR findings (Fig 5.5C).

### 5.3.7 Pyruvate Rescues Cells from Cytotoxic Effects of RC

Upon the supplementation of media with pyruvate, the viability of NB-1691 was rescued from the cytotoxic effects of RC. This was confirmed utilizing an MTS assay, trypan blue exclusion and a clonogenicity assay. Upon viability evaluation using trypan blue exclusion, RC resulted in a 69% reduction in viability without pyruvate, while the addition of pyruvate with RC resulted in only 16.6% reduction in viability, compared to vehicle control. While there was still a significant reduction in viability of pyruvate with RC compared to vehicle control ( $p=0.0361$ ), an improvement in viability upon pyruvate with RC compared to treatment of RC without pyruvate was also significant ( $p<0.001$ , Fig 5.6B).

MTS assay further supported these results as RC treatment alone resulted in approximate 60% reduction in absorbance compared to control while the addition of RC with pyruvate resulted in a 40% reduction in absorbance. Ethanol treatment resulted in a significant reduction in absorbance, regardless of pyruvate supplementation ( $p<0.01$ ), however the addition of pyruvate to RC resulted in a significant improvement in absorbance compared to RC alone ( $p<0.01$ , Fig 5.6A).

Finally, a clonogenicity assay performed evaluating colony growth and formation following treatment with RC supplemented with pyruvate. Treatment with vehicle

control, regardless of the addition of pyruvate, resulted in the development of 70-125 colonies per plate. In contrast, treatment with RC alone resulted in no colony formation, while pyruvate addition lead to a significant increase in the number of colonies observed per plate (an average of 43 colonies per plate,  $p < 0.01$ , Fig 5.6C).

### **5.3.8 Evaluation of Nutrient and Metabolic Intermediate Supplementation on the Effects of RC Treatment.**

An MTS assay was performed on NB-1691 evaluating the effects of glucose, NeAA and glutamax supplementation. No significant difference upon the addition of glucose (Fig 5.7A), NeAA (Fig 5.7B) or glutamax (Fig 5.7C) was observed upon RC treatment alone compared to RC treatment supplementation with any of these nutrients.

The supplementation of RC treatment with citric acid cycle intermediates, including malate, isocitrate,  $\alpha$ kg and succinate, was performed and trypan blue exclusion was utilized to establish the effect. Upon the addition of malate (Fig 5.8B), succinate (Fig 5.8C) or isocitrate (Fig 5.8D) to RC treatment, no improvement in viability was observed. In contrast, cells treated with RC alone exhibited 36% viability compared to RC treated cells supplemented with  $\alpha$ kg which displayed 94% viability. This rescue of the cytotoxic effects of RC upon  $\alpha$ kg supplementation compared to RC treatment alone was significant ( $p < 0.001$ , Fig 5.8A).

### **5.3.9 Effect of Metabolic Inhibitors on RC Treatment upon NB-1691 Cells *In Vitro***

The effects of glycolysis inhibition on the effects of RC was evaluated by treatment with 2DG followed by an MTS assay. Upon treatment of NB-1691 cells with 2DG, a significant reduction in the absorbance of cells treated with 2DG and ethanol compared to ethanol alone was observed ( $p < 0.001$ ). Despite this, cells treated with 2DG and ethanol still displayed greater absorbance than cells treated with 2DG and RC ( $p < 0.001$ ). Additionally, 2DG treatment with RC did result in a slight decrease in absorbance compared to RC treatment alone ( $p < 0.01$ , Fig 5.9A).

Viability was evaluated upon the inhibition of PDK in the setting of RC treatment utilizing DCA. DCA did not result in decreased viability upon cells treated with ethanol (Fig 5.9B). Additionally, the viability of RC treatment remained unchanged upon the addition of DCA as well.

Viability was also evaluated upon the inhibition of oxidative phosphorylation in the setting of RC treatment utilizing rotenone. Similar to DCA, rotenone did not result in reduced viability of NB-1691 cells treated with ethanol (Fig 5.9C). Further, rotenone treatment did not further reduce the viability of cells treated with RC.

### **5.3.10 Evaluation of RC Effect on PK Activity**

PK activity was observed to be significantly increased upon treatment with 200 $\mu$ g/mL RC compared to ethanol treated NB-1691 cells following two hours of treatment ( $p = 0.0081$ ). Ethanol treated cells exhibited an approximate 48nM/min/mL rate of PK activity while RC treated cells displayed an approximate 65nM/min/mL rate of PK activity (Fig 5.10A).

### **5.3.11 Evaluation of RC Effect on LDH Activity**

LDH activity was observed to be significantly reduced upon treatment with 200µg/mL RC compared to ethanol treated NB-1691 cells following two hours of treatment ( $p=0.0196$ ). On average ethanol treated cells exhibited 24mU/mL rate of LDH activity while RC treated cells had a 16mU/mL rate of LDH activity (Fig 5.10B).

### **5.3.12 Evaluation of RC Effects on Total Cellular NAD Levels**

A significant reduction in the total NAD (NAD<sup>+</sup>+NADH) levels was observed upon treatment with 200µg/mL RC in NB-1691 cells following two hours of treatment ( $p<0.001$ , Fig 5.10C). RC treated cells had about 75% less total NAD than ethanol treated cells. The total amount of NAD was increased upon the addition of 1mM pyruvate to cells resulting in no significant difference between ethanol and RC treatment groups in the presence of pyruvate.

### **5.3.13 *In Vivo* Evaluation of RC Effects on Disseminated Neuroblastoma**

The effect of RC on prevention of metastatic when decreasing weights were observed in mice (Fig 5.11A). At the time of euthanasia, there was no difference in the weight of mice between treatment groups (Fig 5.11B). Upon necropsy, the greatest burden of metastatic foci was observed in the liver and kidneys in both treatment groups and there was no gross difference observed in metastatic establishments of tumor between treatment groups. There were no differences in the weights of organs, including

liver, kidney, spleen, heart and lungs, between treatment groups (Fig 5.12A). The liver and kidneys were further evaluated histologically. The average number of metastatic foci observed in representative 10X images of liver and kidneys for all animals again revealed no difference in tumor burden between mice treated with ethanol and RC (Fig 5.12A, B).

#### **5.4 Discussion**

Neuroblastoma remains one of the deadliest childhood cancers. Outcomes of aggressive variants of this disease result in high mortality rates and investigation into novel treatment methods may lead to improved outcomes for this patient population in the future. Through this work, we identified that RC results in the striking development of neuroblastoma cytotoxicity *in vitro*. Further, RC treatment results in reduced growth and proliferation of these cells. These cytotoxic effects are likely secondary to metabolic derangements afforded by treatment with this extract resulting in cell death. While there was no improvement in outcomes observed upon RC treatment in a disseminated model of neuroblastoma, given the *in vitro* findings observed, RC still offers therapeutic potential for the treatment of neuroblastoma.

Upon investigation of RC treatment on neuroblastoma cells *in vitro*, two cell culture lines were evaluated, one which was MYCN amplified (NB-1691) and another without MYCN amplification (SK-N-AS). MYCN is a critical oncogene for determining the aggressiveness of a patient's tumor, as amplification of MYCN is associated with more advanced and aggressive disease as well as poorer outcomes [1-4]. To this end, while RC treatment resulted in reduced viability in both cell lines, surprisingly the effects

of RC were enhanced upon treatment on NB-1691 cells. These effects were even more pronounced upon treatment of cells prior to adherence to the culture dish. In contrast, SK-N-AS cells were more susceptible to the effects of Dox, a common chemotherapeutic agent utilized for the treatment of neuroblastoma in the clinical setting [1,5] while NB-1691 were much less sensitive to Dox. Given these findings, our further efforts into the investigation of the effects of RC on neuroblastoma were focused on the NB-1691 cell line given that these cells remained more susceptible to RC.

In addition to the cytotoxic effects that RC conferred upon neuroblastoma cells, RC also resulted in reduced growth as well as alterations in genetic expression. RC resulted in a significant reduction in the expression of Id genes. Numerous types of cancers have revealed alteration in Id gene expression upon RC treatment [7,9]. As Id genes are associated with cellular differentiation, RC treatment may also result in a reduction in the patterns of cell growth and differentiation resulting in a less aggressive tumor phenotype.

RC treatment resulted in a rapid cytotoxicity, in which reduced growth and increased cell death were observed within 24 hours of treatment. Further, alterations in genetic expression and enzymatic activity were observed in as little as two hours following treatment. Upon RC treatment of NB-1691 in culture, cells began to develop cytoplasmic vacuoles, suggestive of cellular damage and/or autophagy, within several hours. We hypothesized that the causes for these effects could be attributable to nutrient deficiencies, oxidative damage or derangements to cellular metabolism.

In order to evaluate the means to which RC exerts its cytotoxic effects on NB-1691 cells, a variety of metabolic nutrients and intermediates were provided upon RC treatment. Interestingly, pyruvate as well as  $\alpha$ kg resulted in significant rescue in cell viability in the setting of RC treatment. The addition of glucose, NeAA or glutamax, as well as other citric acid cycle intermediates, failed result in any appreciable improvement in cell viability upon RC treatment. This reveals that the effects of RC are, at least partially, reversible and are dependent upon the availability of key nutrients to prevent the development of cell death.

The Warburg effect states that the growth of rapidly proliferating cells, such as cancers, are more dependent on glycolysis, even in aerobic conditions. This is achieved through enhanced cellular glucose uptake as well as promotion of glycolysis over mitochondrial dependent cellular respiration [15-18]. HIF is believed to play a key role in the Warburg Effect as a “switch” in cancer development as it promotes glycolysis as favored cellular metabolism [19, 20]. While we observed that HIF expression and its transcriptional activity are increased upon RC treatment, these results are likely secondary to the cellular stress imposed by RC treatment.

HIF is a key regulator of cellular metabolism and in cancer cells enhances glycolytic activity and reduces mitochondrial respiration. To this end, elevations in HIF activity typically result in enhanced the activity of LDH [21, 22], furthering anaerobic metabolism and restoring cellular levels of NAD for continued use in glycolysis [23]. Despite elevated HIF expression observed upon RC treatment, the activity of LDH was noted to be decreased and PK activity was observed to be increased. Additionally, the



total cellular levels of NAD were significantly reduced upon RC treatment compared to vehicle treated cells. Therefore RC treatment potentially prevents optimal functioning of cellular metabolism that maintains the Warburg Effect as changes in enzymatic activity observed upon RC treatment drives the cells away from glycolysis. Further, given reduced cellular NAD levels observed upon RC treatment, effective cellular metabolism can not be continued efficiently to maintain cellular growth and viability. Future work will focus on further defining the mechanism to which RC affects the cellular metabolism of neuroblastoma and it's association with cellular viability.

Given the observation of the effects that RC exerts on NB-1691 cells, further investigation into the *in vivo* effects of RC on neuroblastoma was performed. To this end, a disseminated model of neuroblastoma was investigated as RC has previously been shown to prevent the establishment of both primary tumors and metastatic lesions [6,8]. Mice were provided RC enterally and then NB-1691 were injected via the lateral tail vein to create a disseminated disease state. Despite positive outcomes upon RC treatment observed upon investigations of other tumors, such as melanoma, we did not observe any difference in the establishment of metastatic neuroblastoma upon RC treatment. Several reasons may have contributed to these results. First, as NB-1691 cells are derived from human neuroblastoma, immunodeficient NOD SCID mice were utilized. RC is known to be immuno-modulatory and through the use of NOD SCID mice, the benefits of the immunologic changes resulting from RC treatment may have been lost. Secondly, as neuroblastoma cells can be rescued from the cytotoxic effects of RC upon supplementation with nutrients such as pyruvate, the availability of these nutrients

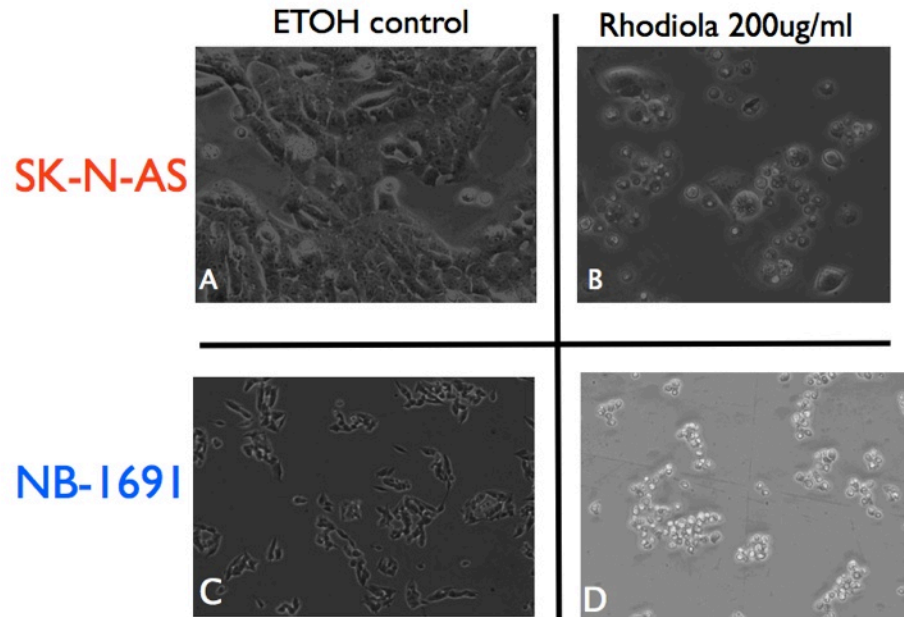
systemically may prevent RC from affecting circulating neuroblastoma cells. Alternative evaluation of orthotopic neuroblastoma or evaluation of alternative neuroblastoma cell lines in an immunocompetent mouse may result in improved outcomes upon RC treatment.

## **5.5 Conclusion**

Through this work, dramatic cytotoxic and anti-proliferative effects following RC treatment on neuroblastoma *in vitro* were observed. Strikingly these effects are more pronounced in NB-1691 cells, despite its MYCN amplified status. The *in vitro* effects of RC appear to result from alterations in the metabolic functioning of the cell resulting in rapid cytotoxicity. These findings are promising as a novel adjuvant therapy for neuroblastoma. Despite our *in vitro* findings, RC treatment failed to result in an improved outcome upon treatment in a disseminated model of neuroblastoma *in vivo*. However, RC treatment may still prove to be efficacious for the treatment of neuroblastoma as it may improve outcomes for the treatment of solid tumors or as an adjunct therapy to other chemotherapeutic agents. Further work is required to assess the therapeutic benefits of *Rhodiola* plant extracts for the treatment of neuroblastoma.

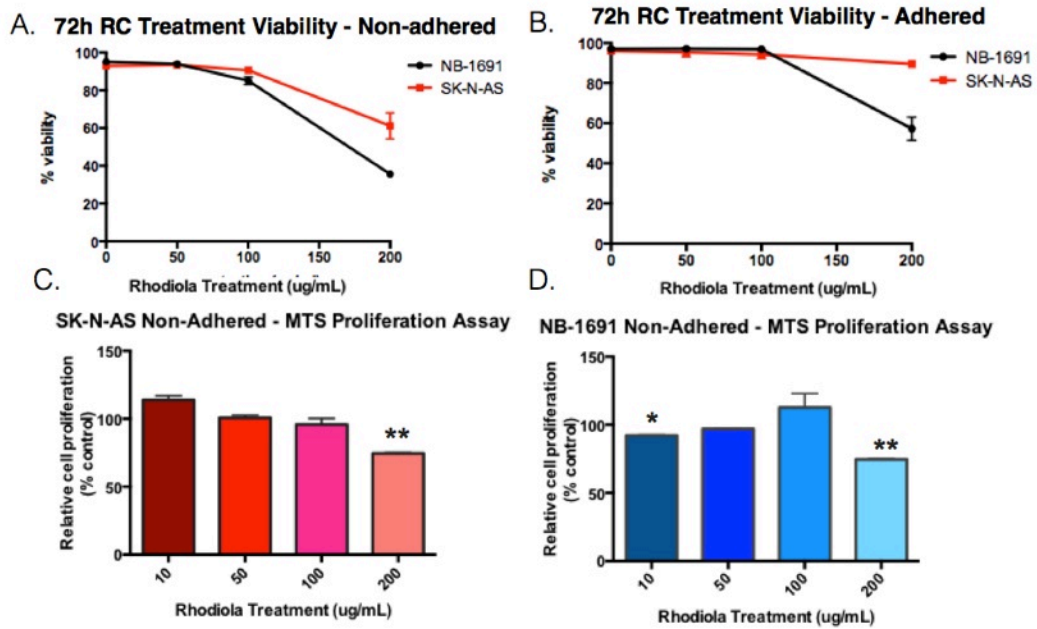
## 5.6 Figures

Figure 5.1: Rhodiola Effects on Neuroblastoma In Vitro



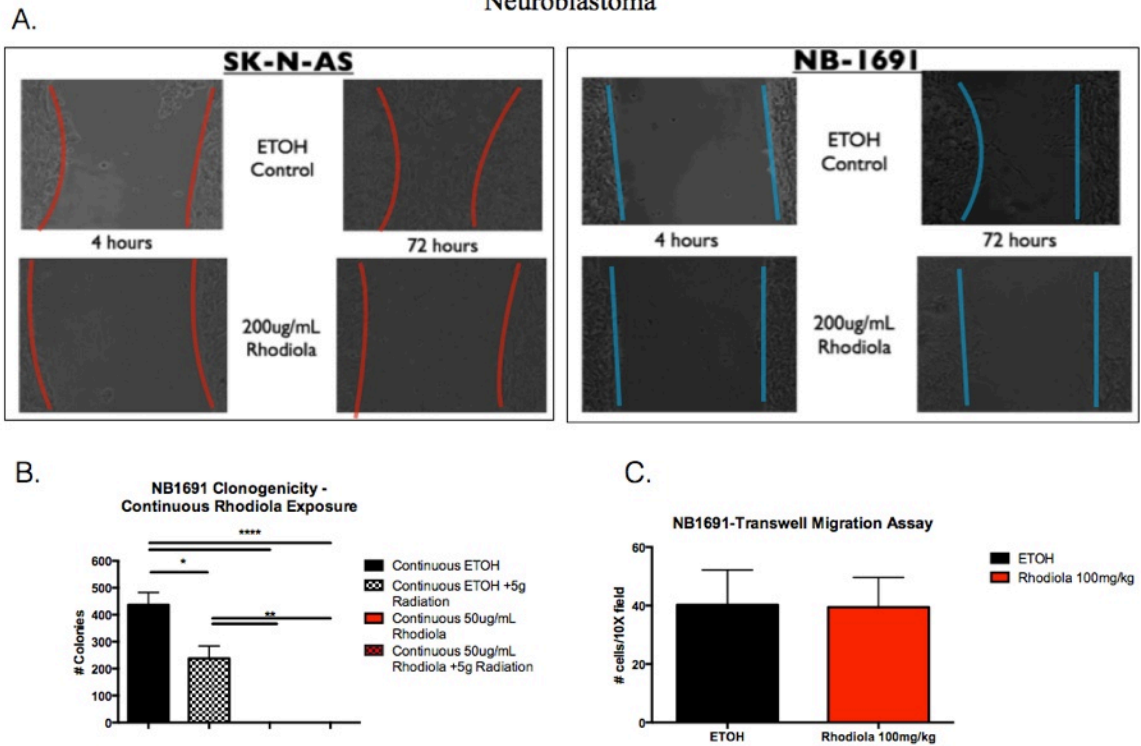
**Figure 5.1.** Morphological Effects of RC Treatment on Neuroblastoma Cells *In Vitro*. Phase contrast images of live neuroblastoma cells, both SK-N-AS (A, B) and NB-1691 (C, D) cell lines, were performed following 24 hours of ethanol vehicle (A, C) and RC treatment (B, D).

Figure 5.2: Cytotoxic Effects of Rhodiola on Neuroblastoma



**Figure 5.2. Cytotoxic Effects of RC on Neuroblastoma *In Vitro*.** A) 72 hour viability evaluated with trypan blue exclusion on NB-1691 (black) and SK-N-AS (red) cells following treatment with RC, dose including 0, 50, 100, 200 $\mu$ g/mL upon treatment in suspension. B) 72 hour viability evaluated with trypan blue exclusion on NB-1691 and SK-N-AS cells treated with 0, 50, 100, 200 $\mu$ g/mL RC following plate adherence. C) MTS assay performed on SK-N-AS cells treated with 0, 10, 50, 100, and 200 $\mu$ g/mL RC in suspension. Results presented as absorbance relative to vehicle control treated cells following 24 hours of treatment. D) MTS assay performed on NB-1691 cells treated with 0, 10, 50, 100, and 200 $\mu$ g/mL RC in suspension. Results presented as absorbance relative to vehicle control treated cells following 24 hours of treatment. Error Bars indicate +/- standard error of the mean, \*=p<0.05, \*\*=p<0.01

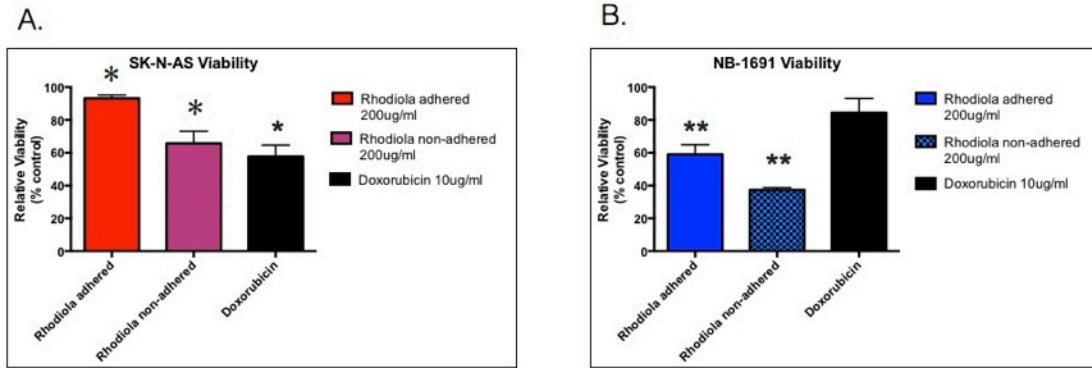
Figure 5.3: Evaluation of Rhodiola's Effects on Migration and Growth in Neuroblastoma



**Figure 5.3. Evaluation of RC's Effect on Migration and Growth on Neuroblastoma In Vitro**

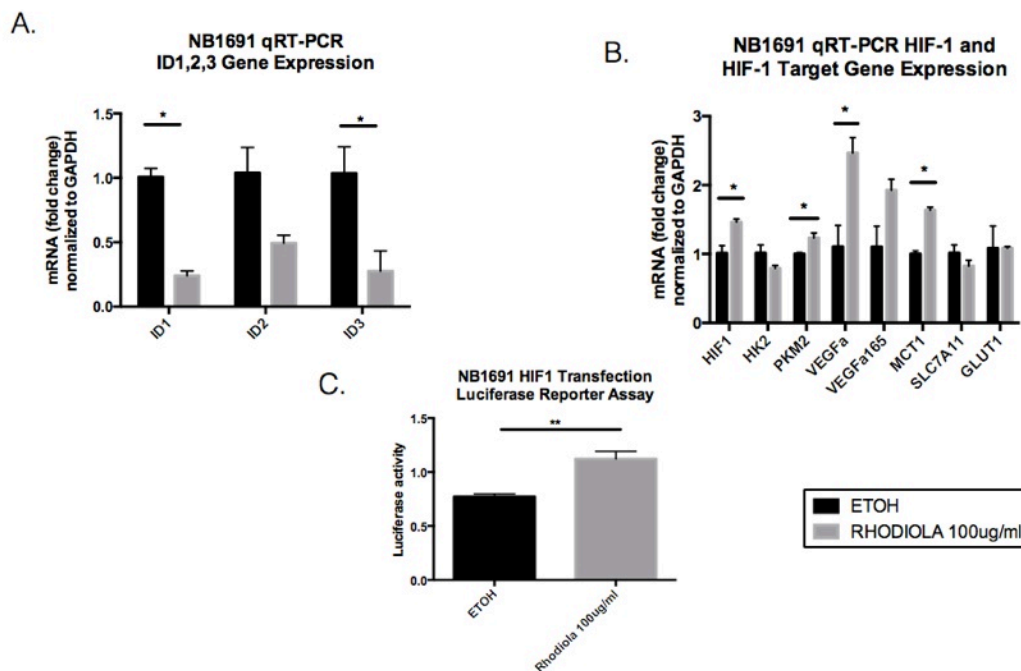
A) Scratch wound was created in confluent monolayer of SK-N-AS and NB-1691 then treated with either ethanol or 200 $\mu$ g/mL RC. Representative images following 4 and 72 hours of treatment with either vehicle control or RC are shown. Red and blue lines outline borders of growth within scratch wound. B) Clonogenicity evaluation of NB-1691 treated with 50 $\mu$ g/mL RC or ethanol vehicle control +/- 5Gy radiation. RC treatment was applied continuously. C) The average number of cells treated with either ethanol or 100 $\mu$ g/mL RC that migrated through transwell migration wells quantified in each representative 10X field. Error Bars indicate +/- standard error of the mean, \*= $p$ <0.05, \*\*= $p$ <0.01, \*\*\*= $p$ <0.0001.

Figure 5.4: *Rhodiola* Vs. Dox Viability



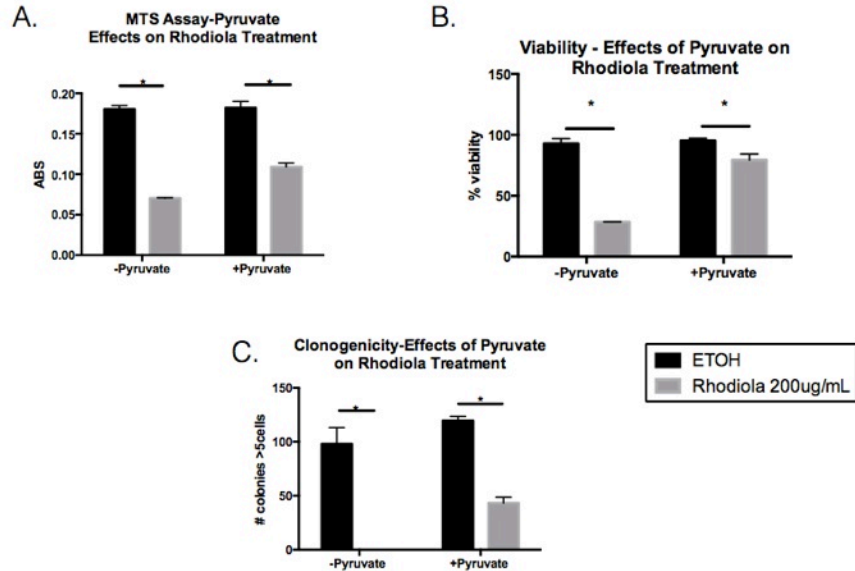
**Figure 5.4. Evaluation of RC vs Dox treatment on Neuroblastoma *In Vitro*.** 72 hour viability evaluated using trypan blue exclusion of SK-N-AS (A) and NB-1691 (B) cells performed following treatment with 200 $\mu$ g/mL RC both before and after adherence to the plate. Results were compared to 10 $\mu$ g/mL Dox treatment. Results presented as viability relative to ethanol control treated cells. Error Bars indicate +/- standard error of the mean, \*= $p$ <0.01, \*\*= $p$ <0.001.

Figure 5.5: NB-1691 Gene Expression Changes Upon *R. crenulata* Treatment



**Figure 5.5. Effects on Gene Expression upon RC treatment in NB-1691 *In Vitro*.** A) Quantitative RT-PCR was performed from RNA extracted from NB-1691 cells treated with 100 $\mu$ g/mL RC or ethanol vehicle control for 24 hours. Changes in mRNA levels normalized to GAPDH expression of ID 1, ID 2, and ID 3 gene expression. B) Changes in mRNA levels normalized to GAPDH expression of HIF-1 targets including HIF1- $\alpha$ , HK2, PKM2, VEGF, VEGF $\alpha$ 165, MCT1, SLC7A11 and GLUT1. C) NB1691 cells transfected with luciferase reporter HIF-1 promoter and treated with 100 $\mu$ g/mL RC or ethanol vehicle for 48 hours. Luciferase activity was evaluated and relative luciferase activity is reported. Error Bars indicate +/- standard error of the mean, \* = p < 0.05 and \*\* = p < 0.01.

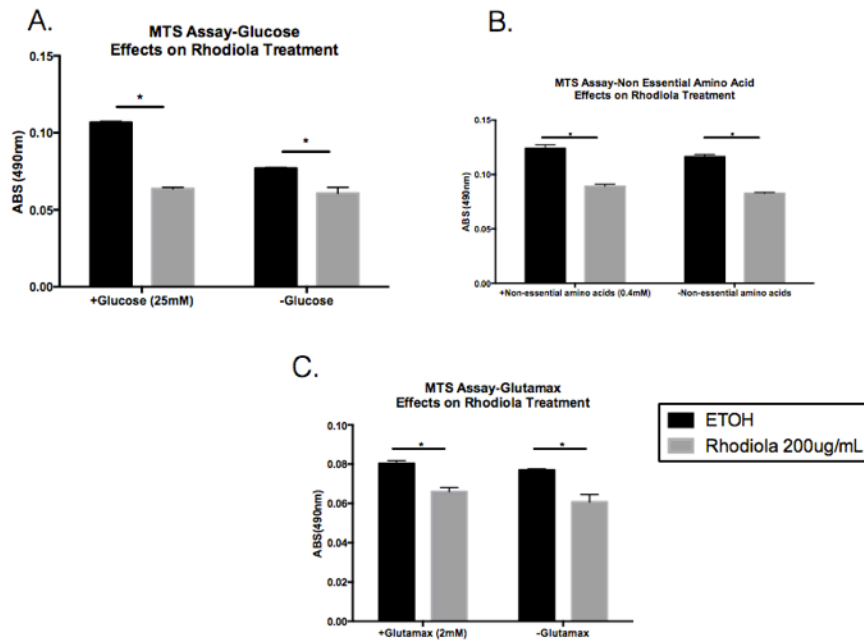
Figure 5.6: Evaluation of the effects of Pyruvate on *Rhodiola* Treatment



**Figure 5.6 Evaluation of the Effects of Pyruvate Upon RC Treatment on Neuroblastoma.** A) MTS assay performed on NB-1691 cells treated with 200 $\mu$ g/mL RC or ETOH +/- Pyruvate (1mM) following 24 hours of treatment. B) Assessment of viability utilizing trypan blue exclusion on NB-1691 cells treated with 200 $\mu$ g/mL RC or ETOH +/- Pyruvate. C) Clonogenicity evaluation of NB-1691 treated with 50 $\mu$ g/mL RC or ethanol vehicle control +/- 1mM Pyruvate. RC treatment was applied continuously and plates were evaluated for the development of colony formation over three weeks. Following this, cells were fixed and stained with crystal violet and total colonies formed were quantified. Error Bars indicate +/- standard error of the mean, \*=p<0.05.

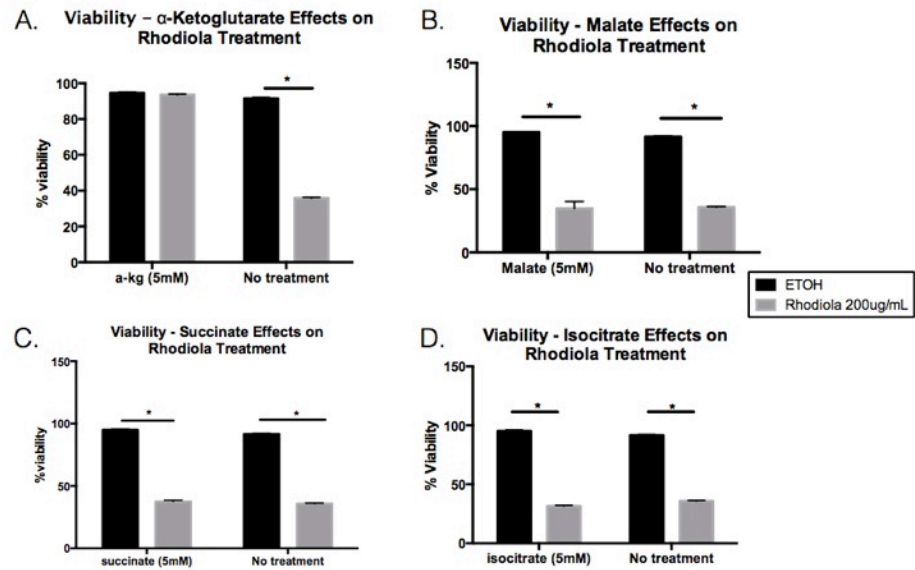


Figure 5.7: Nutrient Supplementation on RC Effects on Viability



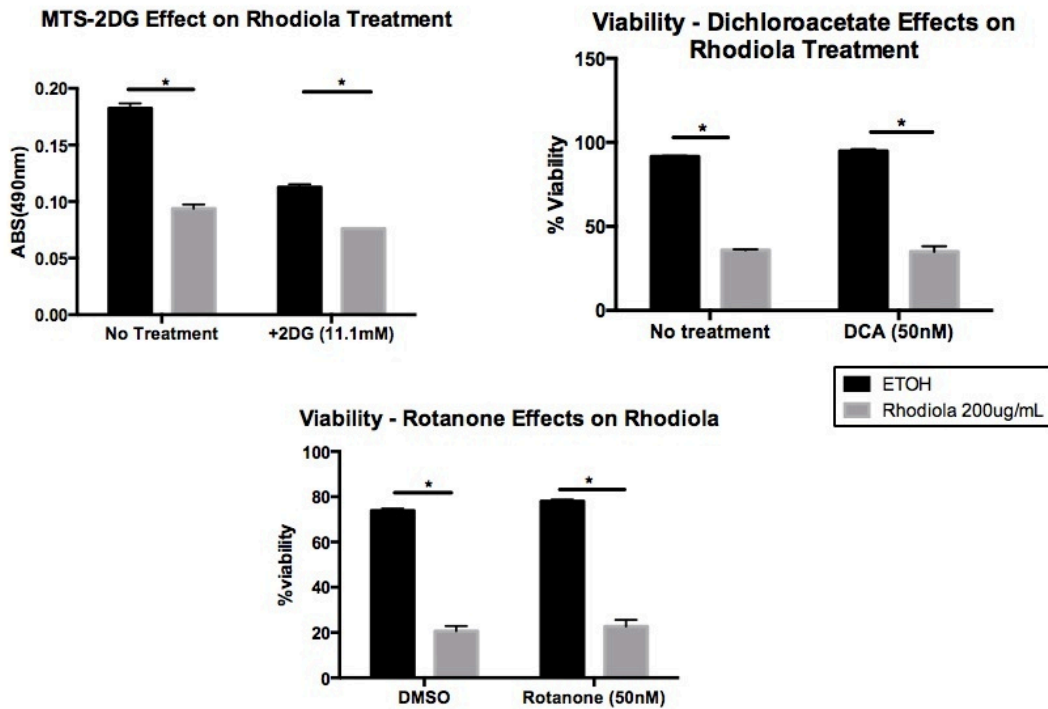
**Figure 5.7. Evaluation of Nutrient Supplementation on RC Effects on Neuroblastoma Viability *In Vitro*.** All experiments were performed on 1X104 NB-1691 cells treated with RC or ethanol in suspension +/- listed nutrient in DMEM lacking pyruvate, glucose and glutamine. Cells were incubated for 24 hours and then an MTS assay was performed to assess for cell viability. A) Evaluation of the effects of glucose (25mM) on RC treatment. B) Evaluation of the effects of non-essential amino acids (0.4mM) on RC treatment. C) Evaluation of the effects of glutamax (2mM) on RC treatment. Error Bars indicate +/- standard error of the mean, \*=p<0.05.

Figure 5.8-Citric Acid Cycle Intermediate Effects on *Rhodiola* Treatment



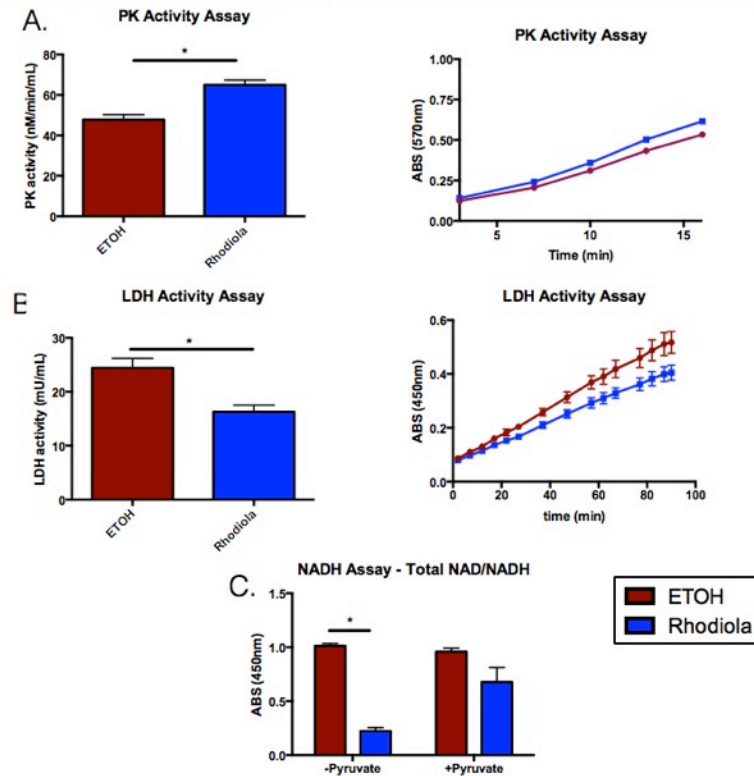
**Figure 5.8. Evaluation of Citric Acid Cycle Intermediate Supplementation on RC Effects on Neuroblastoma Viability *In Vitro*.** All experiments were performed on  $2 \times 10^5$  NB-1691 cells pre-conditioned in pyruvate (1mM) containing medium. Cells were treated with  $200 \mu\text{g/mL}$  RC or vehicle control +/- 5mM  $\alpha$ -ketoglutarate (A), +/- 5mM malate (B), +/- 5mM succinate (C), +/- 5mM isocitrate (D) in suspension and incubated for 24 hours. Viability was evaluated using trypan blue exclusion using a Vi-cell counter. Error Bars indicate +/- standard error of the mean,  $*=p<0.05$ .

Figure 4.9-Metabolic Inhibitor Effects on *Rhodiola* Treatment



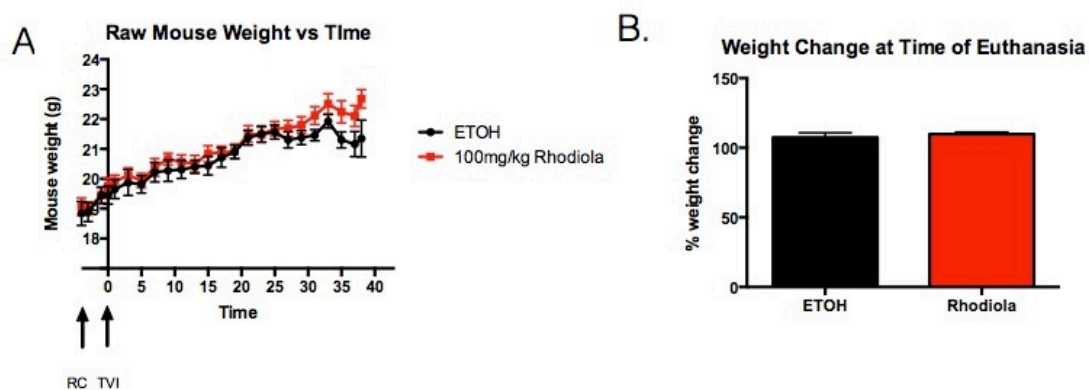
**Figure 5.9. Effect of Metabolic Inhibitors on RC Treatment upon NB-1691 Cells *In Vitro*.** A)  $1 \times 10^4$  cells treated with  $200 \mu\text{g/mL}$  RC or ethanol +/-  $11.1 \text{mM}$  2-deoxy-D-glucose (2DG), treated for 24 hours and MTS assay was performed to assess for viability. B)  $2 \times 10^5$  cells treated with  $200 \mu\text{g/mL}$  RC or ethanol +/-  $20 \text{nM}$  dichloroacetate (DCA), treated in suspension for 24 hours. Trypan blue exclusion performed utilizing a Vicell counter was utilized to assess for viability. C)  $2 \times 10^5$  cells treated with  $200 \mu\text{g/mL}$  RC or ethanol +/-  $50 \text{nM}$  Rotanone, treated in suspension for 24 hours. Trypan blue exclusion performed utilizing a Vicell counter was utilized to assess for viability.

Figure 5.10-Rhodiola Effects on Metabolic Enzymes and Intermediates



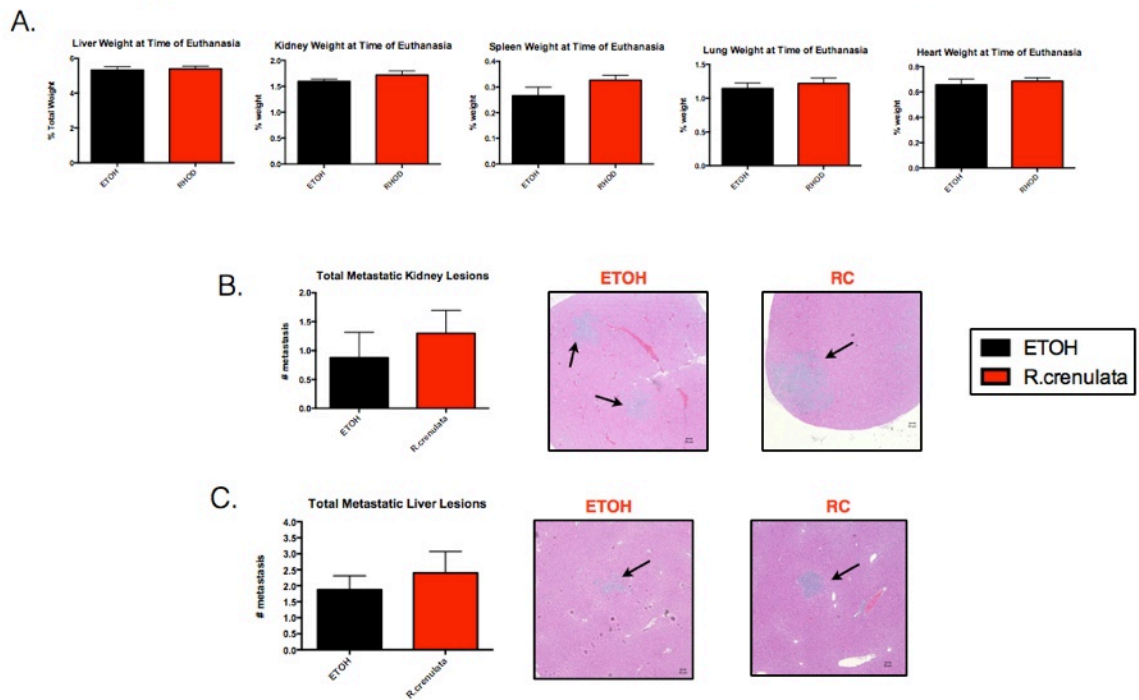
**Figure 5.10 RC Effects on Metabolic Enzyme Activity and Metabolic Intermediate Levels.** A) Pyruvate Kinase Activity levels evaluated upon NB-1691 treated for two hours with either RC 200 $\mu$ g/mL or ETOH. Results show both PK activity (nM/min/mL) for each sample as well as PK activity over time. B) Lactate Dehydrogenase Activity levels evaluated upon NB-1691 treated for two hours with either RC 200 $\mu$ g/mL or ETOH. Results shown include LDH activity (mU/mL) for each sample as well as LDH activity over time. C) NAD Quantification Assay performed in NB-1691 cells treated with 200 $\mu$ g/mL RC or ETOH +/-1mM pyruvate for two hours in which total NAD+NADH levels were quantified. Error bars represent +/- standard error of the mean, \*=p<0.05.

Figure 5.11-*In Vivo* Evaluation of *Rhodiola* in a Disseminated Model of Neuroblastoma



**Figure 5.11.** Evaluation of the *In Vivo* Efficacy of RC Treatment of Disseminated Neuroblastoma. A) Graphic representation of the weight changes of mice treated with 100mg/kg RC or ETOH with disseminated NB-1691 over time. Arrows represent dates of RC treatment initiation (RC) and tail vein injection (TVI). B) Weight change at time of euthanasia of mice treated with 100mg/kg RC or ETOH. Error bars represent +/- standard error of the mean.

Figure 5.12-Outcomes of *Rhodiola* Administration on Disseminated Neuroblastoma



**Figure 5.12. Outcomes of RC treatment in a disseminated *in vivo* neuroblastoma model.** A) Proportional total weights of organs collected at time of euthanasia including from mice treated with either 100mg/kg RC or ETOH. Organs represented include liver, kidney, spleen, lung and heart. B) Average number of metastatic lesions established in kidneys present within each 10X field. Representative 10X images of kidney samples from each treatment group shown, arrows represent metastatic lesions. C) Average number of metastatic lesions established in livers present within each 10X field. Representative 10X images of liver samples from each treatment group shown, arrows represent metastatic lesions. Error bars represent +/- standard error of the mean

## 5.7 Tables

**Table 5.1 - Primers Utilized in qRT-PCR.** List of primers utilized for qRT-PCR to evaluate the effects of RC treatment of NB-1691 cells on genetic expression.

Gene	Forward Sequence	Reverse Sequence
GAPDH	5'-TGCACCACCAACTGCTTAGC-3'	5'-GGCATGGACTGTGGTCATGAG-3'
ID1	5'-CCAGAACCGCAAGGTGAG-3'	5'-GGTCCCTGATGTAGTCGATGA-3'
ID2	5'-GACAGAACCAGGCGTCCA-3'	5'-AGCTCAGAAGGGAATTCAGATG-3'
ID3	5'-CATCTCCAACGACAAAAGGAG-3'	5'-CTTCCGGCAGGAGGGTT-3'
HIF1	5'-CTCACCAGACAGAGCAGGAA-3'	5'-TGCGAAGCTATTGTCTTTGG-3'
HK2	5'-TCGAGTACATGGGCATGAAGG-3'	5'-ACTTGAGGAGGATGCTCTCGT-3'
PKM2	5'-CCACTTGCAATTATTTGAGGAA-3'	5'-GTGAGCAGACCTGCCAGACT-3'
MCT1	5'-GTCATTGGAGGTCTTGGGCT-3'	5'-GCCAATGGTCGCCTCTTGTA-3'
SLC7A11	5'-GGCAACCGCGTAATACTTG-3'	5'-TTGCAAGCTCACAGCAATTC-3'
GLUT1	5'-GGTTGTGCCATACTCATGACC-3'	5'-CAGATAGGACATCCAGGGTAGC-3'
VEGFa	5'-CCACGTCAGAGAGCAACATC-3'	5'-TCTCCTATGTGCTGGCTTTG-3'
VEGFa165	5'-ATCTTCAAGCCATCCTGTGTGC-3'	5'-CAAGGCCACAGGGATTTTC-3'

## 5.8 References

1. Davidoff, A.M. Neuroblastoma. (2010) Ashcraft's Pediatric Surgery. 5th Edition. Chapter 68. 872-894.
2. Grosfeld, J. L. Risk-based management: current concepts of treating malignant solid tumors of childhood. *J Am Coll Surg*. 1999. 189(4): 407-425.
3. Ora, I. and Eggert, A. Progress in Treatment and Risk Stratification of Neuroblastoma: Impact on Future Clinical and Basic Research. *Seminars in Cancer Biology* 2011 21; 217-228.
4. Pelicci, P., Lanfrancone, L., Brathwaite, M.D., et al. Amplification of N-myc in Untreated Human Neuroblastomas Correlates with Advanced Disease Stage. *Science* 1984 224; 1121-1124.
5. Green, A.A., Hayes, F.A. and Hustu, H.O. Sequential Cyclophosphamide and Doxorubicin for Induction of Complete Remission in Children with Disseminated Neuroblastoma. *Cancer* 1981 48; 2310-2317.
6. Pannossian A, Wilkman G, Sarris J. Rosenroot (*Rhodiola rosea*): traditional use, chemical composition, pharmacology and clinical efficacy. *Phytomedicine*. 2010;17:481–93.
7. Gauger KJ, Rodríguez-Cortés A, Hartwich M, et al. *Rhodiola crenulata* inhibits the tumorigenic properties of invasive mammary epithelial cells with stem cell characteristics. *J Med Plants Res*. 2010;4:446–54.
8. Tu Y, Roberts L, Schneider SS. *Rhodiola crenulata* induces death and inhibits growth of breast cancer cell lines. *J Med Food*. 2008;11:413–23.
9. Mora, M.C., Bassa, L.M., Wong, K.E., et al. *Rhodiola Crenulata* Inhibits Wnt/ $\beta$ -catenin Signaling in Glioblastoma. *Journal of Surgical Research*. Accepted for publication February, 2015
10. Dudek, MC, Wong, KE, Bassa, LM, et al. Antineoplastic Effects of *Rhodiola Crenulata* Treatment on B16-F10 Melanoma. *Tumor Biology*. 2015. DOI 10.1007/s13277-015-3742-2
11. Houghton, P.J., Morton, C.L., Tucker, C., et al. The Pediatric Preclinical Testing Program: Description of Models and Early Testing Results. *Pediatric Blood Cancer*. 2007. 49:928-940.



12. Maher, J.C., Krishan, A., Lampidis, T.J. Greater Cell Cycle Inhibition and Cytotoxicity Induced by 2-deoxy-D-glucose in Tumor Cells Treated Under Hypoxic vs Aerobic Conditions. *Cancer Chemother Pharmacol.* 2004. 53: 116-122.
13. Stacpoole, P.W., Henderson, G.N., Yan, Z., James, M.O. Clinical Pharmacology and Toxicology of Dichloroacetate. *Environ Health Perspect.* 1998. 104 (Supp 4): 989-994.
14. Hollingworth, R.M., Ahammadsahib, K.I., Gadelhak, G.G., et al. New Inhibitors of Complex I of the Mitochondrial Electron Transport Chain with Activity as Pesticides. *Biochemical Society Transactions.* 1994. 22 (1): 230-233.
15. Besinger, S.J. and Christofk, H.R. New Aspects of the Warburg Effect in Cancer Cell Biology. *Seminars in Cell & Developmental Biology.* 2012. 23(4):352-361.
16. Hockenberry, D.M., Tom, M. Abikoff, et al. The Warburg Effect and Beyond: Metabolic Dependencies for Cancer Cells. *Cell Death Signaling in Cancer Biology and Treatment.* 2012. Chapter 2: 35-51.
17. Upadhyay, M., Samal, J., Kandpal, M., et al. The Warburg Effect: Insights from the Past Decade. *Pharmacology & Therapeutics.* 2013. 137 (3): 318-330.
18. Kim, J., Dang, C.V. Cancer's Molecular Sweet Tooth and the Warburg Effect. *Cancer Research.* 2006. doi: 10.1158/0008-5472.CAN-06-1501
19. Semenza, G.L. HIF-1 Mediates Metabolic Responses to Intratumoral Hypoxia and Oncogenic Mutations. *J Clin Invest.* 2013. 123 (9):3664-3671.
20. Semenza, G.L. HIF-1: Upstream and Downstream of Cancer Metabolism. *Current Opinions in Genetics & Development.* 2010. 20 (1): 51-6.
21. Vander Heiden, M.G., Cantley, L.C., Thompson, C.B. Understanding the Warburg Effect: The Metabolic Requirements of Cell Proliferation. *Science.* 2009. 22: 1029-1033.
22. Hsu, P.P., Sabatini, D.M. Cancer Cell Metabolism: Warburg and Beyond. *Cell.* 2008. 134 (5): 703-7.
23. Feron, O. Pyruvate into Lactate and Back: From the Warburg Effect to Symbiotic Energy Fuel Exchange in Cancer Cells. *Radiotherapy and Oncology.* 2009. 92 (3): 329-333

## CHAPTER 6

### CONCLUSION

#### 6.1 General Discussion

Cancer remains one of the leading cause of death in the United States today. While significant improvements to commonly used treatment agents as well as creation or identification of novel therapeutic options have been made, the mortality rates of cancer continues to remains high. Further, it's treatments are limited by the toxicities associated with the many of these chemotherapeutic agents. Development and evaluation of novel methods to treat various forms of cancer may lead to improved survival as well as reduced off target side effects and their associated morbidities. This work sought to evaluate novel treatment methods for several types of chemo-resistant cancer both *in vitro* and *in vivo*.

#### 6.2 Utilization of PolyMPC for Cancer Therapeutics

PolyMPC produgs have previously been shown to improve survival upon the treatment of a murine model of breast cancer in immunocompetent mice. While these findings were promising, the safety of the scaffold polyMPC polymer, as well as evaluation of polyMPC prodrugs (polyMPC-Dox), had yet to be evaluated in a human cancer model. Through this work we observed that polyMPC polymers were extremely safe for systemic administration in mice. Limits to therapeutic administration of the polymer were secondary to the viscosity of the polymer solution and the inability to

further dilute higher doses of polymer effectively. No appreciable side effects were observed following administration of large doses of polyMPC. Investigation of the therapeutic efficacy of polyMPC-Dox upon treatment of a human ovarian tumor in NOD SCID mice further confirmed the prior investigation of polyMPC-Dox in immunocompetent mice. Mice treated with polyMPC-Dox displayed increased tumor uptake of Dox. Additionally, treatment with polyMPC-Dox resulted in improved survival of mice compared to control and free Dox treated mice. In comparison to doxil, an alternative Dox formulation, treatment tolerance and survival was much improved in mice treated with polyMPC-Dox.

Further investigation to improve targeting of polyMPC directly to tumors was also evaluated. Mesenchymal stem cells, which have inherent tumoritropic capabilities, were investigated as a vehicle to improved targeted delivery of polyMPC to tumor. We observed that polyMPC can be stably loaded with polyMPC and that the *in vivo* migratory capabilities of these cells were unaltered.

### **6.3 Utilization of *Rhodiola* Extract for the Treatment of Cancer**

RC is an adaptogenic phytochemical that has been observed to have anti-tumor properties, observed both *in vitro* and *in vivo*. Given these findings, we sought to evaluate the effects of RC on two aggressive forms of cancer derived from the neural crest. For both neuroblastoma and melanoma, we observed that RC lead to reduced viability, growth and proliferation *in vitro*. Further investigation into the mechanism to which RC

exerts its cytotoxic effects upon neuroblastoma treatment revealed that RC resulted in changes in the metabolic activity of cells, likely resulting in cell death.

Upon evaluation of both cancers in a disseminated model to mimic metastatic disease *in vivo*, RC lead to reduced establishment of pulmonary melanoma lesions, although no difference in the establishment of neuroblastoma lesions was observed. Upon investigation of the topical application of RC on subcutaneous melanoma lesions, tumors were observed to grow more radially and tumors displayed reduced mitotic activity.

#### **6.4 Conclusion**

Through this thesis, I have evaluated alternative treatment options for the several aggressive and chemo-resistant forms of cancer. Two broad approaches were evaluated for this work in which both polyMPC prodrugs and *Rhodiola* based plant extracts were utilized to treat cancer. Both polyMPC prodrugs and RC have the potential to broaden our arsenal of anti-cancer agents that be to be employed in humans for the treatment of cancer in the future.

## BIBLIOGRAPHY

1. American Cancer Society. Cancer Facts and Figures. 2015. Accessed 2/10/15. Available from <http://www.cancer.org/acs/groups/content/@editorial/documents/document/acspc-044552.pdf>.
2. Agbarya, A., Ruimi, Nili, Epelbaum, R., et al. Natural Products as Potential Cancer Therapy Enhances: A Preclinical Update. Sage. 2014. doi: 10.1177/2050312114546924
3. Azzola MF, Shaw HM, Thompson JF, et al. Tumor mitotic rate is a more powerful prognostic indicator than ulceration in patients with primary cutaneous melanoma. *Cancer*. 2003;97:1488–98.
4. Balch CM, Gershenwald JE, Soong S, et al. Staging and primary tumor mitotic rate. *J Surg Oncol*. 2011;104:379–85.
5. Balch CM, Gershenwald JE, Soong S, et al. Final version of 2009 AJCC melanoma staging and classification. *J Clin Oncol*. 2009;27: 6199–206.
6. Bang, O.Y., Lee, J.S., Lee, P.H., et al. Autologous Mesenchymal Stem Cell Transplantation in Stroke Patients. *Annals of Neurology* 2005 57;874-882
7. Bedrosian I, FariesMB, Guerry D, et al. Incidence of sentinel node metastasis in patients with thin primary melanoma (#1 mm) with vertical growth phase. *Ann Surg Oncol*. 2000;7:262–7.
8. Bertrand, N., Wu, J., Xu, X., et al. Cancer Nanotechnology: The Impact of Passive and Active Targeting in the Era of Modern Cancer Biology. *Advanced Drug Delivery Reviews*. 2014. 66:2-25.
9. Besinger, S.J. and Christofk, H.R. New Aspects of the Warburg Effect in Cancer Cell Biology. *Seminars in Cell & Developmental Biology*. 2012. 23(4):352-361.
10. Bocharova, O. A., B. P. Matveev, et al. The effect of a *Rhodiola rosea* extract on the incidence of recurrences of a superficial bladder cancer (experimental clinical research). *Urol Nefrol (Mosk)*. 1995. 2: 46-47.
11. Breslow A. Thickness, cross-sectional areas and depth of invasion in the prognosis of cutaneous melanoma. *Ann Surg*. 1970;5:902–8.
12. Brown RP, Gerbarg PL. *The rhodiola revolution*. 1st ed. Holtzbrinck Publishers; 2004.

13. Brown, R.P., Gerbarg, P.L., Ramazanov, Z. Rhodiola Rosea A Phytomedicinal Overview. *HerbalGram*. 2002. 56:40-52.
14. Chiang H, Chien Y, Wu C, et al. Hydroalcoholic extract of Rhodiola rosea L. (Crassulaceae) and its hydrolysate inhibit melanogenesis in B16F0 cells by regulating the CREB/MITF/tyrosinase pathway. *Food Chem Toxicol*. 2014;65:129–39.
15. Chin L. The genetics of malignant melanoma: lessons from mouse and man. *Nat Rev Cancer*. 2003;3:559–70.
16. Chen, S., Fang, W., Ye, F., et al. Effect on Left Ventricular Function of Intracoronary Transplantation of Autologous Bone Marrow Mesenchymal Stem cells in Patients with Myocardial Infarction. *The American Journal of Cardiology*. 2004 94; 92-95.
17. Chen X, Parelkar S, Henchey E, Schneider S, Emrick T. PolyMPC-Doxorubicin Prodrugs. *Bioconjugate Chem*. 2012, 23, 1753-1763.
18. Cheng H, Kastrup CJ, Ramanathan R, Siegwart DJ, Ma M, Bogatyrev SR, et al. Nanoparticulate cellular patches for cell-mediated tumoritropic delivery. *ACS Nano*. 2010;4(2):625-31.
19. Davidoff, A.M. Neuroblastoma. (2010) *Ashcraft's Pediatric Surgery*. 5th Edition. Chapter 68. 872-894.
20. Darbinyan V, Aslanyan G, Amrovan E, et al. Clinical trial of Rhodiola rosea L. extract SHR-5 in the treatment of mild to moderate depression. *Nord J Psychiatry*. 2007;61:343–8.
21. Deans, R.J. and Moseley, A.B. Mesenchymal Stem Cells: Biology and Potential Clinical Uses. *Experimental Hematology* 2000 28; 875-884.
22. Delplace, V., Couvreur, P., Nicolas, J. Recent Trends in the Design of Anticancer Polymer Prodrug Nanocarriers. *Polym. Chem*. 2014. 5:1529-1544.
23. Dudek, MC, Wong, KE, Bassa, LM, et al. Antineoplastic Effects of Rhodiola Crenulata Treatment on B16-F10 Melanoma. *Tumor Biology*. 2015. DOI 10.1007/s13277-015-3742-2
24. Duncan R. Polymer conjugates as anticancer nanomedicines. *Nat Rev Cancer*. 2006;6(9):688-701.
25. Dwyer AV, Whitten DL, Hawrelak JA. Herbal medicines, other than St. John's Wort, in the treatment of depression: a systematic review. *J Clin Ther*. 2001;16:40–9.

26. Elder DE. Pathology of melanoma. *Clin Cancer Res.* 2006;12: 2309–11.
27. Feron, O. Pyruvate into Lactate and Back: From the Warburg Effect to Symbiotic Energy Feul Exchange in Cancer Cells. *Radiotherapy and Oncology.* 2009. 92 (3): 329-333
28. Francken AB, Shaw HM, Thompson JF, et al. The prognostic importance of tumor mitotic rate confirmed in 1317 patients with primary cutaneous melanoma and long follow-up. *Ann Surg Oncol.* 2004;11:426–33.
29. Fox, M. E.; Szoka, F. C.; Fréchet, J. M. J. Soluble Polymer Carriers for the Treatment of Cancer: The Importance of Molecular Architecture. *Acc. Chem. Res.* 2009, 42, 1141- 1151
30. Gauger, K.J. *Rhodiola Rosea: A Possible Plant Adaptogen.* *Alternative Medicine Review.* 2001. 6:293-30
31. Gauger KJ, Rodríguez-Cortés A, Hartwich M, et al. *Rhodiola crenulata* inhibits the tumorigenic properties of invasive mammary epithelial cells with stem cell characteristics. *J Med Plants Res.* 2010;4:446–54.
32. Gelderblom, H.; Verweij, J.; Nooter, K.; Sparreboom, A. Cremophor EL: the Drawbacks of Vehicle Selection for Drug Formulation. *Eur. J. Cancer.* 2001, 37, 1590-1598.
33. Grantab R, Sivananthan S, Tannock IF. The penetration of anticancer drugs through tumor tissue as a function of cellular adhesion and packing density of tumor cells. *Cancer Res.* 2006;66(2):1033-9.
34. Green, A.A., Hayes, F.A. and Hustu, H.O. Sequential Cyclophosphamide and Doxorubicin for Induction of Complete Remission in Children with Disseminated Neuroblastoma. *Cancer* 1981 48; 2310-2317.
35. Greish, K. Enhanced Permeability and Retention Effect for Selective Targeting of Anticancer Nanomedicine: Are we There Yet? *Drug Discovery Today: Technologies.* 2012. 9(2):e161-166.
36. Grosfeld, J. L. Risk-based management: current concepts of treating malignant solid tumors of childhood. *J Am Coll Surg.* 1999. 189(4): 407-425.
37. Haag R, Kratz F. Polymer therapeutics: concepts and applications. *Angew Chem Int Ed Engl.* 2006;45(8):1198-215.

30. Hall, B., Dembinski, J., Sasser, A.K., et al. Mesenchymal Stem Cells in Cancer: Tumor-Associated Fibroblast and Cell-Based Delivery Vehicles. *International Journal of Hematology* 2007 86; 8-16.
38. Hasan, N.; Ohman, A. W.; Dinulescu, D. M. The Promise and Challenge of Ovarian Cancer Models. *Transl. Cancer Res.* 2015, 4.
39. Heldin CH, Rubin K, Pietras K, Ostman A. High interstitial fluid pressure - an obstacle in cancer therapy. *Nat Rev Cancer.* 2004;4(10):806-13.
40. Hockenberry, D.M., Tom, M. Abikoff, et al. The Warburg Effect and Beyond: Metabolic Dependencies for Cancer Cells. *Cell Death Signaling in Cancer Biology and Treatment.* 2012. Chapter 2: 35-51.
41. Hollingworth, R.M., Ahammadsahib, K.I., Gadelhak, G.G., et al. New Inhibitors of Complex I of the Mitochondrial Electron Transport Chain with Activity as Pesticides. *Biochemical Society Transactions.* 1994. 22 (1): 230-233.
42. Hoon DS, Bostick P, Kuo C, et al. Molecular markers in blood as surrogate prognostic indicators of melanoma recurrence. *Cancer Res.* 2000;60:2253–7.
43. Houba, P. H. J.; Boven, E.; van der Meulen-Muileman, I. H.; Leenders, R. G. G.; Scheeren, J. W.; Pinedo, H. M.; Haisma, H. J. Pronounced Antitumor Efficacy of Doxorubicin When Given as the Prodrug DOX-GA3 in Combination with a Monoclonal Antibody  $\beta$ -Glucuronidase Conjugate. *Int. J. Oncol.* 2001, 91, 550-554.
44. Houghton, P.J., Morton, C.L., Tucker, C., et al. The Pediatric Preclinical Testing Program: Description of Models and Early Testing Results. *Pediatric Blood Cancer.* 2007. 49:928-940.
45. Hsu, P.P., Sabatini, D.M. Cancer Cell Metabolism: Warburg and Beyond. *Cell.* 2008. 134 (5): 703-7.
46. Huang, X., Zhang, F., Wang, H., et al. Mesenchymal Stem Cell-based Cell Engineering with Multifunctional Mesoporous Silica Nanoparticles for Tumor Delivery. *Biomaterials* 2013 24; 1772-1780.
47. Injac, R.; Strukelj, B. Recent Advances in Protection Against Doxorubicin-Induced Toxicity. *Technol. Cancer Res. Treat.* 2008, 6, 497-516.
48. Ishihara, K. New Polymeric Biomaterials—Phospholipid Polymers with a Biocompatible Surface. *Front Med. Biol. Eng.* 2000, 10, 83-95.



49. Ishihara, K. Highly Lubricated Polymer Interfaces for Advanced Artificial Hip Joints through Biomimetic Design. *Polym. J.* 2015, 47, 585-597.
50. Iwasaki, Y.; Ishihara, K. Phosphorylcholine-Containing Polymers for Biomedical Applications. *Anal. Bioanal. Chem.* 2005, 381, 534-546.
51. Jain RK. Delivery of molecular and cellular medicine to solid tumors. *Adv Drug Deliv Rev.* 2001;46(1-3):149-68.
52. Joshi, M.; Sodhi, K. S.; Pandey, R.; Singh, J.; Goyal, S.; Prasad, S.; Kaur, H.; Bhaskar, N.; Mahajan. Cancer Chemotherapy and Hepatotoxicity: An Update. *IAJPS.* 2014, 6, 2976-2984.
53. Kim, J., Dang, C.V. Cancer's Molecular Sweet Tooth and the Warburg Effect. *Cancer Research.* 2006. doi: 10.1158/0008-5472.CAN-06-1501
54. Khandare, J.; Minko, T. Polymer-Drug Conjugates: Progress in Polymeric Prodrugs. *Prog. Polym. Sci.* 2006, 31, 359-397.
55. Khazir, J., Ahmad Mir, B., Pilcher, L., et al. Role of Plants in Anticancer Drug Discovery. *Phytochemistry Letters.* 2014. 7: 173-81.
56. Kratz, F.; Mansour, A.; Soltau, J.; Warnecke, A.; Fichtner, I.; Unger, C.; Drevs, J. Development of Albumin-Binding Doxorubicin Prodrugs that are Cleaved by Prostate-Specific Antigen. *Arch. Pharm.* 2005, 338, 462-472.
57. Larson, N.; Ghandehari, H. Polymeric Conjugates for Drug Delivery. *Chem. Mater.* 2012, 24, 840-853
58. Less JR, Skalak TC, Sevic EM, Jain RK. Microvascular architecture in a mammary carcinoma: branching patterns and vessel dimensions. *Cancer Res.* 1991;51(1):265-73.
59. Leu AJ, Berk DA, Lymboussaki A, Alitalo K, Jain RK. Absence of functional lymphatics within a murine sarcoma: a molecular and functional evaluation. *Cancer Res.* 2000;60(16):4324-7.
60. Li L, Guan Y, Liu H, Hao N, Liu T, Meng X, et al. Silica nanorattle-doxorubicin-anchored mesenchymal stem cells for tumor-tropic therapy. *ACS Nano.* 2011;5(9):7462-70.

61. Liu Z, Li X, Simoneau AR, Jafari M, et al. Rhodiola rosea extracts and salidroside decrease the growth of bladder cancer cell lines via inhibition of the mTOR pathway and induction of autophagy. *Mol Carcinog.* 2012;51:257–67.
62. Luxenhofer, R.; Schulz, A.; Li, S.; Bronich, T. K.; Batrakova, E. V.; Jordan, R.; Kabanov A. V. Doubly Amphiphilic Polymers as High-Capacity Delivery Systems for Hydrophobic Drugs. *Biomaterials.* 2010, 31, 4972-4979.
63. Loebinger MR, Eddaoudi A, Davies D, Janes SM. Mesenchymal stem cell delivery of TRAIL can eliminate metastatic cancer. *Cancer Res.* 2009;69(10):4134-42.
64. Maeda, H.; Nakamura, H.; Fang, J. The EPR Effect for Macromolecular Drug Delivery to Solid Tumors: Improvement of Tumor Uptake, Lowering of Systemic Toxicity, and Distinct Tumor Imaging In Vivo. *Adv. Drug Deliv. Rev.* 2013, 65, 71-79.
65. Maeda, H.; Wu, J.; Sawa, T.; Matsumura, Y.; Hori, K. Tumor Vascular Permeability and the EPR Effect in Macromolecular Therapeutics: a Review. *J. Control. Release.* 2000, 65, 271-284.
66. Maeda H, Matsumura Y. Tumorotropic and lymphotropic principles of macromolecular drugs. *Crit Rev Ther Drug Carrier Syst.* 1989;6(3):193-210.
67. Maeda H, Sawa T, Konno T. Mechanism of tumor-targeted delivery of macromolecular drugs, including the EPR effect in solid tumor and clinical overview of the prototype polymeric drug SMANCS. *J Control Release.* 2001;74(1-3):47-61.
68. Maher, J.C., Krishan, A., Lampidis, T.J. Greater Cell Cycle Inhibition and Cytotoxicity Induced by 2-deoxy-D-glucose in Tumor Cells Treated Under Hypoxic vs Aerobic Conditions. *Cancer Chemother Pharmacol.* 2004. 53: 116-122.
69. Mehta, R.G., Murillo, G., Naithani, R., et al. Cancer Chemoprevention by Natural Products: How Far Have we Come? *Pharm Res.* 2010. 27:950-61.
70. Matsumura, Y.; Maeda, H. A New Concept for Macromolecular Therapeutics in Cancer Chemotherapy: Mechanism of Tumor Tropic Accumulation of Proteins and Antitumor Agents SMANCS. *Cancer Res.* 1986, 46, 6387-6392.
71. McRae Page S, Martorella M, Parelkar S, Kosif I, Emrick T. Disulfide cross-linked phosphorylcholine micelles for triggered release of camptothecin. *Mol Pharm.* 2013;10 (7):2684-92.
72. McRae Page S, Henchey E, Chen X, Schneider S, Emrick T. Efficacy of polyMPC-DOX prodrugs in 4T1 tumor-bearing mice. *Mol Pharm.* 2014;11(5):1715-20.

73. Meier F, Satyamoorthy K, Nesbit M, et al. Molecular events in melanoma development and progression. *Front Biosci.* 1998;3: 1005–10.
74. Melanoma of the Skin. In: turning cancer data into discovery. surveillance, epidemiology, and end results (SEER) program. 2004–2010. <http://seer.cancer.gov/statfacts/html/melan.html>. Accessed 12 March 2015.
75. Mellado B, Gutierrez L, Castel T, et al. Prognostic significance of the detection of circulating malignant cells by reverse transcriptase polymerase chain reaction in long-term clinically disease-free melanoma patients. *Clin Cancer Res.* 1999;5:1843–8.
76. Milosevic MF, Fyles AW, Wong R, Pintilie M, Kavanagh MC, Levin W, et al. Interstitial fluid pressure in cervical carcinoma: within tumor heterogeneity, and relation to oxygen tension. *Cancer.* 1998;82(12):2418-26.
77. Minchinton AI, Tannock IF. Drug penetration in solid tumours. *Nat Rev Cancer.* 2006;6(8):583-92.
78. Mora MC, Bassa LM, Wong KE, et al. *Rhodiola Crenulata* inhibits Wnt/ $\beta$ -catenin signaling in glioblastoma. *J Surg Res.* 2015;197(2): 247–55.
79. Motulsky HJ, Brown RE. Detecting outliers when fitting data with nonlinear regression – a new method based on robust nonlinear regression and the false discovery rate. *BMC Bioinf.* 2006. doi: 10.1186/1471-2105-7-123.
80. National Cancer Institute. A Snapshot of Ovarian Cancer. <http://www.cancer.gov/research/progress/snapshots/ovarian> (accessed Sep 28, 2015).
81. Overwijk WW, Restifo NP. B16 as a mouse model for human melanoma. *Curr Protoc Immunol.* 2001. doi:10.1002/0471142735.im2001s39.
82. Ora, I. and Eggert, A. Progress in Treatment and Risk Stratification of Neuroblastoma: Impact on Future Clinical and Basic Research. *Seminars in Cancer Biology* 2011 21; 217-228.
83. Page, S. M.; Henchey, E.; Chen, X.; Schneider, S.; Emrick, T. Efficacy of polyMPCDOX Prodrugs in 4T1 Tumor-Bearing Mice. *Mol. Pharmaceutics.* 2014, 11, 1715-1720
84. Pannossian A, Wilkman G, Sarris J. Rosenroot (*Rhodiola rosea*): traditional use, chemical composition, pharmacology and clinical efficacy. *Phytomedicine.* 2010;17:481–93.

85. Pardoll, D., Allison, J. Cancer Immunotherapy: Breaking the Barriers to Harvest the Crop. *Nature Medicine*. 2004. 10: 887-892.
86. Pastorino, F., Di Paolo, D., Piccardi, F., et al. Enhanced Antitumor Efficacy of Clinical-Grade Vasculature-Targeted Liposomal Doxorubicin. *Clinical Cancer Research* 2008 14; 7320-7329.
87. Pasut G, Veronese FM. PEG conjugates in clinical development or use as anticancer agents: an overview. *Adv Drug Deliv Rev*. 2009;61(13):1177-88.
88. Pelicci, P., Lanfrancone, L., Brathwaite, M.D., et al. Amplification of N-myc in Untreated Human Neuroblastomas Correlates with Advanced Disease Stage. *Science* 1984 224; 1121-1124.
89. Primeau AJ, Rendon A, Hedley D, Lilge L, Tannock IF. The distribution of the anticancer drug Doxorubicin in relation to blood vessels in solid tumors. *Clin Cancer Res*. 2005;11(24 Pt 1):8782-8.
90. Rahman, A. M.; Yusuf, S. W.; Ewer, M. S. Anthracycline-induced Cardiotoxicity and the Cardiac Sparing Effect of Liposomal Formulation. *Int. J. Nanomedicine*. 2007, 2, 567-583.
91. Ren C, Kumar S, Chanda D, Chen J, Mountz JD, Ponnazhagan S. Therapeutic potential of mesenchymal stem cells producing interferon-alpha in a mouse melanoma lung metastasis model. *Stem Cells*. 2008;26(9):2332-8.
92. Ren C, Kumar S, Chanda D, Kallman L, Chen J, Mountz JD, et al. Cancer gene therapy using mesenchymal stem cells expressing interferon-beta in a mouse prostate cancer lung metastasis model. *Gene Ther*. 2008;15(21):1446-53.
93. Richmond, A.; Su, Y. Mouse Xenograft Models vs GEM Models for Human Cancer Therapeutics. *Dis. Model Mech*. 2008, 1, 78-72.
94. Roger M, Clavreul A, Venier-Julienne MC, Passirani C, Sindji L, Schiller P, et al. Mesenchymal stem cells as cellular vehicles for delivery of nanoparticles to brain tumors. *Biomaterials*. 2010;31(32):8393-401.
95. Rose, P. G. Pegylated Liposomal Doxorubicin: Optimizing the Dosing Schedule in Ovarian Cancer. *Oncologist*. 2005, 10, 205-214.
96. Saenz del Burgo, L., Pedraz, J.L., Orive, G., et al. Advanced Nanovehicles for Cancer Management. 2014. 19 (10): 1659-1670.

97. Semenza, G.L. HIF-1 Mediates Metabolic Responses to Intratumoral Hypoxia and Oncogenic Mutations. *J Clin Invest.* 2013. 123 (9):3664-3671.
98. Semenza, G.L. HIF-1: Upstream and Downstream of Cancer Metabolism. *Current Opinions in Genetics & Development.* 2010. 20 (1): 51-6.
99. Seo SH, Kim KS, Park SH, Suh YS, Kim SJ, Jeun SS, et al. The effects of mesenchymal stem cells injected via different routes on modified IL-12-mediated antitumor activity. *Gene Ther.* 2011;18(5):488-95.
100. Shim, G-s.; Manandhar, S.; Shin, D.; Kim, T-H.; Kwak, M-K. Acquisition of Doxorubicin Resistance in Ovarian Carcinoma Cells Accompanies Activation of the NRF2 Pathway. *Free Radic. Biol. Med.* 2009, 47, 1619-1631.
101. Siegal, R., DeSantis, C., Virgo, K., et al. Cancer Treatment and Survivorship Statistics, 2012. *CA A Cancer Journal for Clinicians.* 2012. DOI: 10.3322/caac.21149
102. Singal, P.K.; Iliskovic, N. Doxorubicin-Induced Cardiomyopathy. *N. Engl. J. Med.* 1998, 339, 900-905.
103. Skopińska-Różewska E, Hartwich M, Siwicki AK, et al. The influence of *Rhodiola rosea* extracts and rosavin on cutaneous angiogenesis induced in mice after grafting of syngeneic tumor cells. *Cent Eur J Immunol.* 2008;33:102–7.
104. Stacpoole, P.W., Henderson, G.N., Yan, Z., James, M.O. Clinical Pharmacology and Toxicology of Dichloroacetate. *Environ Health Perspect.* 1998. 104 (Supp 4): 989-994.
105. Studeny M, Marini FC, Champlin RE, Zompetta C, Fidler IJ, Andreeff M. Bone marrow-derived mesenchymal stem cells as vehicles for interferon-beta delivery into tumors. *Cancer Res.* 2002;62(13):3603-8.
106. Tacar, O., Sriamornsak, P. and Dass, C.R. Doxorubicin: an Update on Anticancer Molecular Action, Toxicity and Novel Drug Delivery Systems. *Journal of Pharmacy and Pharmacology.* 2013. 65(2): 157-170.
107. Tadokoro Tet al. UV-induced DNA damage and melanin content in human skin differing in racial/ethnic origin. *FASEB J.* 2003. doi:10. 1096/fj.02-0865fje.
108. Ten Tjie, A. J.; Verweij, J.; Loos, W. J.; Sparreboom A. Pharmacological Effects of Formulation Vehicles: Implications for Cancer Chemotherapy. *Clin. Pharmacokinet.* 2003, 42, 665-685.

109. Thompson JF, Soong S, Balch S, et al. Prognostic significance of mitotic rate in localized primary cutaneous melanoma: an analysis of patients in the Multi-Institutional American Joint Committee on cancer melanoma staging database. *J Clin Oncol.* 2011;29:2199– 205.
110. Tu Y, Roberts L, Schneider SS. *Rhodiola crenulata* induces death and inhibits growth of breast cancer cell lines. *J Med Food.* 2008;11:413–23.
111. Upadhyay, M., Samal, J., Kandpal, M., et al. The Warburg Effect: Insights from the Past Decade. *Pharmacology & Therapeutics.* 2013. 137 (3): 318-330.
112. Vander Heiden, M.G., Cantley, L.C., Thompson, C.B. Understanding the Warburg Effect: The Metabolic Requirements of Cell Proliferation. *Science.* 2009. 22: 1029-1033.
113. Wei X, Yang X, Han ZP, Qu FF, Shao L, Shi YF. Mesenchymal stem cells: a new trend for cell therapy. *Acta Pharmacol Sin.* 2013;34(6):747-54.
114. Weir, H.K., Thompson, T.D., Soman, A, et al. The Past, Present, and Future of Cancer Incidence in the United States: 1975-2020. *Cancer.* 2015. DOI: 10.1002/cncr.2925
115. Zhang X, Yao S, Liu C, Jiang Y. Tumor tropic delivery of doxorubicin-polymer conjugates using mesenchymal stem cells for glioma therapy. *Biomaterials.* 2015;39:269-81.